



***A MEASUREMENT  
ARCHITECTURE BASED ON  
COMPRESSIVE SAMPLING  
FOR THE MONITORING OF  
ELECTRICAL POWER  
TRANSMISSION GRIDS***

***A THESIS PRESENTED TO  
"DIPARTIMENTO DI INGEGNERIA ELETTRICA E DELLE  
TECNOLOGIE DELL'INFORMAZIONE  
UNIVERSITÀ DI NAPOLI FEDERICO II"  
BY  
BONAVOLONTÀ FRANCESCO***

***IN PARTIAL FULFILLMENT  
OF THE REQUIREMENTS FOR THE DEGREE  
DOCTOR OF PHILOSOPHY  
IN ELECTRICAL ENGINEERING***

***ADVISOR: PROF. MAURO D'ARCO***

***ASSISTANT ADVISOR: ING. R. SCHIANO LO MORIELLO***

***MARCH 2015***

# CONTENTS

Abstract.....	5
Introduction .....	7
1 Compressive Sampling .....	13
1.1 Compressible signals .....	14
1.2 Transform coding and its inefficiencies .....	15
1.3 Compressive Sampling .....	15
1.4 Sensing Matrix Determination .....	16
1.5 Sparse Solution Evaluation.....	17
1.6 References .....	19
2 Compressive Sampling Approach for the Measurement of Electrical Power Quality	20
2.1 Introduction .....	20
2.2 The Proposed Method.....	21
2.2.1 Transformation Matrix Determination .....	21
2.2.2 Sampling Matrix Determination.....	22
2.2.3 Sensing Matrix Determination .....	23
2.2.4 Input Signal Recovering .....	23
2.3 Numerical results .....	23
2.4 Conclusions .....	27
2.5 References .....	27
3 Multi-channel Simultaneous Data Acquisition Systems. ....	30
3.1 Introduction .....	30
3.2 The Proposed CS-based Acquisition Approach .....	31

3.3	CS-based simultaneous data acquisition.....	35
3.4	Numerical results.....	37
3.5	Experimental Results.....	41
3.5.1	Tests conducted through 32-bit microcontroller .....	42
3.5.2	Tests conducted on 8-bit microcontroller.....	50
3.5.3	Tests conducted on a FPGA-based platform.....	54
3.6	Conclusions .....	56
3.7	References .....	57
4	Sample Rate Enhancement In DASs For Low-Cost Sensing Nodes.....	59
4.1	Introduction .....	59
4.2	Increasing the effective sample rate of embedded DAS.....	60
4.2.1	Traditional Sampling Approach .....	61
4.2.2	CS-based Sampling Approach.....	61
4.2.3	Proposed Sample Rate Improvement .....	62
4.3	Proposed Sampling Approach .....	62
4.3.1	Sampling Instants Determination .....	63
4.4	Numerical Results .....	65
4.4.1	ADC Sample Rate and Vertical Resolution .....	66
4.4.2	Noise.....	68
4.4.3	Number of Acquired Samples and Effective Sample Rate.....	69
4.4.4	Jitter .....	70
4.4.5	Input Signal Sparsity .....	72
4.5	Experimental Tests .....	73
4.5.1	Tests conducted on 32-bits microcontroller .....	75
4.5.2	Tests conducted on 8-bits microcontroller .....	80
4.6	Conclusions .....	84

4.7	References .....	85
5	Compliance assessment of the CS based architecture in Harmonic and Interharmonic Measurements .....	88
5.1	Introduction .....	88
5.2	The proposed approach.....	89
5.3	Test Assessment .....	92
5.3.1	Aims of the tests .....	92
5.3.2	Selection of the Test Signal .....	94
5.3.3	Simulation Results.....	96
5.3.4	Experimental Results.....	100
5.4	Conclusions .....	106
5.5	References .....	107
	Conclusions and Future Developments .....	108

## **Abstract**

In recent years significant change in the power grid for the distribution of electrical energy have been observed. Thanks to liberalization of the electrical market and the incentives offered to the production of energy from renewable sources, the number of medium and small producers has increased. Moreover, with the development of communication technology, the transmission grid has been increasingly equipped with automated devices capable of monitoring and transmitting some information about the grid and, in some cases, to control the actuation devices connected to the grid itself. In this scenario, the term smart grid was born, used to describe energy networks that can automatically monitor energy flows and adjust to changes in energy supply and demand accordingly. When coupled with smart metering systems, smart grids reach consumers and suppliers by providing information on real-time consumption. As an example, consumers can adapt their energy usage to different energy prices throughout the day with personal smart meters, saving money on their energy bills by consuming more energy in lower price periods. As it can be expected, the wider the grid, the larger the number of smart meters required for its monitoring. However, deploying thousands of such devices turns rapidly to be too expensive. Consequently, the realization of the distributed measurement system could not be economically sustainable.

## *Abstract*

To overcome the considered limitations, the research activities have been focused on the possibility to move towards a different approach for monitoring grid deployed on wide geographical areas, exploiting the advantages of an innovative acquisition paradigm: the Compressed Sampling (CS). CS is a signal processing technique for efficiently acquiring and reconstructing a signal from far fewer samples than those required by the Shannon-Nyquist sampling theorem. In particular, the proposed architecture consists of low cost nodes mandated only to sample and digitize a limited number of input signal samples and transmit them to a central measurement unit, thus saving the costs related to large memory supports and expensive digital processing units. Once the samples are received, the central unit recovers the signal spectrum thanks to CS-based algorithm and carries out the desired measurements. Thanks to the CS-based approach, it is possible to design and realize a measurement node, characterized by reduced memory depth and only one ADC, suitable for poly-phase system with neutral wire that allows meeting the requirements of a distributed measurement system. Numerical and experimental test verified highlight the capability of CS-based acquisition approach of correctly measuring the root-mean-square amplitude of voltage waveforms and assuring simultaneous multi-channel acquisitions. Finally, the compliance of the measurement node based on CS approach with the current Power Quality standards is assessed and discussed.

## **Introduction**

Electricity is the most versatile and widely used form of energy and global demand is growing continuously. The electrical power system was built up over more than 100 years. It is now one of the most effective components of the infrastructure on which modern society depends. It delivers electrical energy to industry, commercial and residential consumers, meeting ever-growing demand. Most of today's generation capacity relies on fossil fuels and contributes significantly to the increase of carbon dioxide in the world's atmosphere, with negative consequences for the climate and society in general. To satisfy both the increasing demand for power and the need to reduce carbon dioxide emissions, there is need of an electric system that can handle these challenges in a sustainable, reliable and economic way. To this aim, it is necessary to modernize the whole grid infrastructure.

In particular, the challenges and needs for future transmission grids can be summarized in four main aspects:

- ***Environmental challenges.*** Traditional electric power production, as the largest man-created CO<sub>2</sub> emission source, must be changed to mitigate the climate change. Also, a shortage of fossil energy resources has been foreseen in the next few decades. Natural catastrophes, such as hurricanes, earthquakes, and tornados can destroy the transmission grids easily. Finally, the available and suitable space for the future expansion of transmission grids has decreased dramatically.
- ***Market/customer needs.*** Full-fledged system operation technologies and power market policies need to be developed to sustain the transparency and liberty of the competitive market. Customer satisfaction with electricity consumption should be improved by providing high quality/price ratio electricity and customers' freedom to interact with the grid.
- ***Infrastructure challenges.*** The existing infrastructure for electricity transmission has quickly aging components and insufficient investments for improvements. With the pressure of the increasing load demands, the network congestion is becoming worse.

The fast online analysis tools, wide-area monitoring, measurement and control, and fast and accurate protections are needed to improve the reliability of the networks.

- ***Innovative technologies.*** On one hand, the innovative technologies, including new materials, advanced power electronics, and communication technologies, are not yet mature or commercially available for the revolution of transmission grids; on the other hand, the existing grids lack enough compatibility to accommodate the implementation of spear-point technologies in the practical networks

Whereas the innovation of the transmission grid was driven by technology in the past, the current power industry is being modernized and tends to deal with the challenges more proactively by using state-of-the-art technological advances in the areas of sensing, communications, control, computing, and information technology. The shift in the development of transmission grids to be more intelligent has been summarized with the term “Smart Grid”.

Smart grids will provide more electricity to meet rising demand, increase reliability and quality of power supplies, increase energy efficiency, be able to integrate renewable energy sources into power networks. The benefits associated with the Smart Grid include:

- ✓ More efficient transmission of electricity
- ✓ Quicker restoration of electricity after power disturbances
- ✓ Reduced operations and management costs for utilities, and ultimately lower power costs for consumers
- ✓ Reduced peak demand, which will also help lower electricity rates
- ✓ Increased integration of large-scale renewable energy systems
- ✓ Better integration of customer-owner power generation systems, including renewable energy systems
- ✓ Improved security

Deploying a suitable distributed measurement system is a fundamental early step to grid modernization. The distributed measurement system will give consumers the information they need to make intelligent decisions, the ability to execute those decisions and a variety of choices leading to substantial benefits they do not currently enjoy. In addition, system operators will be able to greatly improve consumer service by refining utility operating and asset management processes based on distributed measured system data. Each measurement

node has to perform acquiring, processing, control, and communication task. Moreover it has to be equipped with Power Quality (PQ) monitoring capabilities, in order to enable more rapid detection, diagnosis and resolution of PQ problems. The IEC 61000-4-30 standard defines the methods for measurement and interpretation of results of PQ parameters involved in 50/60 Hz power supply systems. The considered parameters concern with power frequency, magnitude of the supply voltage, flicker, supply voltage dips and swells, voltage interruptions, transient voltages, supply voltage unbalance, voltage and current harmonics and interharmonics, signaling on the supply voltage and rapid voltage changes. In particular, the standard referenced in IEC 61000-4-7 suggests the realization of measurement instruments which, after a suitable synchronization pre-processing, adopt suitable Fast Fourier Transform (FFT) calculations on consecutive, and without gaps, periods of 200 ms. Consider a poly-phase system with neutral wire, where four currents and four voltages have to be detected, synchronized, measured and analyzed with good accuracy and spectral resolution. As a consequence, the measurement instrument has to be able to: (i) simultaneous acquisition of multiple signals (i) estimate the frequency of incoming signals, (ii) change (in a digital or analog way) the sampling frequency, (ii) store and manage a large number of data; (iii) calculate in sequence or simultaneously, eight FFTs in a very short time, and (iv) detect and classify events. The compliance with IEC 61000-4-30 using the suggested synchronized FFT analysis needs processing and memory capabilities, notable increases the cost of the each measurement node. As it can be expected, the number of measurement nodes increases according to the extension of the monitored grid. If wide grid have to be monitored, it should be necessary to deploy thousands of these measurement nodes over the area. Therefore, the realization of the distributed measurement system could not be economically sustainable. At the same time, it is very important to carry out a distributed monitoring of the PQ phenomena in many points of the electrical plant to detect and to isolate the distorting loads. It is evident that to allow the realization of cost effective PQ monitoring network efforts have to be done in minimizing both the memory and computational burden. Hardware platform as low-cost microcontrollers are frequently taken into account to realize low-cost sensor node for a distributed measurement system. Typical microcontroller integrate sensing, data acquisition system (DAS), processing unit and communication block in a single chip allowing cost-effective realization of measurement nodes (Fig.0.1). However, they are generally characterized by limited hardware resources, in term of number of available analog-to-digital

converters (ADCs) and in term of memory depth. The considered platform can, in fact, scarcely store more than few kilobytes of data, and typically adopt multiplexer to share different physical channels over the same ADC. In order to recognize, without ambiguity, the power quality disturbances, PQ standards often require a long-time analysis, thus, a great number of samples has to be stored and transmitted.

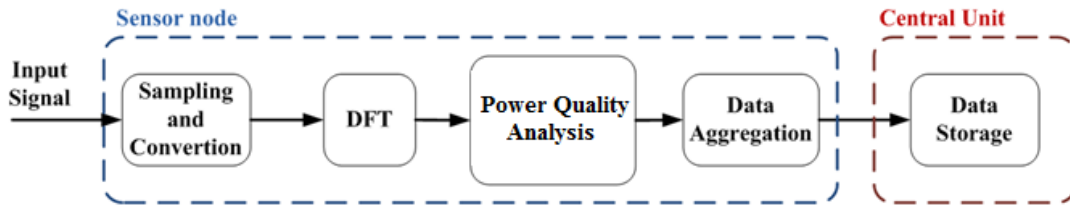


Fig. 0.1 Traditional architecture for PQ monitoring.

Unfortunately, this requirement is in contrast with the characteristics of the low-cost microcontroller. In addition, the adoption of a multiplexer to share different physical channels over the same ADC, allows only sequential acquisitions. As a consequence, overall measurement performance is limited, because an unwanted phase displacement turns out to be imposed on the acquired signals. This phase shift is mainly due to the inter-channel delay the multiplexer spends to acquire two samples on different channels, and proves to be a deep constraint that typically reduces the applicability of low-cost measurement nodes. As an example, the measurement of power flows, requiring the process of the voltages and currents waveform, digitized in the same instants, could be strongly degraded from the use of DASs based on low-cost microcontrollers. Therefore, low-cost measurement nodes, based on microcontroller architectures, do not meet the desired requirements for smart grid monitoring. To overcome the considered limitation, the research activity suggests the possibility to move towards a different approach for monitoring grid deployed on wide geographical areas, exploiting the advantages of an innovative measurement approach: the Compressed Sampling (CS). CS is a signal processing technique for efficiently acquiring and reconstructing a signal from far fewer samples than those required by the Shannon-Nyquist sampling theorem . In particular, the proposed architecture consists of low cost nodes mandated only to sample and digitize a limited number of input signal samples and transmit them to a central measurement unit, saving, thus, the costs related to large memory supports and expensive digital processing units. Once the samples have been received, the central unit recovers the signal spectrum thanks to CS-based algorithm and carries out the desired measurements. The proposed

architecture is shown in Fig.0.2, where two main blocks can be observed: the single Sampling Node (SN) and the Central Measurement Unit (CMU).

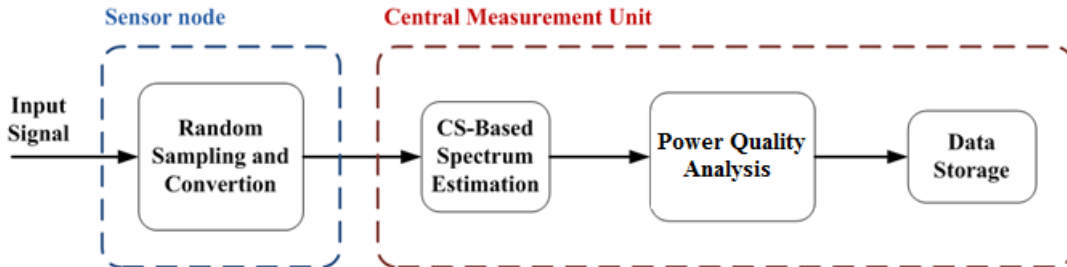


Fig. 0.2 Proposed architecture based on CS approach.

The CMU, with high computational capability and equipped with a high capacity hard disk, is mandated to both process the acquired samples and estimates PQ parameters. The CMU stores the entire reconstructed spectrum, so that the details of the voltage waveform are permanently saved for successive observations. In other words, thanks to the CS-based approach, it has been possible to design and realize a measurement node, characterized by reduced memory depth and only one ADC, that allows meeting the following requirements of a distributed measurement system:

- recording of long traces for off-line analysis
- simultaneously acquiring voltages and currents waveforms
- monitoring Power Quality
- reducing costs for a single node

thus proving suitable for Smart Grid environment.

The present Ph.D. final work is organized as follows: in Chapter 1, a brief theoretical background on the Compressive Sampling is given. In Chapter 2 the applicability of compressive sampling techniques in PQ measurements is investigated. In particular, aim of the research activity in this first step, is definition of a PQ measurement method, based on the compressive sampling, capable of (i) assuring measurement performance comparable with those required by standards and granted typical PQ measurement methods and instruments, and (ii) drastically reducing the required memory with respect to traditional measurement methods. In Chapter 3 a novel acquisition approach, based on CS, capable of carrying out multichannel simultaneous data acquisition also through inherently sequential DASs is

presented. To this aim, the approach exploits a unique time-basis for all the input channels adopted, along with a compressive random sampling, in order to assure the reconstruction of desired signals without any artefact due to the inter-channel delay and/or sequential acquisition scheme. It is worth noting that for distributed measurement systems consisting of distributed acquisition nodes and a central computing unit that processes measurement data, improving the performance of the embedded DAS, in terms of sample rate, can be crucial for the improvement of the whole measurement system. To this aim, a new method based on compressive sampling, which permits to increase the maximum sample rate of DAS integrated in low-cost microcontrollers, is proposed in Chapter 4. Finally, in the Chapter 5, by means of numerical and experimental tests, the compliance of the measurement node based on CS approach with the current Power Quality standard is assessed. In particular, the capability of CS-based acquisition approach of correctly measuring root-mean-square amplitude of harmonic and interharmonic voltage pollution has been verified.

## 1 Compressive Sampling

The Shannon-Nyquist sampling theorem states that one must sample at least two times faster than the signal bandwidth to prevent harmful information loss when capturing a signal [1]. In many applications, including digital image and video cameras, the required Nyquist rate is so high that too many samples are acquired, making compression a necessity before storing or transmitting operations. In other applications, including imaging systems (medical scanners and radars) and high-speed analog-to-digital converters, increasing the sampling rate is very expensive. Recently a novel sensing/sampling paradigm, known as Compressive Sampling (CS), that goes against the common wisdom in data acquisition has been proposed [2]. Compressive Sampling theory asserts that one can recover certain signals and images from far fewer samples or measurements than traditional methods use [3]. In other words, the new method is able to capture and represent compressible signals at a rate significantly below the Nyquist rate. A CS technique can be divided in two fundamental stages: (i) A first stage in which the input signal is acquired directly in a compressed form; (ii) A second stage in which the input original signal is correctly reconstructed by means a suitable CS-Solver [4].

To make this possible, CS relies on two principles: (i) *sparsity*, which pertains to the signals of interest, and (ii) *incoherence*, which pertains to the sensing modality.

- Sparsity expresses the idea that the “information rate” of a continuous time signal may be much smaller than suggested by its bandwidth, or that a discrete-time signal depends on a number of degrees of freedom that is comparably much smaller than its (finite) length. More precisely, CS exploits the fact that many natural signals are sparse or compressible in the sense that they have concise representations when expressed in the proper basis  $\Psi$  [5].
- Incoherence extends the duality between time and frequency and expresses the idea that objects having a sparse representation in  $\Psi$  must be spread out in the domain in which they are acquired, just as a Dirac or a spike in the time domain is spread out in the frequency domain. In a different way, incoherence says that unlike the signal of interest, the sampling/sensing waveforms have an extremely dense representation in  $\Psi$  [6].

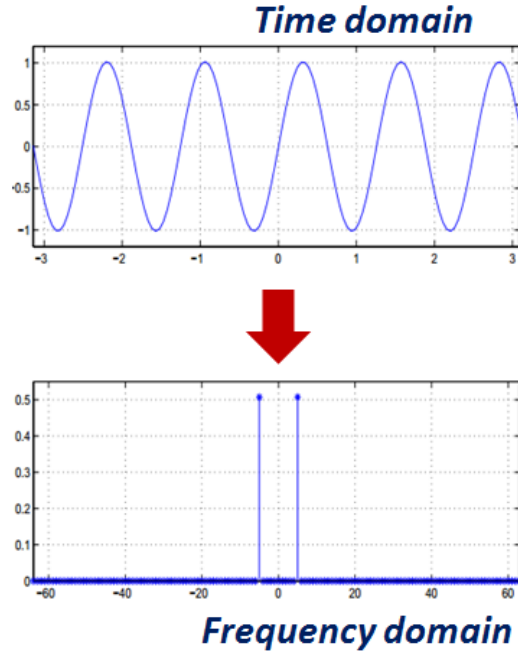


Fig.1.1 As an example, a sinusoidal signal is characterized by an endless evolution versus time, while its Fourier transform contain the same information in only two coefficients different from zero.

The crucial observation is that one can design efficient sensing or sampling protocols that capture the useful information content embedded in a sparse signal and condense it into a small amount of data [7]. These protocols are nonadaptive and simply require correlating the signal with a small number of fixed waveforms that are incoherent with the sparsifying basis. What is most remarkable about these sampling protocols is that they allow a sensor to very efficiently capture the information in a sparse signal without trying to comprehend that signal. Further, there is a way to use numerical optimization to reconstruct the full-length signal from the small amount of collected data.

### 1.1 Compressible signals

Consider a real-valued, finite-length, one-dimensional, discrete-time signal  $\mathbf{x}$ , which can be viewed as an  $N \times 1$  column vector in  $R^N$  with elements  $x[n]$ ,  $n = 1, 2, \dots, N$ . Any signal in  $R^N$  can be represented in terms of a basis of  $N \times 1$  vectors  $\{\psi_i\}_{i=1}^N$ . For the sake of simplicity, let us assume that the basis is orthonormal. Using the  $N \times N$  matrix  $[\psi_1 | \psi_2 | \dots | \psi_N]$  with the vectors  $\{\psi_i\}$  as columns, a signal  $\mathbf{x}$  can be expressed as:

$$\mathbf{x} = \sum_{i=1}^N f_i \cdot \psi_i \quad \text{or} \quad \dots \quad \mathbf{x} = \Psi \mathbf{f} \quad (1.1)$$

where  $\mathbf{f}$  is the  $N \times 1$  column vector of weighting coefficients  $f_i = \langle \mathbf{x}, \boldsymbol{\psi}_i \rangle = \boldsymbol{\psi}_i^T \mathbf{x}$  and  $\cdot^T$  denotes transpositions. Clearly,  $\mathbf{x}$  and  $\mathbf{f}$  are equivalent representations of the signal, with  $\mathbf{x}$  in the time or space domain and  $\mathbf{f}$  in the  $\boldsymbol{\Psi}$  domain. The signal  $\mathbf{x}$  is said to be  $K$ -sparse if it is a linear combination of only  $K$  basis vectors; that is, only  $K$  of the coefficients in (1.1) are nonzero and  $(N - K)$  are zero. The case of interest is when  $K \ll N$ . The signal  $\mathbf{x}$  is *compressible* if the representation (1.1) has just a few large coefficients and many small coefficients.

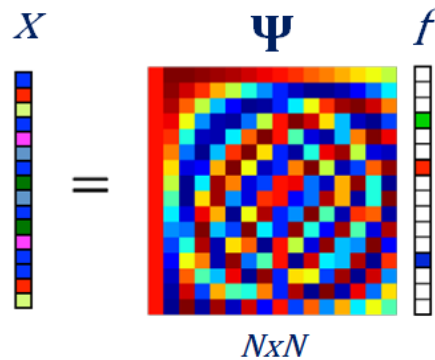


Fig. 1.2 Compressible signals

### 1.2 Transform coding and its inefficiencies

The fact that compressible signals are well approximated by  $K$ -sparse representations forms the foundation of transform coding [8]. In data acquisition systems (for example, digital cameras) transform coding plays a central role: the full  $N$ -sample signal  $\mathbf{x}$  is acquired; the complete set of transform coefficients  $\{f_i\}$  is computed via  $f = \boldsymbol{\psi}^T \mathbf{x}$ ; the  $K$  largest coefficients are located and the  $(N - K)$  smallest coefficients are discarded; and the  $K$  values and locations of the largest coefficients are encoded. Unfortunately, this sample-then-compress framework suffers from three inherent inefficiencies. First, the initial number of samples  $N$  may be large even if the desired  $K$  is small. Second, the set of all  $N$  transform coefficients  $\{f_i\}$  must be computed even though all but  $K$  of them will be discarded. Third, the locations of the large coefficients must be encoded, thus introducing an overhead.

### 1.3 Compressive Sampling

Compressive Sampling address these inefficiencies by directly acquiring a compressed signal representation without going through the intermediate stage of acquiring  $N$  samples. Consider a general linear measurement process that computes  $M \ll N$  inner products between  $\mathbf{x}$  and a

collection of vectors  $\{\phi_j\}_{j=1}^M$  as in  $y_j = \langle x, \phi_j \rangle$ . Arrange the measurements  $y_j$  in a  $M \times 1$  vector  $\mathbf{y}$  and the measurements vectors  $\phi_j^T$  as rows in a  $M \times N$  matrix  $\Phi$ .

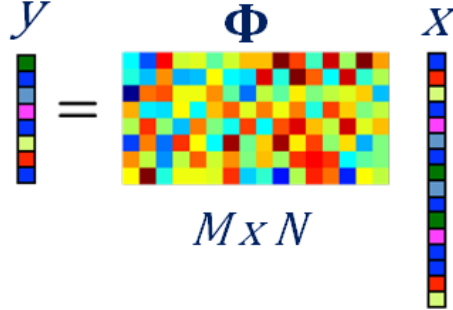


Fig. 1.3 Sampling matrix  $\Phi$  allows selecting  $M$  measured values from which reconstructing the original signal.

Thus, from a mathematical point of view, the relation between the sequence of acquired samples  $\mathbf{y} \in \mathbb{R}^m$  and the input signal of interest  $\mathbf{x} \in \mathbb{R}^n$  can be expressed as:

$$\mathbf{y} = \Phi \mathbf{x} \quad (1.2)$$

In other words, the sampling matrix  $\Phi$  allows selecting  $M$  measured values from which reconstructing the original signal.

#### 1.4 Sensing Matrix Determination

Unfortunately, the system described in (1.2) turns out to be an underdetermined system of linear equations; this kind of systems have usually infinitely many solutions, meaning that there are infinitely many candidate signals  $\hat{\mathbf{x}}$  [6]

Under the assumption that  $\mathbf{x}$  is characterized by a sparse representation in a proper basis, the sequence of acquired measurements can be expressed in terms of the sparse representation of  $\mathbf{x}$  by combining eq. (1.1) and (1.2),

$$\mathbf{y} = \Phi \mathbf{x} = \Phi \Psi \mathbf{f} \quad (1.3)$$

Introducing a new matrix, referred to as sensing matrix, according to

$$\mathbf{A} = \Phi \Psi \quad (1.4)$$

where  $\mathbf{A} \in \mathbb{R}^{m \times n}$ , the following equation system has to be solved to achieve the sparse signal  $\mathbf{f}$

$$\mathbf{y} = \mathbf{A} \mathbf{f} \quad (1.5)$$

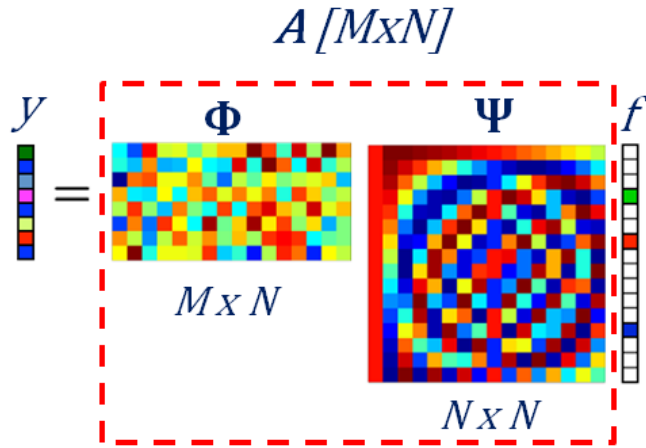


Fig. 1.4 Sensing Matrix A

### 1.5 Sparse Solution Evaluation

Even though the equations system in (1.5) is still underdetermined, the sparsity of  $f$  can be exploited to find a suitable solution [9]. More specifically, it is possible to recover  $x$  by solving the following optimization problem

$$\hat{f} = \underset{f}{\operatorname{argmin}} \|f\|_1 \quad \text{s. t. } f \in \mathcal{B}(y) \quad (1.6)$$

where  $\|\cdot\|_1$  stands for the  $l_1$ -norm (i.e. the sum of the absolute values of the  $f$  components) and  $\mathcal{B}(y)$  is a proper constraint that assures the consistence with the samples  $y$ . In particular, in the presence of noise-free samples, the feasible set  $\mathcal{B}(y)$  can be expressed as

$$\mathcal{B}(y) = \{f: Af = y\} \quad (1.7)$$

If the acquired samples have been contaminated with small amount of noise  $\epsilon$  (such as the quantization noise) a better expression would be

$$\mathcal{B}(y) = \{f: \|Af - y\|_2 \leq \epsilon\} \quad (1.8)$$

In other words, the best estimate  $\hat{f}$  of the input signal spectrum turns out to be the sparse representation characterized by the minimum  $l_1$ -norm. The use of  $l_1$ -norm grants, in fact, that obtained solution will be sparse, condition that is usually not met when least square minimization approaches are adopted. Moreover, the constraints (1.7) and (1.8) define the so-called feasible set and assure that the required estimate  $\hat{f}$  is a solution (either absolute or approximated) of the equations system (1.5).

Once the solution  $\hat{f}$  is obtained, the input signal of interest can easily be recovered by means of (1.1):

$$\hat{x} = \Psi \hat{f} \quad (1.9)$$

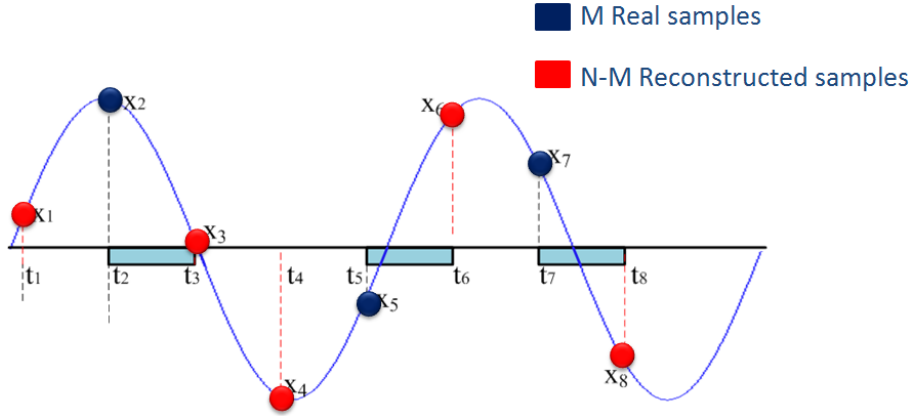


Fig. 1.5 Real and reconstructed samples

The following inequality furnishes the lower limit of the number of samples  $M$  of  $x$  to be acquired, according to the sparsity of  $x$  and the characteristics of the sampling:

$$M \geq C \cdot \mu^2(\Phi, \Psi) \cdot S \cdot \log N \quad (1.10)$$

where  $M$  is the number of measurements,  $C$  is a positive constant,  $\mu$  the coherence between the matrices  $\Phi$  and  $\Psi$ ,  $S$  the sparsity, and  $N$  the number of points to be reconstructed. The coherence is defined as the quantity:

$$\mu(\Phi, \Psi) = \sqrt{n} \max_{1 \leq k, j \leq n} |\langle \varphi_k, \psi_j \rangle| \quad (1.11)$$

and  $\varphi_k$  and  $\psi_j$  stand, respectively, for the  $k$ -th row and the  $j$ -th column of the matrices  $\Phi$  and  $\Psi$  and  $\langle \cdot, \cdot \rangle$  indicates the traditional inner product. It is clearly that the number of measurements mainly depends on the sparsity  $S$  of  $x$ , and coherence  $\mu$ . In order to exploit effectively a compressive sampling technique, a low value both sparsity  $S$  and coherence  $\mu$  has to be met. The lower their values, the fewer the samples required for a reliable reconstruction of  $f$  and consequently of the original signal  $x$ . The sparsity  $S$  depend both by a suitable choosing of the orthonormal base and the intrinsic characteristics of signal  $x$ . If  $\Phi$  and  $\Psi$  contain uncorrelated elements, the coherence is small. The minimum level of coherence is equal to 1, whereas the maximum level is  $\sqrt{N}$ . In a CS-based approach, the coherence should be as much as possible close to 1. Surprisingly, it has been demonstrated

that random matrices are largely incoherent with any fixed orthonormal bases  $\Psi$ . Thus, by selecting a random sampling matrix  $\Phi$ , it is possible to obtain a small coherence [10].

## 1.6 References

- [1] H. Nyquist, "Certain topics in telegraph transmission theory," AIEE Trans., Vol. 47, 1928.
- [2] E. J. Candès, M. B. Wakin, "An Introduction To Compressive Sampling," IEEE Signal Processing Magazine, March 2008, pp.21-30.
- [3] E. Candès, J. Romberg, and T. Tao, "Robust uncertainty principles: Exact signal reconstruction from highly incomplete frequency information," IEEE Trans. Inform. Theory, vol. 52, no. 2, pp. 489–509, Feb. 2006.
- [4] E. Candès and T. Tao, "Near optimal signal recovery from random projections: Universal encoding strategies?," IEEE Trans. Inform. Theory, vol. 52, no. 12, pp. 5406–5425, Dec. 2006.
- [5] Mesecher, D.; Carin, L.; Kadar, I.; Pirich, R., "Exploiting signal sparseness for reduced-rate sampling," Systems, Applications and Technology. IEEE Long Island, Conference, 2009. LISAT '09, pp 1-6, 2009.
- [6] E. Candès and J. Romberg, "Sparsity and incoherence in compressive sampling," Inverse Prob., vol. 23, no. 3, pp. 969–985, 2007.
- [7] D. Donoho, "Compressed sensing," IEEE Trans. Inform. Theory, vol. 52, no. 4, pp. 1289–1306, Apr. 2006.
- [8] S. Mallat, A Wavelet Tour of Signal Processing. New York: Academic, 1999.
- [9] Eldar, Y.C.; Kutyniok, G.; Compressed sensing Theory and Applications. Cambridge University Press, New York, USA, 2012.
- [10] D.L. Donoho and X. Huo, "Uncertainty principles and ideal atomic decomposition," IEEE Trans. Inform. Theory, vol. 47, no. 7, pp. 2845–2862, Nov. 2001.

## **2 Compressive Sampling Approach for the Measurement of Electrical Power Quality**

### **2.1 Introduction**

Nowadays, large scale monitoring of Power Quality (PQ) in electrical power plants is a pressing need in many countries due to both liberalization of the electrical market and deeper interconnections of electrical networks. Today, quality objectives have become more and more explicit either in the form of contracts negotiated with customers, or as definite objectives agreed with the Regulator that may even impose penalties in the case of non-observance of the PQ objectives. To meet PQ targets, it is indispensable that the interested parties agree on the method of gathering and presenting estimated data. For these reasons many standards regulate PQ disturbances by means of suitable indices[1-4].

The IEC 61000-4-30 standard [3] defines the methods for measurement and interpretation of results of PQ parameters involved in 50/60 Hz power supply systems. The considered parameters concern with power frequency, magnitude of the supply voltage, flicker, supply voltage dips and swells, voltage interruptions, transient voltages, supply voltage unbalance, voltage and current harmonics and interharmonics, mains signaling on the supply voltage and rapid voltage changes. In particular, the standard referenced in [4] suggests the realization of measurement instruments which, after a suitable synchronization pre-processing, adopt suitable Fast Fourier Transform (FFT) calculations on consecutive, and without gaps, periods of 200 ms. Let it consider a poly-phase system with neutral wire, where four currents and four voltages have to be detected, synchronized, measured and analyzed with good accuracy and spectral resolution. This means that the measurement instrument has to be able to: (i) estimate the frequency of incoming signals, (ii) change (in a digital or analog way) the sampling frequency, (ii) store and manage a large number of data; (iii) calculate in sequence or simultaneously, eight FFTs in a very short time, and (iv) detect and classify events. The compliance with [5] and [6] using the suggested synchronized FFT analysis needs processing and memory capabilities, that may limit the cost effective of the measurement solutions present on the market. Several approaches, based on alternative analysis principles, for automatic detection and classification of PQ disturbances were proposed in literature [7]-[11]. Some of them are based on time-frequency representations such as wavelet transform or short time Fourier transform, which are assisted e.g. by neural networks or fuzzy expert systems.

Methods based on pattern recognition using support vector machines are also used as useful techniques for disturbance classifications. Other approaches apply mathematical morphology and/or the calculation of the root mean square (RMS) value. Finally some methods proposed the use of digital filter based techniques [12], [13].

Taking into account what stated above, two huge requirements have to be satisfied: (i) the contemporaneously acquisition of multiple signals (up to 8) at very high data rate for a minimum time of 200 ms required by PQ standards;(ii) the use of numerical techniques with high computational burden required by the most of the presented PQ measurement methods. At the same time, it is very important to carry out a distributed monitoring of the PQ phenomena in many points of the electrical plant to detect and to isolate the distorting loads. It is evident that to allow the realization of cost effective PQ monitoring network efforts have to be done in minimizing both the memory and computational burden of PQ measurement instruments. A valuable help to deal with the considered problem is given by Compressive Sampling (CS) approach. This way, in this Chapter the applicability of compressive sampling techniques in PQ measurements is investigated. In particular, the preliminary research activities have been focused on the definition, implementation and assessment of a novel PQ measurement method, based on the compressive sampling, capable of

- i. assuring as good measurement accuracies as those required by current standards and granted by typical PQ measurement methods and instruemnts,
- ii. drastically reducing the required memory with respect to traditional measurement methods.

## **2.2 The Proposed Method**

### **2.2.1 Transformation Matrix Determination**

According to what stated in Chapter 1, a necessary condition to apply CS-based methods is that the unknown  $N$ -dimensional signal  $\mathbf{x}$  has to be sparse in a suitable orthonormal basis. For the sake of simplicity, let us consider the PQ analysis of only stationary signals. In the specific application, input signals consists of the sum of a limited number sinusoidal components (at harmonic and/or interharmonic frequency). This way, it turns out to be natural to choose the traditional DFT as transformation matrix relating the input signal  $\mathbf{x}$  with its complex spectrum  $\mathbf{f}$ . This way, the corresponding entries of the transformation matrix  $\Psi$  are defined as:

$$\psi_{i,p} = \frac{1}{\sqrt{n}} e^{j\frac{2\pi}{n}i \cdot p} \quad \forall i, p \in [0, \dots, n-1] \quad (2.1)$$

## 2.2.2 Sampling Matrix Determination

In order to assure a low level of coherence, a sampling random matrix has to be adopted to obtain  $M$  measurements  $\mathbf{y}$  from the unknown input signal  $\mathbf{x}$ . A simple random matrix can be obtained by randomly deleting  $N-M$  rows from the square identity matrix  $\mathbf{I}$  (obtaining, thus, a rectangular sampling matrix having  $M \times N$  size). This is equivalent to perform a non uniform sampling of  $M$  samples in the considered observation interval.

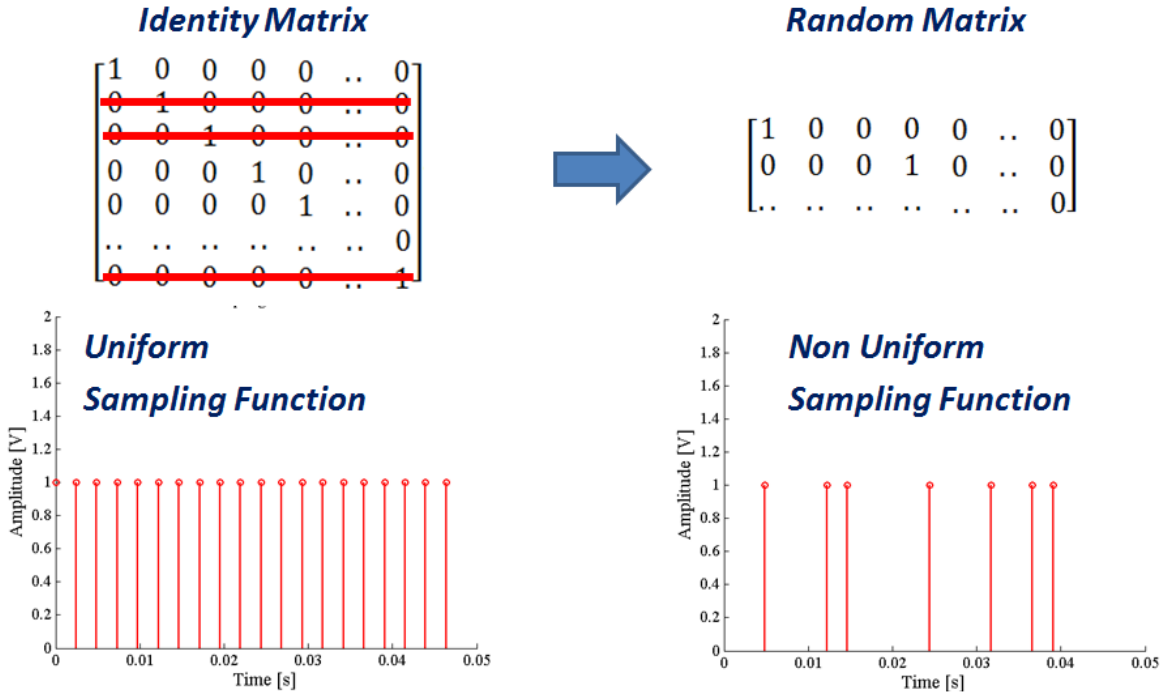


Fig. 2.1 Random matrix obtained by randomly deleting  $N-M$  rows from the square identity matrix  $\mathbf{I}$ .

For the sake of the clarity, let us assume to be interested in recovering an 8-samples input signal  $\mathbf{x}$  from 3 samples  $\mathbf{y}$  acquired in time domain. The equations system (1.2) can be rewritten as

$$\begin{bmatrix} y(0) \\ y(1) \\ y(2) \end{bmatrix} = \begin{bmatrix} 1 & 0 & 0 & 0 & 0 & 0 & 0 & 0 \\ 0 & 0 & 0 & 0 & 1 & 0 & 0 & 0 \\ 0 & 0 & 0 & 0 & 0 & 0 & 0 & 1 \end{bmatrix} * \begin{bmatrix} x(0) \\ x(1) \\ \dots \\ x(6) \\ x(7) \end{bmatrix} = \begin{bmatrix} x(0) \\ x(4) \\ x(7) \end{bmatrix} \quad (2.2)$$

### 2.2.3 Sensing Matrix Determination

Thanks to the specific choice of the sampling matrix, the matrix  $\mathbf{A}$  can be generated as a submatrix of  $\Psi$ , thus reducing the computational burden of the method, since  $\mathbf{A}$  doesn't have to be calculated from actual multiplications. It is, in fact, evaluated as the rows of the matrix  $\Psi$ , whose indexes match those the sampling instants  $k_i$ , thus granting its possible implementation also on devices characterized by reduced memory depth. With reference to the sampling matrix in (2.2), the corresponding sensing matrix is given by

$$\mathbf{A} = \begin{bmatrix} \frac{1}{\sqrt{8}} & \frac{1}{\sqrt{8}} & \dots & \frac{1}{\sqrt{8}} \\ \frac{1}{\sqrt{8}} & \frac{1}{\sqrt{8}} e^{j\frac{2\pi}{8}4} & \dots & \frac{1}{\sqrt{8}} e^{j\frac{2\pi}{8}28} \\ \frac{1}{\sqrt{8}} & \frac{1}{\sqrt{8}} e^{j\frac{2\pi}{8}7} & \dots & \frac{1}{\sqrt{8}} e^{j\frac{2\pi}{8}49} \end{bmatrix} \quad (2.3)$$

### 2.2.4 Input Signal Recovering

Once determined the matrix  $\mathbf{A}$ , the spectrum of the input signal can be obtained by finding the sparse sequence  $\hat{\mathbf{f}}$  that is solution of the equation system (1.5) and characterized by the minimum  $l_1$ -norm. The estimated input signal  $\hat{\mathbf{x}}$  can thus be evaluated according to (1.9) and the obtained reconstruction is characterized by a resolution in time domain equal to

$$\frac{T_W}{N} \quad (2.4)$$

where  $T_W$  is the observation time interval and  $N$  is the number of sample of the reconstructed input signal  $\hat{\mathbf{x}}$ . Once obtained the time domain evolution of the signal of interest, the desired value of voltage is achieved by evaluating the RMS value of the reconstructed signal.

## 2.3 Numerical results

In order to preliminarily assess the performance of the proposed method, a number of tests were carried out by means of numerical simulations. With regard to the signal reconstruction, as for the successive numerical and experimental tests performed in the research activity, a free-tool (namely CVX by CVX Research [14] and working in MATLAB<sup>TM</sup> environment) has been adopted for the solution of convex optimization problem associated with (1.5). As an

example, an input signal has been generated according to the parameters shown in Table 1; acquisition parameters have been set according to those provided by Fluke 1760 [15].

Table 1- Signal and acquisition parameters

Samples number $n$	2048
Sampling rate [kSa/s]	10.24
Carrier frequency [Hz]	50
Max Harmonic order	40
Acquired samples $m$	200
Vertical resolution [bit]	14

With regard to the harmonic content, the amplitude of each component has randomly been set in the interval from 0% up to 5%. Fig. 2.2 shows the original signal along with the  $m$  samples acquired for its reconstruction by means of CS.

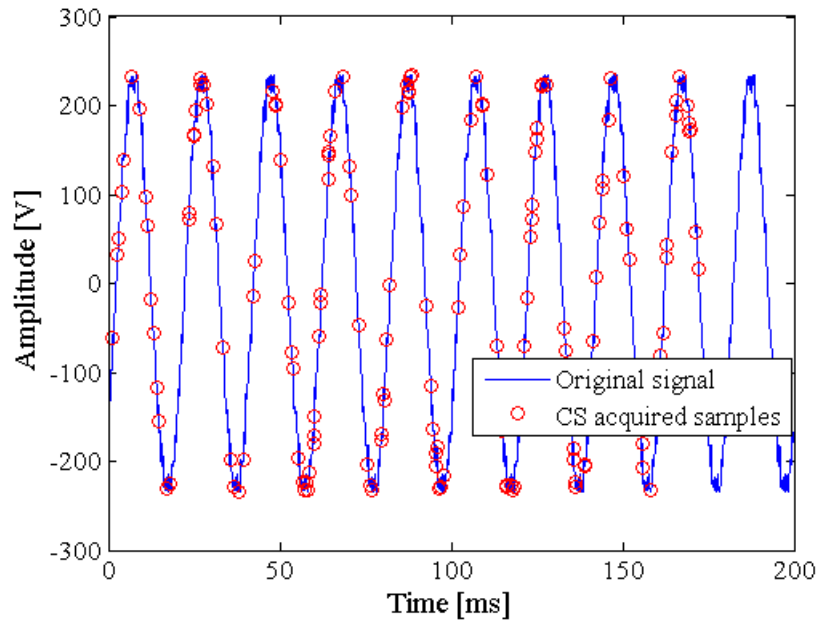


Fig. 2.2 Example of signal acquired according to the CS paradigm.

The results obtained by means of the proposed method are given in Fig.2.3, where the remarkable concurrence between original and reconstructed spectrum of the input signal can be noticed. The difference between nominal and estimated RMS voltage equal to 0.06% confirms the efficacy of the method and suggest its use for the implementation of an embedded meter whose specification would be very close to that granted by Fluke 1760.

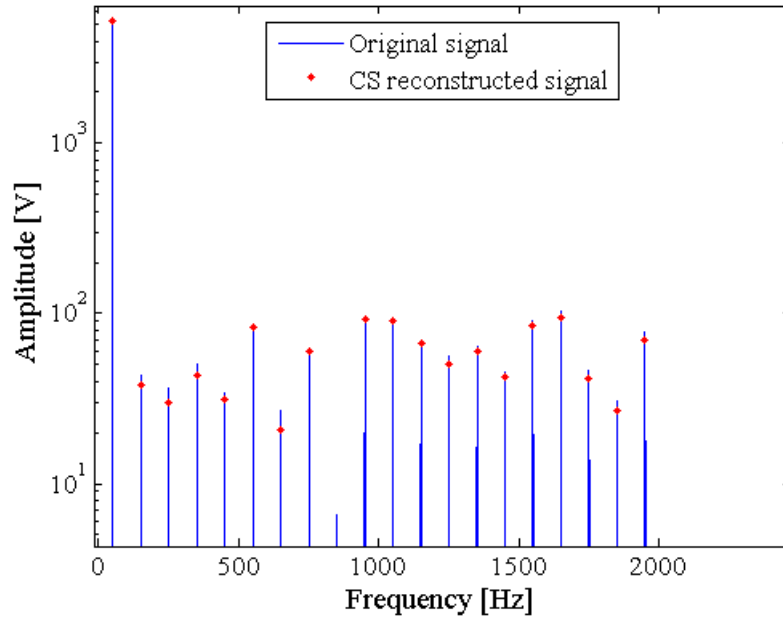


Fig. 2.3 Original (blue) and reconstructed (red dots) spectrum.

To better appreciate the capability of the method, Fig.2.4 and Fig.2.5 show the reconstructed signal along with the amplitude difference with respect to the original signal.

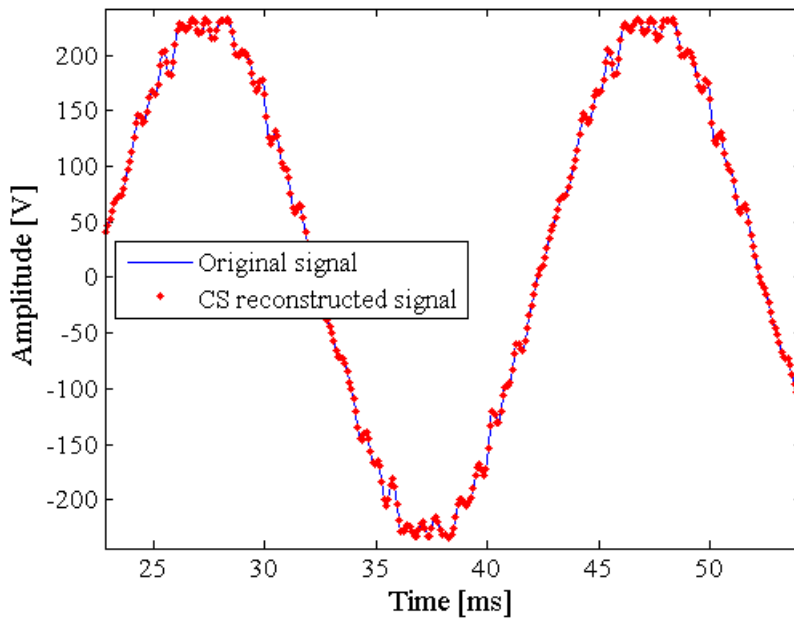


Fig. 2.4 Original and reconstructed signal.

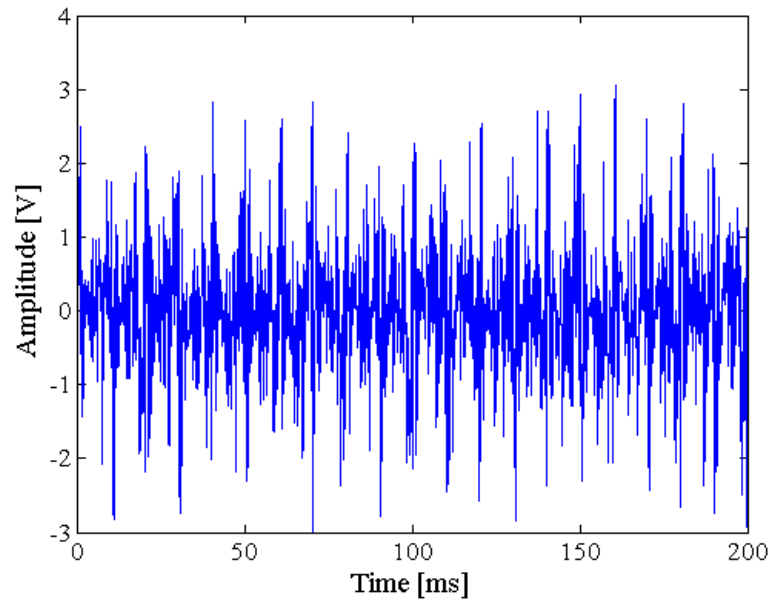


Fig. 2.5 Amplitude difference between original and reconstructed signal.

To further investigate the capabilities of the method, the evolution of the difference between estimated and nominal rms voltage has been measured versus different values of number of acquired samples and normalized bandwidth (Fig.2.6). The input signal is characterized by the same frequency of the previous example; the same guard interval has also been taken into account. As it can be noticed, the higher the number of acquired samples, the better the associated power estimate, whatever the spectral content of the considered signal. Nevertheless, a defined region characterized by the best performance (difference lower than 0.1%) can be highlighted.

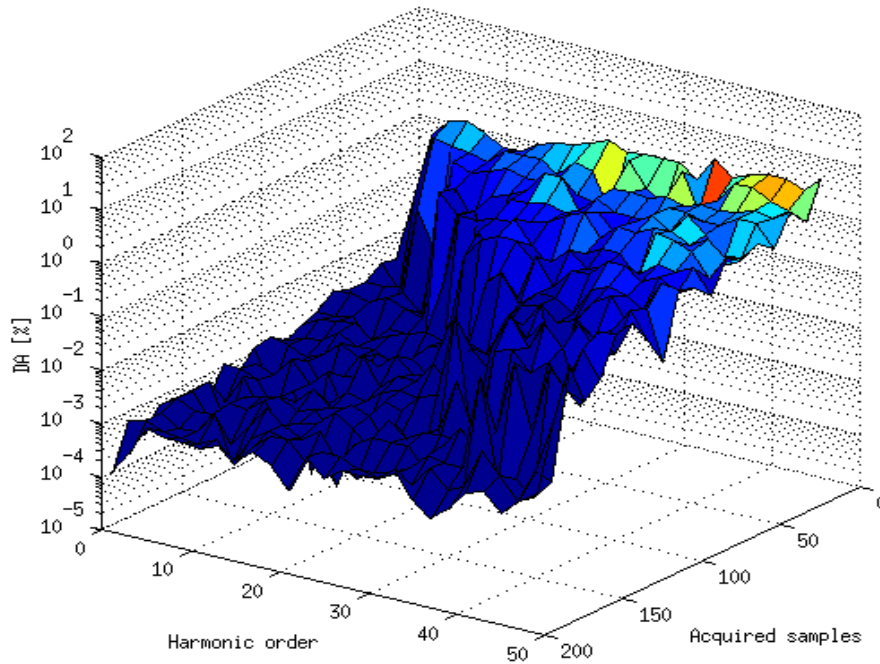


Fig.2.6 Evolution of the difference between estimated and nominal RMS voltage versus the number of acquired samples and harmonic order

## 2.4 Conclusions

The first steps of the research was activities focused of the definition of a new measurement method based on compressive sampling techniques for Power Quality measurements. In particular, the suitability of the method at measuring the RMS voltage of signal characterized by different levels of harmonic distortion has been assessed. Thanks to the attractive properties of CS, it has been possible to reconstruct signals of interest from a very limited number of samples (down to 20 random samples for pure sinusoidal tones). In other words, it has been proved that by using a compressive sampling approach, a notably reduction of the required memory depth, to perform long-time analysis, has been obtained. Several tests conducted on numerical signals showed the promising results granted by the method; differences between estimated and nominal RMS value never greater than 0.01% also in the presence of severe harmonic distortion if the suitable number of samples are taken.

## 2.5 References

[1] *IEEE Recommended Practice for Monitoring Electric Power Quality*, IEEE Standard

- 1159, 1995.
- [2] *IEEE Recommended Practices and Requirements for Harmonic Control in Electrical Power System*, IEEE Standard 519, 1992.
  - [3] *Electromagnetic Compatibility - Testing and Measurement Techniques – Power Quality Measurement Methods*, International standard IEC 61000-4-30, 2003.
  - [4] *Electromagnetic Compatibility - Testing and Measurement Techniques – General Guide on Harmonics and Interharmonics Measurements and Instrumentation, for Power Supply Systems and Equipment Connected thereto*, International standard IEC 61000-4-7.
  - [5] M.Aiello, A.Cataliotti, V.Cosentino and S.Nuccio, "Synchronization Techniques for Power Quality Instruments," *IEEE Trans. Instr. Meas.*, vol. 56, no. 5, pp. 1511-1519, Oct. 2007.
  - [6] A.Bracale, G.Carpinelli, Z.Leonowicz, T.Lobos, J.Rezmer, "Measurement of IEC Groups and Subgroups using Advanced Spectrum Estimation Methods," *IEEE Trans. Instr. Meas.*, vol. 57, no. 4, pp. 672-681, Apr. 2008.
  - [7] B.Perunicic, M.Mallini, Z.Wang, Y.Liu, "Power quality disturbance detection and classification using wavelets and artificial neural networks," *Proc. of 8th International Conference on Harmonics And Quality of Power*, vol. 1, 1998, pp. 77-82.
  - [8] E.Styvaktakis, M. H. J.Bollen, I. Y. H.Gu, "Automatic Classification of Power System Events Using RMS Voltage Measurements," *Power Engineering Society Summer Meeting*, vol. 2, 2002, pp. 824-829.
  - [9] A. M.Gaouda, S. H.Kanoun, M. M. A.Salama, A. Y.Chikhani, "Pattern Recognition Applications for Power System Disturbance Classification," *IEEE Trans. Power Del.*, vol. 17, no. 3, pp. 677-683, July 2002.
  - [10] F. F. Zhu, G. S. Hu, J. Xie, "Classification of power quality disturbances using wavelet and fuzzy support vector machines," in *Proc. 4th International Conference on Machine Learning and Cybernetics*, vol. 7, 2005, pp. 3981-3984.
  - [11] P.K.Dash, M.V.Chilukuri, "Hybrid S-Transform and Kalman Filtering Approach for Detection and Measurement of Short Duration Disturbances in Power Networks," *IEEE Trans. Instr. Meas.*, vol. 53, no. 2, pp. 588-596, Apr. 2004.
  - [12] L. Ferrigno, C. Landi, M. Laracca, C. Luongo, "A Study on the Feasibility and Effectiveness of a Digital Filter Approach for Harmonic and Interharmonic Measurements in Compliance with IEC 61000-4-7", *Metrology and Measurement Systems International*

Journal, Vol. XIV, N°4, pp. 577-593, Dicembre 2007.

- [13] L. Ferrigno, C. Landi, M. Laracca, "FPGA-based Measurement Instrument for Power Quality Monitoring according to IEC Standards", IEEE International Instrumentation and Measurement Technology Conference, I2MTC 2008, Victoria, Vancouver Island, Canada, 12-15 Maggio 2008.
- [14] S. Boyd, and L. Vandenberghe, *Convex Optimization*, Cambridge University Press, 2004. (available at <http://www.stanford.edu/~boyd/cvxbook/>).
- [15] "Fluke 1760 Three-Phase Power Quality Recorder Topas," Fluke Literature, Technical Data, Note 2635073 D-EN-N Rev B, 2006.

## **3 Multi-channel Simultaneous Data Acquisition Systems.**

### **3.1 Introduction**

In most of the Power Quality applications, the monitoring networks can be thought as the connection of wireless cost-effective and tiny nodes, which have to cooperate in order to perform measurement, processing, control and communication tasks. To better appreciate the meaning of concepts as “cost-effective” and “tiny”, it has to be considered that, if no compliance is needed, the cost of each wireless node, involving sensing, data acquisition system (DAS), processing unit and radio communication blocks, has to be lower than few euros. To this aim, hardware platforms as low-cost microcontrollers, field programmable gate arrays (FPGAs) with a reduced number of gates, or cheap digital signal Processors (DSPs) are frequently taken into account. All of them integrate most of the abovementioned blocks in a single chip allowing cost-effective realization of measurement nodes; however, limited hardware resources, in terms of internal memory depth and number of available analog-to-digital converters (ADCs), generally characterize them. The considered platforms can, in fact, scarcely store more than few tens of kilobytes of data, and typically adopt multiplexers to share different physical channels over the same ADC.

To accomplish the measurement tasks, long time intervals are usually observed and, consequently, acquisition, storage and transmission of a great number of samples is involved; moreover, problems related to time base errors have to be taken into account [1], not to mention EMC issues presented by the acquisition system [2]. Unfortunately, the associated hardware requirements clash with the typical features of the considered platforms as well as with the “cost-effective” and “tiny” issues.

To face the considered problem, new acquisition and processing strategies, capable of reducing hardware requirements of the nodes and allowing reliable measurements to be carried out, have recently been proposed in literature. One of the most promising technique is the Compressive Sampling (CS) [3]-[5]. The application of CS drastically reduces the number of acquired, stored, processed and transmitted information data, making it reliable the adoption of the considered low-cost hardware platforms for the above-mentioned applications.

Moreover, in most of PQ applications, the measurement node is required to simultaneously acquire a number of quantities (e.g. voltage and current acquisition for smart metering applications). This requirement cannot be met on most of the considered platforms, since, as stated above, they multiplex input physical channels to reduce the cost of the ADC section (i.e. one of the most expensive), thus allowing only sequential data acquisition to be performed. Therefore, overall measurement performance is limited, because an unwanted phase displacement turns out to be imposed on the acquired signals. This phase shift is mainly due to the inter-channel delay the multiplexer spends to acquire two samples on different channels, and proves to be a deep constraint that typically reduces the applicability of low-cost measurement nodes.

Although many studies can be found in scientific literature concerning with the application of CS to measurement applications (in particular, to WSNs), the attention has been generally paid to aspect as memory management, energy consumption, and communication optimizations [6],[7] or single channel implementation of acquisition strategies [8], [9]. Examples of multi-channel DASs based on CS are also present in the literature [10]; however, most of them requires hardware modifications to be implemented. Finally, the effect of the CS on the phase shift of the acquired signals due to the inter-channel delay in multichannel platforms has to be yet deeply investigated. In this chapter a novel acquisition approach, based on CS, capable of carrying out multichannel simultaneous data acquisition also through inherently sequential DASs is presented. To this aim, the approach exploits a unique time-basis for all the input channels adopted, along with a compressive random sampling, in order to assure the reconstruction of desired signals without any artefact due to the inter-channel delay and/or sequential acquisition scheme.

### ***3.2 The Proposed CS-based Acquisition Approach***

Taking advantage of some attractive features of CS theory, a new sampling method based on the application of the CS is proposed with the aim of realizing low-cost multi-channel simultaneous DASs, capable of overcoming the limitations due to their inherent multiplexed architecture in cost effective hardware platform as microcontrollers or FPGAs. The generality of the proposed method allows it to be able of working with success whatever the number of considered input channels. For the sake of the clarity, it is described with references to an application example, which involves a DAS consisting of four independent input channels

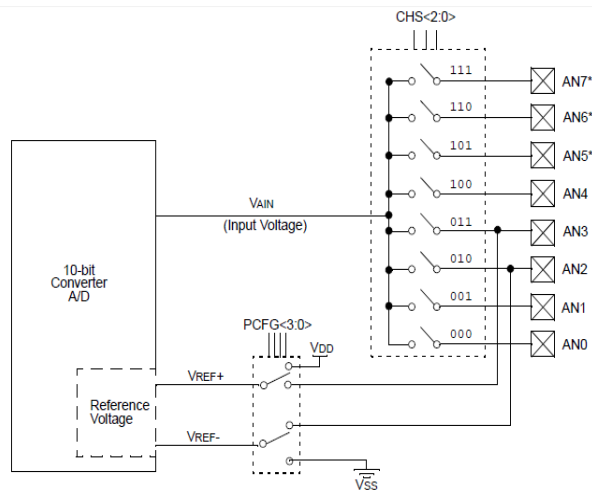


Fig.3.1 Typical DAS architecture of low cost devices,

multiplexed on a single ADC. The multiplexed structure of the ADC imposes that the acquisition of the same signal on the four channels turns out in four digitized waveforms, whose channel to channel phase shifts are mainly due to the sampling interval and inter-channel delay. In particular, the higher the frequency of the input signal, the lower the sampling interval, and the worse the associated phase shift among the channels due to the presence of the inter-channel delay. This is a very important consideration since the deeper worsening in the channel to channel phase reconstruction are obtained when the sampling frequency increases and when the user expects to have more resolution and accuracy on the acquired signal.

#### A. Problem statement

The traditional sequential acquisition scheme adopted by most of the available low-cost embedded systems is shown in Fig.3.1. Several input channels (sometimes up to 64) can exploit a very limited number of sampling and analog-to-digital-conversion blocks (usually not greater than 4), thus making it necessary to multiplex the data acquisition stage among the different channels (as an example, Fig.3.1 shows the considered problem with reference to eight input channels multiplexed on a single ADC). Such a condition gives rise to drawbacks that can be harmful for some applications; in particular:

1. the lowest available sampling interval grows, thus reducing the bandwidth of the signals that can be acquired and measured according to the traditional sampling

theorem. With reference to Fig.3.2, the minimum allowed sampling interval  $T_{sAct}$  is, in fact, equal to

$$T_{sAct} = n_{Chan}(T_s + T_{id}) \quad (3.1)$$

where  $T_s$  indicates the sampling time, i.e. the time interval required to complete the operations of acquisition and analog-to-digital conversion of a single sample,  $T_{id}$  stands for the interchannel delay (i.e. the time interval needed by the hardware to change the input channel connected with the ADC) and  $n_{Chan}$  is the number of active input channels.

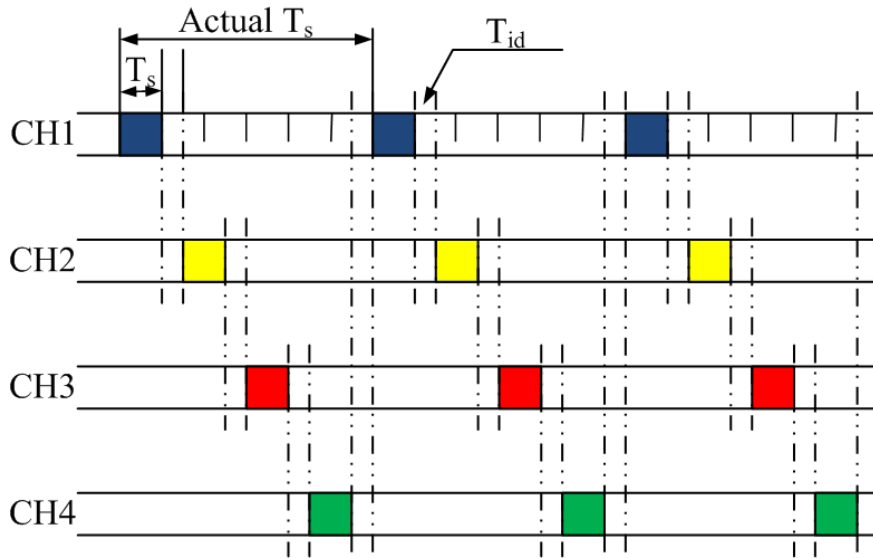


Fig.3.2. Sequential data acquisition involving different physical channels.

2. even though the available sampling period would be sufficient for assuring an alias-free sampling of the desired input signals, the sequential acquisition scheme introduces an artificial phase shift (equal to  $2\pi f_x(T_s + T_{id})$ ) in consecutive channels in the acquisition sequence,  $f_x$  being the frequency of the input signal). The considered phase shift could distort some measurement results (as an example, active power measurement in Power Quality applications); the higher the frequency of the input signal, the worse the effect of the considered phase shift.

Moreover, the limited resources usually available in terms of memory depth do not allow the acquisition of long sequences of samples when several input channels are involved. As an example, even though the dimension of the random access memory of embedded devices have been increasing in recent years, only a few of them allow a real time acquisition of 16-bit

sample sequences longer than 5 kSamples if the number of input channels is equal or greater than 4.

To overcome the considered drawbacks, hereinafter it is presented a suitable acquisition approach based on compressive sampling in order to make it possible to carry out multi-channel simultaneous data acquisition also in the presence of an inherently sequential DAS. From an operating point of view (Fig.3.3), a unique, common time-basis, whose period is equal to  $T_s$ , is exploited to set the sampling instants on the different channels; the instants are defined according to the CS theory and randomly determined (as stated in the successive Section). Even though the channels order in the acquisition sequence could in principle be randomly chosen (thus improving the performance in terms of randomness and matrices incoherence), it is here considered sequential, without loss of generality.

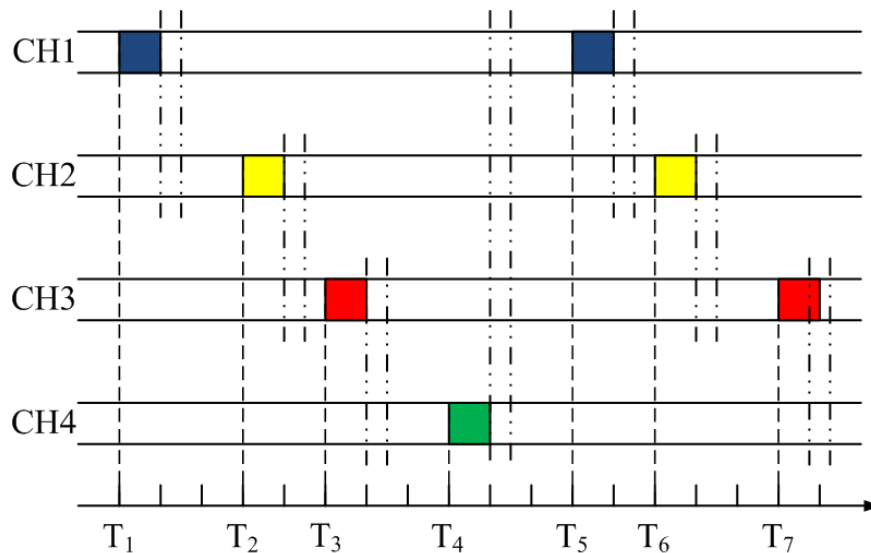


Fig.3.3. Proposed data acquisition approach involving different physical channels.

As it can be appreciated in Fig.3.3, the only constraint for the proposed approach to work with success is that the time interval between two successive sampling instants should be greater than  $T_{id}$ . The considered strategy generates the following advantages:

- thanks to the “compressive” approach, it is possible to acquire a limited number of samples for each channel, and successively reconstruct the signals of interest, whose dimensions could be greater than the available memory depth of the device;

- the adopted time-basis allows the reconstruction of the input signals on the different channels as they were simultaneously acquired, being both the starting time of reconstruction and reconstruction/sampling period  $T_s$  common.

### 3.3 CS-based simultaneous data acquisition

#### ➤ Sampling instants selection

Let us suppose that each input signal can suitably be reconstructed through  $m \ll n$  samples, according to CS approach; this way, four times  $m$  samples have to be digitized for all the channels. A traditional random number generator can be adopted in order to set the sequence of sampling instants indices  $s_j$  (with  $j=1, \dots, 4m$ ), i.e. the multiples of the common sampling period  $T_s$  adopted for signal reconstruction ( $T_j = s_j T_s$  in Fig.3.3). According to the acquisition approach presented in Fig.3.3, the sampling matrix can be arranged to have  $4m$  rows and  $n$  columns, as shown in Fig.3.4 where  $y \in \mathbb{R}^{4m}$ ,  $\Phi \in \mathbb{R}^{4m \times n}$ , and  $x_1, x_2, x_3$  and  $x_4 \in \mathbb{R}^n$ , are the input signals connected to each of the four channels. As for the entries of the matrix, for each row only one element, whose column index is equal to the associated sampling instant index  $s_j$ , is different from zero and equal to one. This way, the vector  $y$  contains the interleaved samples acquired on all the input signals. To suitably reconstruct the associated input signals, the entries of  $y$  have to be reordered and separated in four sequences, referred to as  $y_1, y_2, y_3$  and  $y_4 \in \mathbb{R}^m$ . Moreover, starting from the whole sampling matrix  $\Phi \in \mathbb{R}^{4m \times n}$ , four different matrices  $\Phi_i \in \mathbb{R}^{m \times n}$  (one for each channel) can be attained in a similar way.

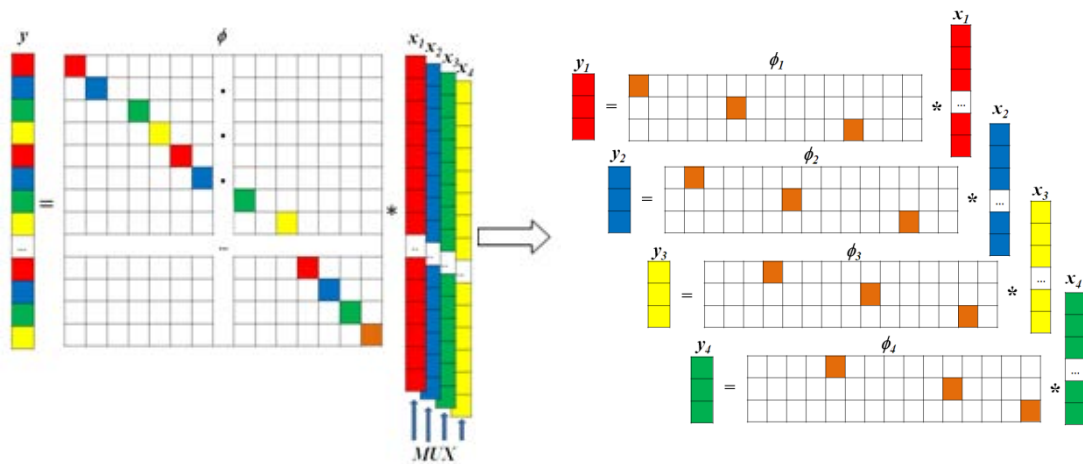


Fig.3.4. CS implementation: the sampling matrix is iteratively applied to the signals acquired on the different channels.

➤ **Optimal generation of the transformation matrix and input signals reconstruction**

The sequence of acquired samples for each input signal can be expressed in terms of the sparse representation of  $x_i$

$$y_i = \Phi_i \cdot \Psi \cdot f_i \quad (3.2)$$

With regard to the transformation matrix  $\Psi$ , it has to be chosen according to specific features both of the input signal and sampling matrix; in particular, an orthonormal basis capable of simultaneously assuring the lowest value of (i) transformed signals sparsity and (ii) coherence with the sampling matrices has to be preferred. For the application considered in the research activity,  $\Psi$  is calculated according to the aforementioned discrete Fourier transform rules, under the assumption of stationary and periodic signals (i.e. characterized by sparse representation in the frequency domain) in the observation interval. A new matrix, referred to as sensing matrix  $\mathbf{A}_i$ , can be determined by applying the following expression

$$\mathbf{A}_i = \Phi_i \cdot \Psi \quad (3.3)$$

This way, in order to reconstruct the sparse signal  $f$ , the following equation system has to be solved

$$\mathbf{y}_i = \mathbf{A}_i \cdot \mathbf{f}_i \quad (3.4)$$

Thanks to the particular choice of the sampling matrix  $\Phi_i$ , the sensing matrix  $\mathbf{A}_i$  turns out to be a submatrix of  $\Psi$ ; this way, the computational burden of the method is reduced since the matrix  $\mathbf{A}_i$  is not real-time calculated through a pure multiplication, but it is evaluated as the rows of the discrete Fourier transform matrix, whose indexes are equal to those of the sampling instants. In other words, each  $\mathbf{A}_i$  is obtained randomly selecting  $n$  rows from the  $N \times N$  discrete Fourier transform  $\Psi$ .

According to what stated above, after determining the matrix  $\mathbf{A}_i$ , the spectrum of the input signal can be obtained by finding the sparse sequence  $\hat{f}_i$  that solves the equation system (3.4) and is characterized by the minimum  $l_1$ -norm. The estimated input signal  $\hat{x}_i$  can thus be evaluated according to (3), and the obtained reconstruction is characterized by a resolution in the time domain equal to  $T_s$ .

It is worth noting that, thanks to the proposed approach, it is possible to reconstruct the input

signal on each channel in such a way that all channels have a common, unique time base. This way, no phase shift due to the inter-channel delay is introduced, to the detriment of the computational burden.

### 3.4 Numerical results

A number of numerical tests have been conducted to preliminarily verify the capability of the proposed method in overcoming the inherent limitations of multiplexed acquisition architecture. To this aim, a DAS, involving 4 physical channels and equipped with only one ADC, has been simulated; a channel period  $T_s$  (including the time needed to sample, convert and change channel) always equal to  $2 \mu\text{s}$  has been considered (corresponding to an equivalent sample rate of 500 kS/s). The sequence of sampling instants have been generated through a traditional pseudo-random number generator and the obtained sequence has been divided for each channel according to what stated in Section 2.3 to set the corresponding  $m$  random samples. This way, 4 physical channels connected to the same input signal have been simulated.

With regard to the signal reconstruction, as for the successive experimental tests, a free-tool (namely CVX by CVX Research [11] and working in MATLAB<sup>TM</sup> environment) has been adopted for the solution of convex optimization problem associated with (17). Signals have been reconstructed in such a way as to cover an observation interval equal to 2 ms; in other words, the number  $n$  of samples of the final reconstruction has been set equal to 1000. Their phase has been evaluated in the frequency domain, and the phase shift  $\Delta\varphi_i$  ( $i = 2,3,4$ ) between the signal reconstructed for the  $i$ -th channel and that reconstructed for the first channel, taken as reference, has been calculated. As expected, the lower the magnitude of  $\Delta\varphi_i$ , the better the capability of the proposed method of exploiting the simulated sequential DAS as a simultaneous one. Moreover, the availability of the nominal input signal has allowed the evaluation of the so-called reconstruction error according to the traditional expression:

$$\varepsilon_i = \frac{\|\hat{x}_i - x_i\|_2}{\|x_i\|_2} 100 \quad (3.5)$$

and, consequently, the assessment of the capability of the proposed approach of correctly reconstructing the signal of interest.

Even though the past experiences ([12],[13]) proved that the proposed approach works with success in the presence of any periodic signal, for the sake of simplicity only sinusoidal

signals have been taken into account in all the conducted tests. According to the general CS theoretical framework, the proposed approach, in fact, assures reliable results as long as the constraint on the number of acquired samples  $m$  and the spectral content (i.e. the sparsity of the input signal in frequency domain) is met.

A first set of tests has aimed at assessing the performance of the proposed method in the best operating conditions, i.e. no noise has been added to the input signal and no quantization of the acquired samples has been considered. The maximum  $\Delta\varphi_i$  and  $\varepsilon_i$  achieved in each test configuration (characterized by different values of  $m$ , varying within the interval 20-100, and signal frequency  $f_x$ , varying within the interval 500-50000 Hz) have been adopted as performance factors. The obtained results are shown in Tab.I. As it can be appreciated, the proposed method has assured a complete “synchronization” of the four input channels; phase shifts never greater than  $9.3 \cdot 10^{-10}$  rad have, in fact, been experienced. Negligible values of  $\varepsilon$ , experienced throughout the tests, corroborates the satisfying results.

Tab.I. Maximum phase shifts and reconstruction errors, expressed respectively in radians and relative percentage terms, for different values of  $m$  and  $f_x$ .

$f_x$ [Hz] $m$	500	1000	5000	10000	50000	
20	$6.3 \cdot 10^{-10}$	$9.3 \cdot 10^{-10}$	$5.1 \cdot 10^{-11}$	$7.2 \cdot 10^{-12}$	$3.9 \cdot 10^{-11}$	$\Delta\varphi$
	$3.0 \cdot 10^{-7}$	$2.0 \cdot 10^{-7}$	$9.6 \cdot 10^{-8}$	$6.4 \cdot 10^{-8}$	$1.1 \cdot 10^{-8}$	$\varepsilon$
40	$-7.0 \cdot 10^{-11}$	$4.6 \cdot 10^{-10}$	$2.8 \cdot 10^{-12}$	$4.8 \cdot 10^{-11}$	$7.5 \cdot 10^{-10}$	$\Delta\varphi$
	$5.2 \cdot 10^{-8}$	$2.5 \cdot 10^{-7}$	$8.3 \cdot 10^{-8}$	$7.4 \cdot 10^{-8}$	$1.4 \cdot 10^{-7}$	$\varepsilon$
60	$1.8 \cdot 10^{-10}$	$8.7 \cdot 10^{-12}$	$1.9 \cdot 10^{-11}$	$-1.2 \cdot 10^{-11}$	$2.4 \cdot 10^{-10}$	$\Delta\varphi$
	$2.3 \cdot 10^{-7}$	$5.4 \cdot 10^{-8}$	$1.0 \cdot 10^{-8}$	$3.5 \cdot 10^{-8}$	$3.9 \cdot 10^{-8}$	$\varepsilon$
80	$-1.1 \cdot 10^{-11}$	$2.4 \cdot 10^{-11}$	$-9.6 \cdot 10^{-12}$	$3.1 \cdot 10^{-10}$	$-3.9 \cdot 10^{-11}$	$\Delta\varphi$
	$1.3 \cdot 10^{-8}$	$3.8 \cdot 10^{-8}$	$1.7 \cdot 10^{-8}$	$1.4 \cdot 10^{-7}$	$1.8 \cdot 10^{-7}$	$\varepsilon$
100	$1.3 \cdot 10^{-13}$	$9.9 \cdot 10^{-13}$	$3.4 \cdot 10^{-12}$	$-5.6 \cdot 10^{-11}$	$1.3 \cdot 10^{-10}$	$\Delta\varphi$
	$1.3 \cdot 10^{-9}$	$2.3 \cdot 10^{-9}$	$1.3 \cdot 10^{-8}$	$5.2 \cdot 10^{-8}$	$1.5 \cdot 10^{-8}$	$\varepsilon$

The effect of the quantization on the method's performance has then been analyzed; to this aim, different vertical resolutions ( $nBit$ ), within the interval 6-14 bit, have been taken into account. In each executed simulation, the amplitude and frequency of the input signal have been equal respectively to the converter full scale ( $2^{nBit-1}$ ) and 5 kHz. As expected, the higher

the value of  $nBit$ , the better the performance of the method (Tab.II). Moreover, satisfying results have been granted also for a higher number of random samples, to the detriment of the computational burden. As an example, signals reconstructed from 100 random samples, digitized by means of a 6-bit ADC, have been very close to those reconstructed from a lower number of samples (up to 60), digitized by means of a 10-bit ADC.

Tab.II. Maximum phase shifts and reconstruction errors, expressed respectively in radians and relative percentage terms, for different values of  $m$  and  $nBit$ .

$nBit$ $m$	6	8	10	12	14	
20	0.0039	0.0012	0.00027	$5.8 \cdot 10^{-5}$	$4.67 \cdot 10^{-5}$	$\Delta\varphi$
	1.3	0.36	0.11	0.020	0.014	$\varepsilon$
40	0.0011	0.00042	0.00030	$-9.0 \cdot 10^{-6}$	$5.5 \cdot 10^{-6}$	$\Delta\varphi$
	0.89	0.22	0.053	0.011	0.0034	$\varepsilon$
60	0.0016	-0.00066	$-6.5 \cdot 10^{-5}$	$1.0 \cdot 10^{-5}$	$-2.3 \cdot 10^{-6}$	$\Delta\varphi$
	0.68	0.17	0.043	0.0096	0.0028	$\varepsilon$
80	0.00099	$6.61 \cdot 10^{-5}$	0.00010	$2.3 \cdot 10^{-5}$	$5.97 \cdot 10^{-7}$	$\Delta\varphi$
	0.68	0.11	0.039	0.0080	0.0028	$\varepsilon$
100	0.00062	-0.00013	$8.4 \cdot 10^{-5}$	$9.4 \cdot 10^{-6}$	$-2.7 \cdot 10^{-6}$	$\Delta\varphi$
	0.44	0.093	0.027	0.0064	0.0019	$\varepsilon$

To investigate the effect of randomness in sample selection, further tests have been conducted considering a 12-bit ADC; in particular, the same values of number of samples and signal frequency as in the first tests have been considered. Moreover, for each couple  $m$  and  $f_x$ , 100 simulations have been carried out by randomly varying the sequence of sampling instants; the mean and experimental standard deviation of the phase shift are given, respectively, in Tab.III and Tab.IV. Mean values of  $\Delta\varphi$  never greater than  $1 \cdot 10^{-5}$  rad have assured an unbiased reconstruction of the input signals, i.e. no phase artifact due to the application of the proposed approach has been introduced. With regard to the experimental standard deviation, it decreases upon the increasing of the number of acquired samples. Moreover, as it can be appreciated in Tab.IV, it decreases upon the increasing of the frequency; the reason of this behavior has to be found in the growing number of signal periods included in the observation

interval, that helps the phase estimation process in a similar way as in other traditional reconstruction algorithms (e.g. time domain sine-fit).

Tab.III. Mean phase shift, expressed in radians, for different values of  $m$  and  $f_x$ .

$f_x$ [Hz] $m$	500	1000	5000	10000	50000
20	$2.4 \cdot 10^{-6}$	$-2.1 \cdot 10^{-6}$	$-8.2 \cdot 10^{-6}$	$9.3 \cdot 10^{-6}$	$1.7 \cdot 10^{-6}$
40	$-1.2 \cdot 10^{-6}$	$7.5 \cdot 10^{-6}$	$8.5 \cdot 10^{-6}$	$-2.5 \cdot 10^{-6}$	$-2.6 \cdot 10^{-7}$
60	$-1.2 \cdot 10^{-7}$	$-5.7 \cdot 10^{-7}$	$5.1 \cdot 10^{-6}$	$-1.9 \cdot 10^{-7}$	$1.6 \cdot 10^{-11}$
80	$7.4 \cdot 10^{-7}$	$-1.8 \cdot 10^{-7}$	$-1.8 \cdot 10^{-6}$	$1.1 \cdot 10^{-6}$	$2.7 \cdot 10^{-12}$
100	$-9.6 \cdot 10^{-6}$	$5.4 \cdot 10^{-6}$	$7.3 \cdot 10^{-7}$	$6.5 \cdot 10^{-7}$	$-8.6 \cdot 10^{-10}$

Tab.IV. Experimental standard deviation of the phase shift, expressed in radians, for different values of  $m$  and  $f_x$ .

$f_s$ [Hz] $m$	500	1000	5000	10000	50000
20	$8.7 \cdot 10^{-5}$	$8.2 \cdot 10^{-5}$	$6.7 \cdot 10^{-5}$	$4.5 \cdot 10^{-5}$	$3.8 \cdot 10^{-5}$
40	$4.7 \cdot 10^{-5}$	$5.3 \cdot 10^{-5}$	$4.1 \cdot 10^{-5}$	$4.1 \cdot 10^{-5}$	$2.6 \cdot 10^{-6}$
60	$4.1 \cdot 10^{-5}$	$4.0 \cdot 10^{-5}$	$2.9 \cdot 10^{-5}$	$2.3 \cdot 10^{-5}$	$2.7 \cdot 10^{-10}$
80	$4.2 \cdot 10^{-5}$	$3.1 \cdot 10^{-5}$	$1.8 \cdot 10^{-5}$	$1.1 \cdot 10^{-5}$	$8.8 \cdot 10^{-11}$
100	$2.9 \cdot 10^{-5}$	$2.8 \cdot 10^{-5}$	$1.6 \cdot 10^{-5}$	$5.2 \cdot 10^{-6}$	$8.7 \cdot 10^{-9}$

Also, some tests have been conducted with the aim of assessing the robustness of the proposed acquisition approach to additive noise. Different signal-to-noise ratios ( $SNRs$ ), varying within the interval 0-70 dB, have been considered and, for each  $SNR$  value, the input signal has been buried in additive white Gaussian noise, the root mean square (RMS) amplitude of which,  $\sigma_{rms}$ , has been evaluated according to

$$\sigma_{rms} = A_{rms} 10^{-\frac{SNR}{20}} \quad (3.6)$$

where  $A_{rms}$  stands for the RMS value of the input signal. As in the previous tests, for each configuration of  $SNR$  and  $m$ , 100 simulations have been executed; the obtained results, in terms of mean and experimental standard deviation, are shown in Tab.V and Tab.VI,

respectively. As it can be appreciated, the proposed method is capable of granting reliable results only for SNR values greater than 40 dB, whatever the number of acquired samples.

Tab.V. Mean phase shift, expressed in radians, for different values of SNR and  $m$ .

$\begin{matrix} \text{SNR [dB]} \\ m \end{matrix}$	0	10	20	30	40	50	60	70
20	-0.052	0.040	0.012	0.0024	0.00022	0.000194	$-5.5 \cdot 10^{-5}$	$2.5 \cdot 10^{-5}$
40	-0.014	0.0059	0.0039	-0.00083	$9.8 \cdot 10^{-5}$	0.000121	$-1.6 \cdot 10^{-5}$	$5.9 \cdot 10^{-6}$
60	0.038	-0.0053	-0.0025	-0.0012	$-6.0 \cdot 10^{-5}$	-0.00012	$2.1 \cdot 10^{-5}$	$-7.4 \cdot 10^{-6}$
80	0.0085	-0.0018	-0.0017	-0.00014	$-9.6 \cdot 10^{-5}$	$7.0 \cdot 10^{-5}$	$-6.4 \cdot 10^{-7}$	$4.2 \cdot 10^{-7}$
100	0.022	-0.00097	0.00092	0.00055	-0.0002	$6.3 \cdot 10^{-5}$	$2.0 \cdot 10^{-5}$	$-6.1 \cdot 10^{-6}$

Tab.VI. Experimental standard deviation of the phase shift, expressed in radians, for different values of SNR and  $m$ .

$\begin{matrix} \text{SNR [dB]} \\ m \end{matrix}$	0	10	20	30	40	50	60	70
20	0.46	0.16	0.049	0.016	0.0050	0.0015	0.00049	0.00015
40	0.27	0.078	0.023	0.0075	0.0026	0.00088	0.00024	$7.5 \cdot 10^{-5}$
60	0.23	0.066	0.022	0.0067	0.0021	0.00061	0.00019	$6.8 \cdot 10^{-5}$
80	0.18	0.04	0.018	0.0058	0.0016	0.00052	0.00017	$4.8 \cdot 10^{-5}$
100	0.15	0.050	0.015	0.0040	0.0016	0.00057	0.00016	$5.0 \cdot 10^{-5}$

### 3.5 Experimental Results

A number of experimental tests have also been carried out in order to assess the performance of the proposed method implemented on actual cost-effective platform. To this aim, a proper measurement station have been realized; it consisted of (i) microcontroller (both 8 and 32 bit architecture) and FPGA-based platforms, (ii) a dual –channel arbitrary function generator AFG3252C by Tektronix (vertical resolution equal to 14 bits, analog bandwidth of 240 MHz, maximum output update frequency equal to 1GS/s), and (iii) a personal computer mandated to:

1. generate the random sequence of the sampling instants;

2. transmit it to the acquisition platform;
3. receive the digitized random samples;
4. reconstruct the input signals according to the CS theory.

As for the numerical tests, the phase shift among the signals digitized or reconstructed for each input channel has been adopted as performance factor.

### 3.5.1 Tests conducted through 32-bit microcontroller

A first set of experiments have been carried out through a STMicroelectronics microcontroller, namely STM32F303VC<sup>TM</sup>, based on 32-bit ARM Cortex M4 family and featuring a maximum operating frequency equal to 72 MHz, data memory depth of 40 KB, four ADCs with selectable vertical resolution (6, 8, 10, and 12 bit) and full scale of 3.3 V, and a minimum sampling time equal to 200 ns@12 bit. The experiments have aimed at comparing the performance of the proposed sampling approach to that inherently granted by the microcontroller, and have been performed with a sample rate equal to 150 kS/s. In particular, the three following acquisition strategies have been taken into account:

- 1) Sequential acquisition: according to Fig.3.1, only one ADC has alternately digitized 3 kSamples on 4 physical input channels, spending a time interval equal to 6.67 $\mu$ s to switch from one channel to the next;
- 2) “Simultaneous” acquisition: the four ADCs of the device have been employed, each of which configured to digitize 3 kSamples on a specific physical channel at a rate of 150 kS/s. The availability of four ADCs has allowed an acquisition process as close as possible to a pure simultaneous one. In this configuration, the time delay between samples associated with successive channels is only due to the time the microcontroller takes to execute the few instructions needed to send the Start Of Conversion to the ADC, i.e. about 50 ns.
- 3) Compressed acquisition: according to Fig.3.2, just one ADC converting 4 physical channels has been employed; the acquisition instants (and, consequently, the delays between samples of successive channels) are determined as a random sequence. As stated above, the algorithm generating the random sequence has been implemented in order to assure a minimum distance between two successive sampling instants equal or greater than 6.67  $\mu$ s. To compare the results with those provided by the previous acquisition strategies, the compressive sampling algorithm has been configured in

such a way as to provide signals reconstructed on 3 kSamples. Finally, regarding the acquired samples, tests have been performed with a number of  $m$  equal to 20, 40, 60, 80, and 100, respectively. The vertical resolution of the ADC has been set equal to 12 bits.

For each considered acquisition configuration, the 4 channels of the device have been fed with the same signal, consisting of a sinusoidal waveform whose amplitude and offset were equal to 2.8Vpp and 1.4V, respectively. Five tests have been conducted for five different signal frequencies: 150Hz, 300Hz, 1500Hz, 3000Hz, 15000Hz, and, for each test, the phase difference between the waveforms acquired on 4 channels have been measured in frequency domain. As for the numerical tests, the maximum absolute value of the phase shifts measured over three channels with respect to that of the signal on the first channel, taken as the reference, has been assumed as indicator of the method performance. The tests were repeated 30 times for each couple of frequency and number of samples, in order to gain the mean value and experimental standard deviation of the phase shifts . The obtained results are shown in Fig.3.5.

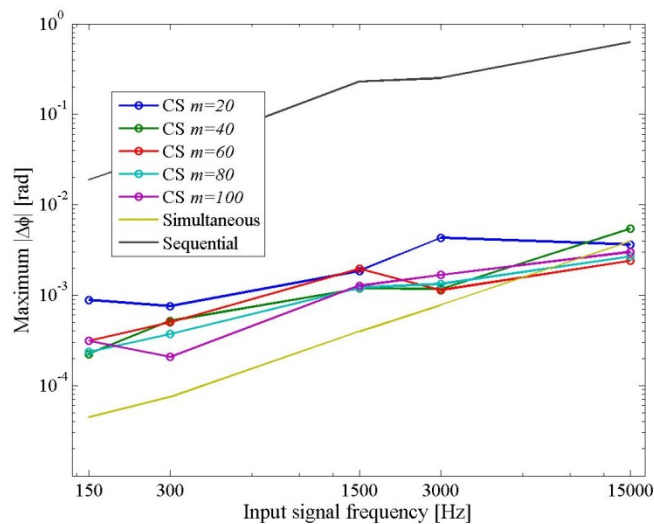


Fig.3.5. Measured phase shift in different acquisition modes.

As expected, in the "simultaneous" and sequential acquisition modes, the values of the phase shift between channels linearly evolved versus frequency, since they are due to the delay between the acquisition of two successive channels. For the sequential acquisition, the phase shift reaches 0.6 radians, making this method unfit to measure quantities depending on the phase relationship between the signals on different channels (as an example measurements of

electrical power or energy). The acquisition in "simultaneous" mode exhibits the same evolution versus frequency, but, of course, the phase shift grows with a lower slope; it can be seen as a lower bound of the ADC performance .

On the contrary, signals reconstructed by means of the proposed method shows a phase shift between channels only slightly dependent on the input frequency and always lower than 0.7centiradian, even though only 20 samples per channel are acquired (i.e., with a compression ratio of 99.3 %). The maximum phase shift is reduced to values lower than about 1 milliradian (equal to 0.016 % of the signal period) if 80 or 100 samples are acquired, i.e. if the compression ratio drops to 96.7%.

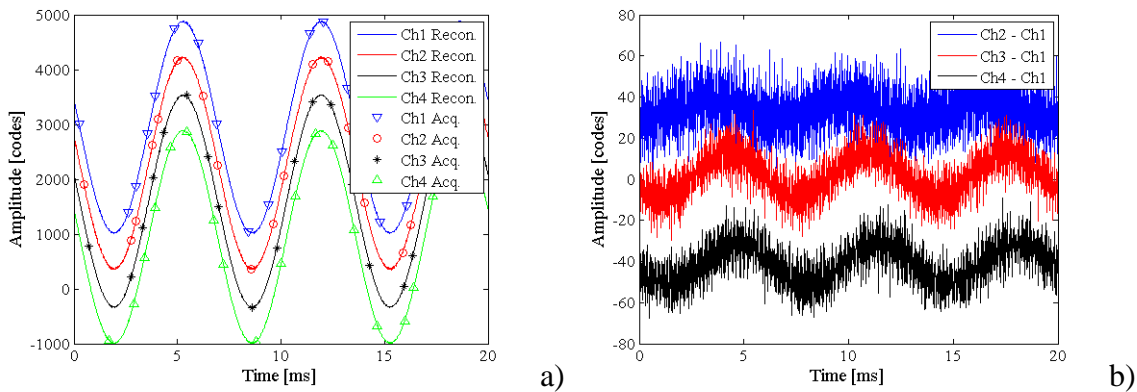


Fig.3.6. a) Reconstructed signals and b) sample-by-sample differences between the obtained waveforms when the proposed acquisition approach is applied to 20 random samples per channel.

As an example, Fig.3.6a shows the signals reconstructed by means of the proposed acquisition approach when a sinusoidal signal with a frequency equal to 150 Hz is considered; only 20 random samples per channel have been acquired. To better appreciate the performance of the proposed approach, sample-by-sample differences between the signal of each input channel and that peculiar of the first one, taken as reference, are shown in Fig.3.6b. For the sake of clarity, a different artificial offset has been added to each signal in order to separate the considered waveforms. The improvement granted by a higher number of acquired samples is highlighted in Fig.3.7a and Fig.3.7b, where the same quantities of Fig.3.6 are gained with respect to signals reconstructed from 100 acquired random samples.

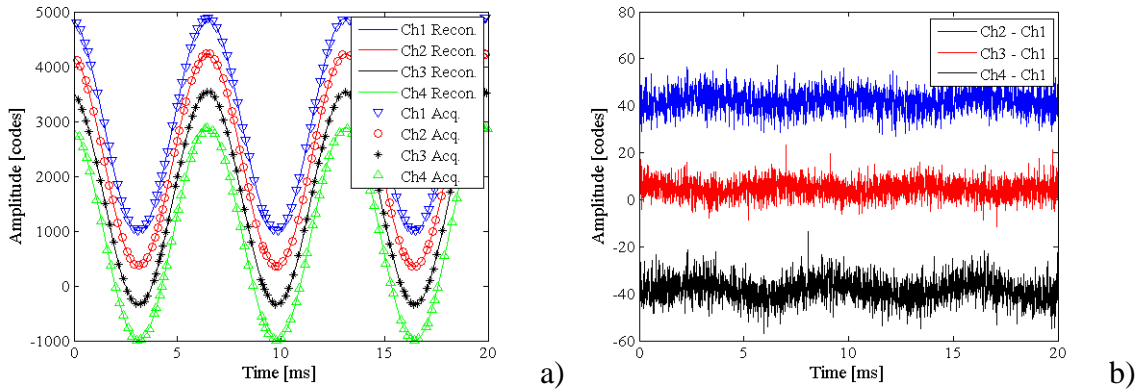


Fig.3.7. a) Reconstructed signals and b) sample-by-sample differences between the obtained waveforms when the proposed acquisition approach is applied to 100 random samples per channel.

Comparing the obtained results with those given in Tab.III and Tab.IV for numerical tests in similar conditions, a slight performance degradation has been experienced; it is mainly related to (i) spectral leakage phenomena due to the finite time-basis resolution and (ii) an effective number of the bits of the ADC lower than 12.

Ultimately, obtained results prove that the proposed acquisition approach allows to reconstruct the input waveform on 3000 samples with a phase error practically negligible, even though a multiplexed converter characterized by an inter-channel delay of  $6.67\mu\text{s}$  is employed and a number of samples per channel lower than 100 is stored. In other words, the used low-cost architecture, combined with the proposed approach, appears to be equivalent to a much expensive device, constituted by four ADCs that work simultaneously, which has to assure a synchronization error as low as few tens of nanosecond at the highest input frequency.

Further tests have been carried out in order to assess the performance of the CS-based approach in different operating conditions. As an example, Tab.VII shows the mean value along with experimental standard deviation of the phase shifts experienced for different vertical resolutions of the converter; the considered phase shifts have been obtained by applying at the four input channels a sinusoidal waveform whose frequency was equal to 500Hz.

Tab. VII Phase shifts of reconstructed waveforms at signal frequency equal to 500Hz.

	m=20		m=100	
	Mean [rad]	Standard deviation [rad]	Mean [rad]	Standard deviation [rad]
Nbit=8	0.0017	0.0041	0.0003	0.0013
Nbit=10	0.0008	0.0042	0.0001	0.0013
Nbit=12	0.0006	0.0042	0.0003	0.0015

In a similar way, the results given in Tab.VIII have been obtained when the frequency of the input signal has been set equal to 50kHz. As for the previous test, the sampling instants have been determined as a random sequence; according to what stated in Section 2.3, the minimum distance between two successive instants has been forced equal to  $2\mu\text{s}$ , since the equivalent sampling frequency was 500kS/s.

Tab.VIII Phase shift of reconstructed waveforms at signal frequency equal to 50kHz.

	m=20		m=100	
	Mean [rad]	Standard deviation [rad]	Mean [rad]	Standard deviation [rad]
Nbit=8	0.0029	0.0059	0.0021	0.0043
Nbit=10	0.0024	0.0073	0.0018	0.0044
Nbit=12	0.0020	0.0059	0.0014	0.0040

For tests conducted on sinusoidal signals with frequency equal to 500Hz, the measured phase shift was negligible, but for 8-bits resolution; in this case, the acquisition of 100 samples is, in fact, required to obtain phase shift value lower than 1 mrad. With regard to tests involving 50kHz sine-wave, the mean is affected by the converter resolution and exhibits higher values of the phase shift, although it is still lower than 3 mrad. On the contrary, the standard deviation of the results do not seem to depend on the resolution of the used converter, whatever the frequency of the input signal.

Other tests have been carried out to characterize the proposed acquisition approach with respect to the compression ratio. The four input channels has received a sinusoidal signal characterized by a frequency of 5 kHz, and the converter has been exploited to acquire 100 random samples per channel. The processing algorithm has been configured to reconstruct the acquired signals respectively on 1000, 3000, 5000, and 10000 samples, with an equivalent sampling rate of 500 kS/s.

Measurement results (Fig.3.8) have shown that the mean phase shift of the reconstructed signals, estimated on 30 measures, is slightly influenced by the compression ratio and is always lower than 0.8 milliradians (i.e. 0.01% of the signal period).

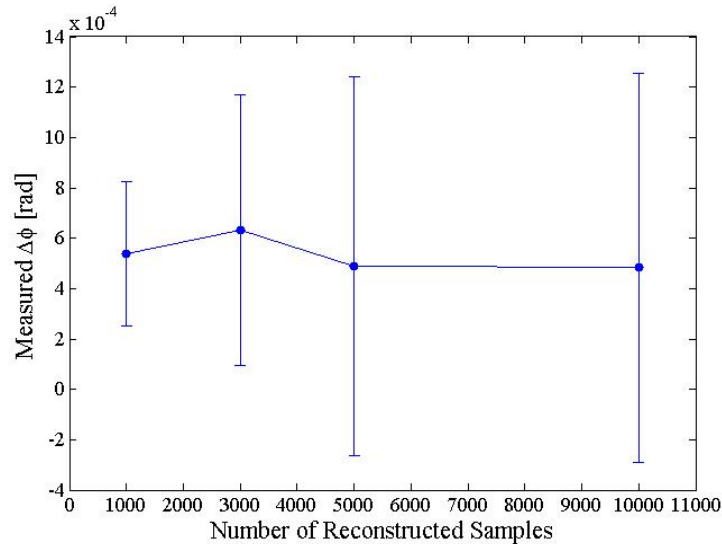


Fig.3.8. Evolution of the maximum phase shift of reconstructed waveforms versus the number of reconstructed samples; all tests have been carried out starting from 100 random samples digitized for each channel.

The associated standard deviation is, instead, lower than 0.3 milliradians when the compression ratio is equal to 96.7%, and increases up to 0.8 milliradians when the compression ratio reaches 99% (i.e., for  $n$  equal to 10 kSamples). Moreover, thanks to the proposed approach, it has been possible to reconstruct up to 40 kSamples; this result cannot be achieved through the traditional acquisition approach on the considered platform, since 80 KB memory depth is at least required.

Further tests have been conducted in order to assess the performance of the approach when the acquired waveforms exhibit a nominal phase shift, i.e. to assess that the reconstruction algorithm does not introduce artifacts in the signal phase. In particular, two physical channels have been supplied with two signals presenting a phase shift respectively equal to  $0^\circ$ ,  $5^\circ$ ,  $10^\circ$ ,  $15^\circ$ ,  $20^\circ$ . Tests have been carried out for two values of input signal frequency (500Hz and 50kHz) and number of acquired samples  $m$  (20 and 100).

Fig.3.9 shows the evolution of mean and associated experimental standard deviation of the reconstructed phase shifts versus the nominal values, when the frequency of the input signal is

500Hz; to better appreciate the performance of the proposed approach, Fig.3.10 shows the differences between the measured and nominal phase shifts.

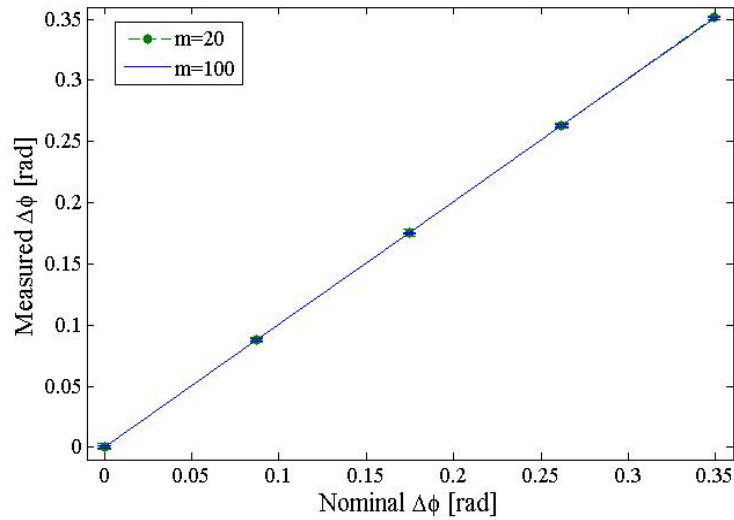


Fig.3.9 Measured phase shift versus nominal one with signal frequency equal to 500Hz.

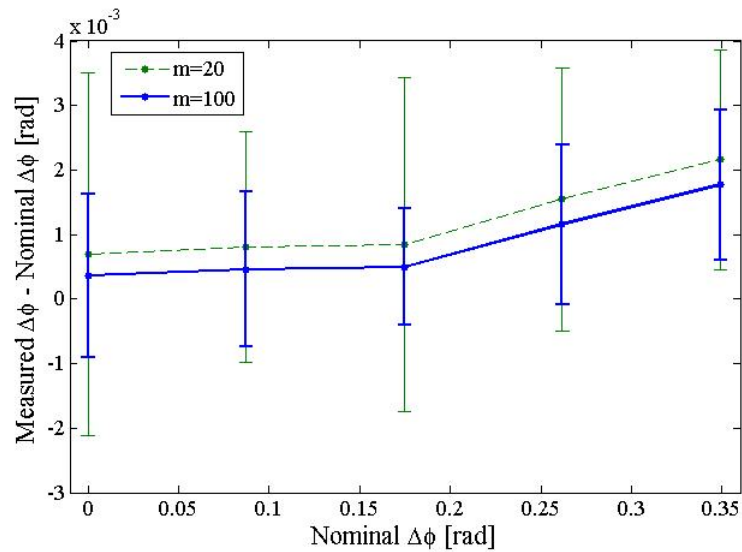


Fig.3.10 Difference between measured and nominal phase shift with signal frequency equal to 500Hz.

In a similar way, the results obtained for a signal frequency of 50kHz are plotted in Fig.3.11 and Fig.3.12.

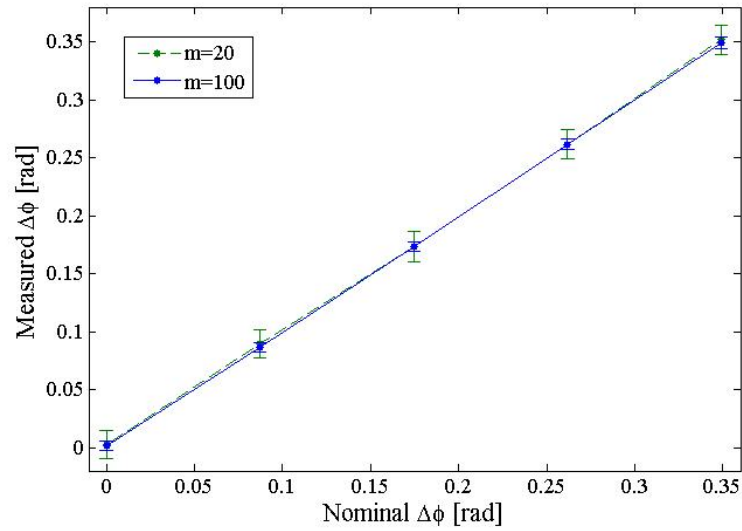


Fig.3.11 Measured phase shift versus nominal one for a signal frequency equal to 50kHz.

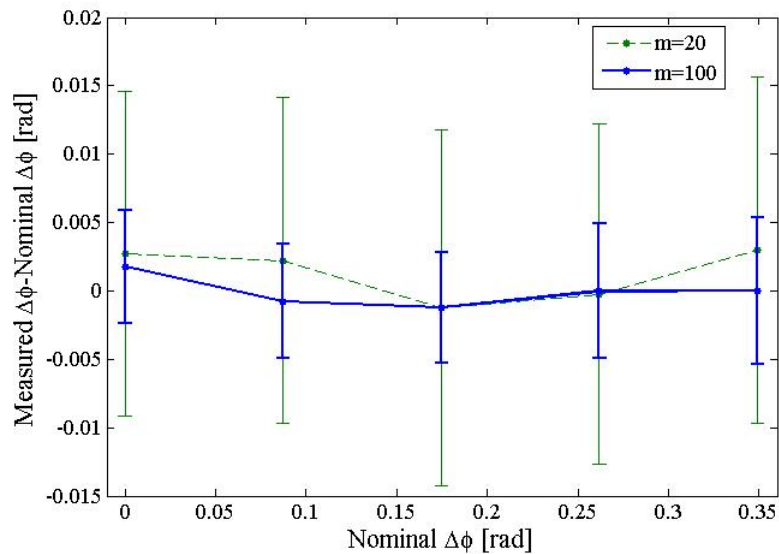


Fig.3.12 Difference between measured and nominal phase shift with signal frequency equal to 50kHz.

When the signal frequency is 500Hz, the difference between the phase shift of the reconstructed signals and the actual phase shift has always been lower than 2 milliradians even for the outstanding compression ratio obtained by acquiring 20 samples and reconstructing the waveform on 3000 points. As it can be expected, if the compression ratio is so high, the measurement results are characterized by a worst standard deviation. As a matter of practice, the measurements performed at different compression ratios have proved to be

compatible with one other, with a standard deviation that increases when the number of acquired samples decreases. The same conclusions can be drawn when the signal frequency is 50kHz; in this case, as expected, the standard deviations increase, causing the reconstructed phases to be affected by greater uncertainty.

### **3.5.2 Tests conducted on 8-bit microcontroller**

Similar test have been conducted on a 8 bit-microcontroller, namely PIC18F4620™ by Microchip, mounted on a PICDEM Plus board and characterized by an actual operating frequency equal to 1 MHz, data memory depth of 4 KB, a single ADC with vertical resolution and full scale voltage equal respectively to 10 bits and 5V, 13 input channels, and a minimum sampling time of 20µs@10bit. The microcontroller has been programmed in such a way as to digitize the signal connected simultaneously to four physical channels. Once again, the phase shift among the different channels has been chosen as performance factor.

Due to the limited operating frequency and the inherent 8-bit architecture of the PIC18F4620, the tests presented in the following have been carried out at 5 kS/s; channel selection and sample storage have, in fact, required several atomic instructions, thus reducing the maximum available sample rate. This way, the minimum time difference between successive samples in the random sequence has been configured equal or greater than 200 µs. The tests have been designed to randomly digitize from 20 up to 100 samples for each channel, covering an observation interval of 600 ms, and to obtain reconstructed signals characterized by 3000 samples for each channel, i.e. a whole set of 12 kSamples, a number unfeasible to be acquired through the considered microcontroller, which makes it outperform more expensive devices.

A sinusoidal waveform, with a peak-to-peak amplitude and offset equal respectively to 4.9 V and 2.5 V, has been used as input signal for the considered four physical channels. Tests have been conducted for different signal frequencies: 5Hz, 10Hz, 50Hz, 100Hz, 500Hz. Similar considerations to those concerning the tests presented in the previous section can be drawn with regard to the phase shift measurement and the number of repetitions for each configuration of signal frequency and number of acquired samples. The obtained results are shown in Fig.3.13.

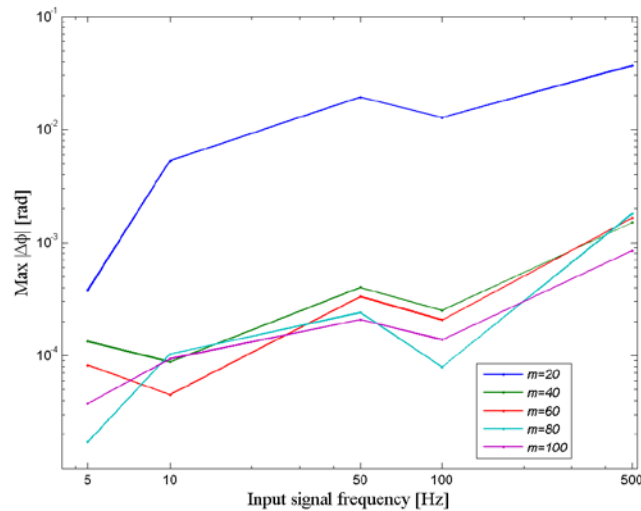


Fig.3.13 Measured phase shift in different acquisition configurations.

Similarly to what experienced with the 32 bit-microcontroller, the reconstructed signals show a phase shift between channels only slightly dependent on the input frequency. In particular, the phase shift has always been lower than 2 milliradians, with a number of digitized random samples within the interval 40-100; the superior performance with respect that exhibited in the presence of the 32 bit-microcontroller has to be associated with the lower value of the involved signal frequencies. By reducing the number of acquired random samples down to 20, the phase shift has grown to 4 centiradians, thus proving it unsuitable to reconstruct signals with a sufficient accuracy. The superior performance with respect to the results shown in Fig.3.5 for the 12 bit ADC has to be ascribed to the lower values of the involved signals and sampling frequencies; in spite of the lower number of bits of the PIC4620<sup>TM</sup> than that of the STM32<sup>TM</sup> (10 vs. 12), the PIC4620<sup>TM</sup> has worked in less critical conditions thus assuring better results. In the same way as the 32 bit-architecture, further tests have been conducted in order to assess the performance of the approach when the acquired waveforms exhibit a nominal phase shift equal to 0°, 5°, 10°, 15°, 20°. Two values of the input signal frequency (5 Hz and 500 Hz) and number of acquired samples (20 and 100) have been considered. Fig 3.14 shows the evolution of the mean and associated experimental standard deviation of the reconstructed phase shift versus the nominal value, when the frequency of the input signal is 5 Hz.

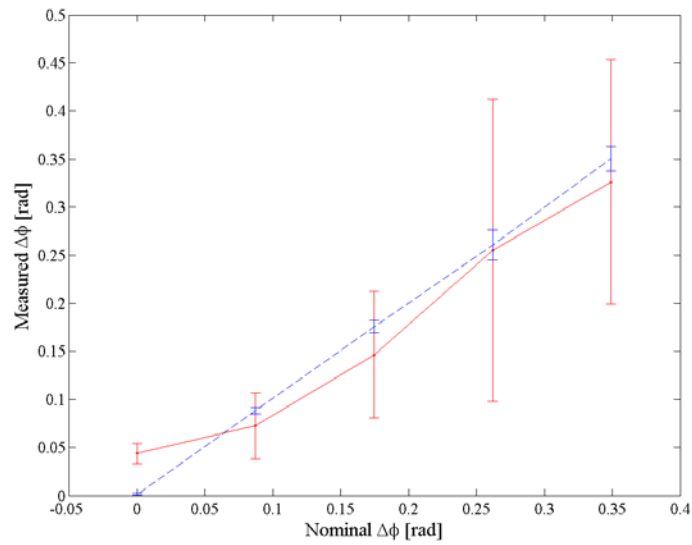


Fig.3.14 Measured phase shift versus nominal one for a signal frequency equal to 500Hz.

To better appreciate the performance of the approach, Fig.3.15 shows the difference between the measured and nominal phase shift.

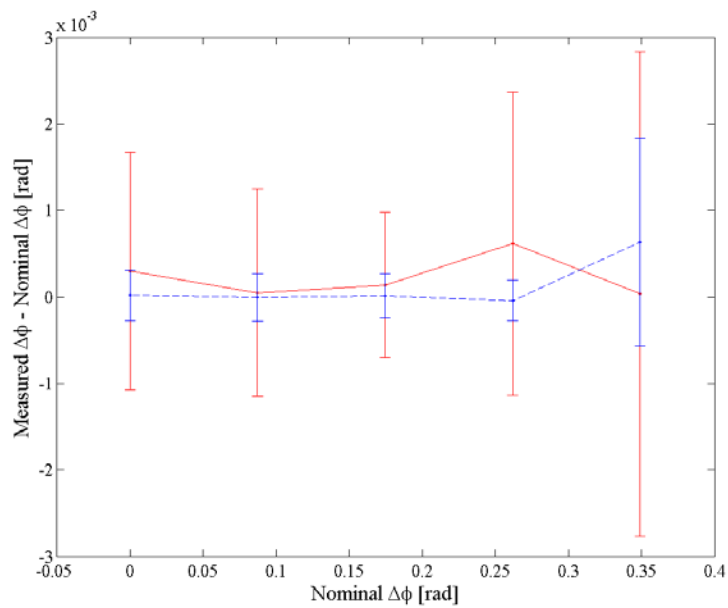


Fig.3.15. Difference between measured and nominal phase shift for a signal frequency equal to 5Hz.

Results obtained for an input signal frequency equal to 500 Hz are shown in Fig.3.16 and Fig.3.17.

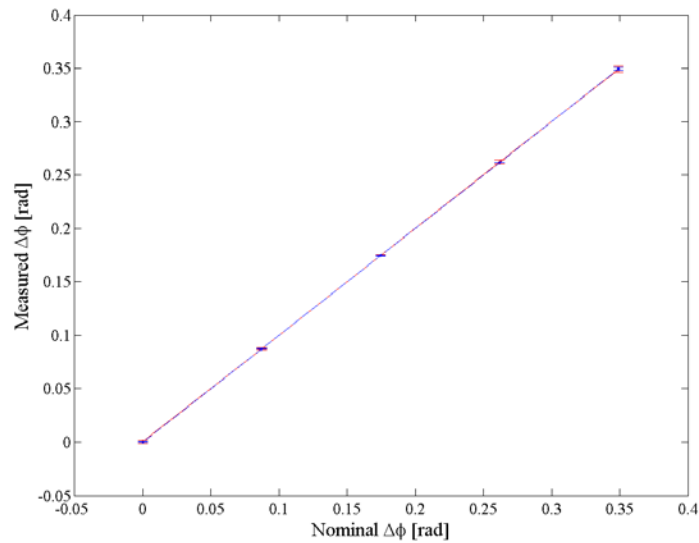


Fig.3.16 Measured phase shift versus nominal one for a signal frequency equal to 5Hz.

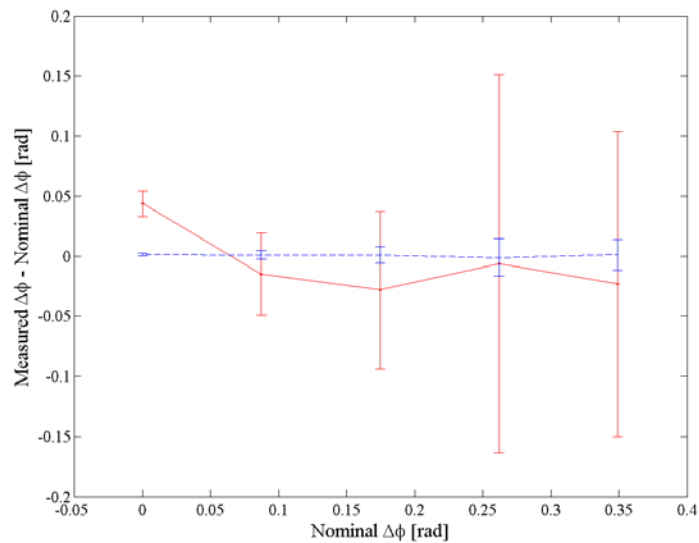


Fig.3.17 Difference between measured and nominal phase shift for a signal frequency equal to 500Hz.

For tests conducted with a signal frequency equal to 5 Hz, the difference between the measured and nominal phase shift has always been lower than 1 milliradians, whatever the number of acquired samples; as expected, the value of  $m$  has highly affected the experimental standard deviation. On the contrary, when the signal frequency has been set equal to 500 Hz, the approach's performance proved to be dependent on the number of acquired samples; differences and experimental standard deviations up to 5 and 15 centiradians, respectively, have been experienced in the tests with 20 random samples. However, the tests conducted

reconstructing the input signals from 100 acquired samples confirmed the satisfying performance of the acquisition approach.

### **3.5.3 Tests conducted on a FPGA-based platform**

The last set of tests has been carried out on a National Instruments sbRIO-9632<sup>TM</sup> Embedded Device. The considered device is a 2MGates FPGA-based hardware with analog inputs and digital input/output pins. As for the analog inputs, it features up to 16 differential channels (32 single ended) and two analog to digital converters that receive up to 8 differential channels through a multiplexer device. The maximum vertical resolution is equal to 16 bits, while the maximum sample rate is equal to 250 kS/s on a single channel and reduces to about 15 kS/s when the whole channel set is considered. This device allows the development of Labview-based software and communicate with a personal computer through a Ethernet connection with a TCP/IP protocol.

Since the manufacturer does not specify its value, the inter-channel delay has preliminarily been estimated in a number of operating conditions involving different sample rates and signal frequencies) A mean value of 19.7  $\mu\text{s}$  with an experimental standard deviation of 3.1  $\mu\text{s}$  has been experienced on the whole operating frequency range of the onboard ADC channels.

Then, two tests have been carried out on several sinusoidal signals characterized by a peak to peak amplitude equal to 1 V and different frequency values. In the former test, a sampling frequency equal to 10 kS/s (very close to the maximum one allowed by the device) has been adopted, while in the latter a lower sampling frequency (50 S/s) has been chosen. In particular, the former test has aimed at investigating the approach's performance when the inter-channel delay is very close to the sampling interval (equal to 100  $\mu\text{s}$ ), while in the latter test the inter-channel delay produces a reduced phase shift among the multiplexed channels. Sinusoidal signals with frequencies within the interval 50-4000 Hz have been considered in the former test, while sinusoidal signals with frequencies within the interval 1-20 Hz have been considered in the latter test.

As in the previous numerical and experimental tests, the effect of multiplexed channels have been analyzed in terms of phase shift of the second, third and fourth channel with respect to the first one, when a sequential acquisition is considered. In particular, the obtained values for the two considered scenarios are given in Fig.3.18.

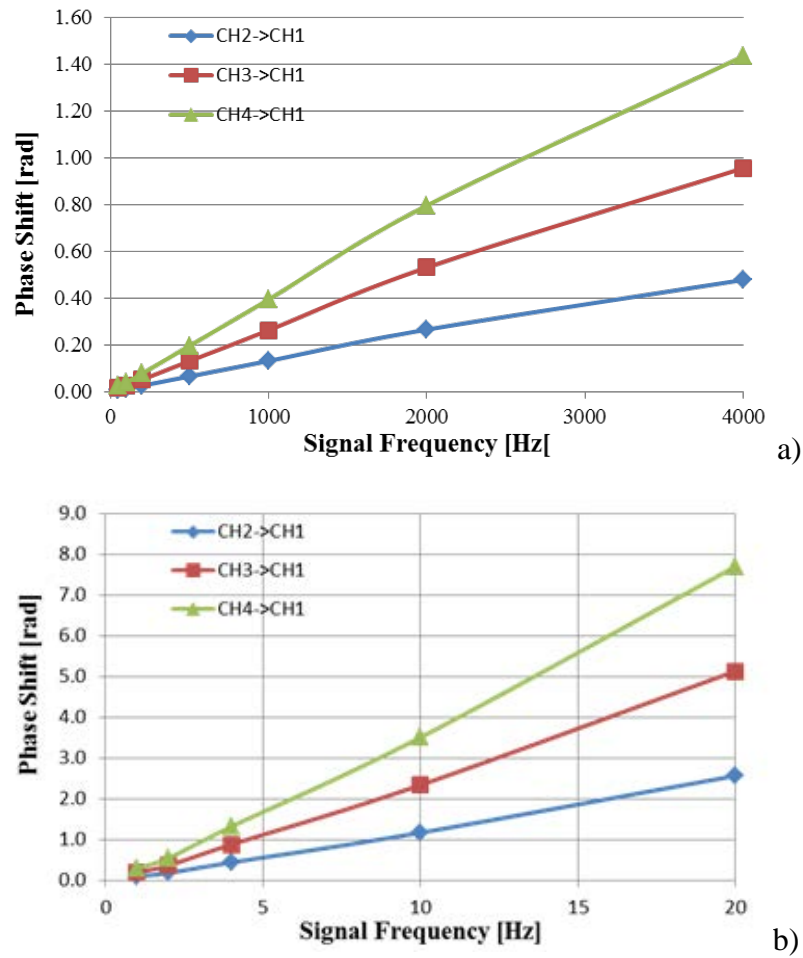


Fig.3.18 Measured phase shift for the four channels versus signal frequency: a) sampling frequency equal to 10kS/s; b) sampling frequency equal to 50 S/s. Multiplexed acquisition is involved.

It is worth noting that, without the proposed acquisition approach, the presence of the multiplexer worsens the phase alignment among channels, giving rise to phase shifts in the range from few milliradians, for low sample rates, up to more than 1 radian, when the sample rate increases.

As for the proposed CS-based acquisition approach, a number of tests have been executed in the same operating conditions involving multiplexed acquisitions. For the sake of brevity, only the results related to a compression ratio equal to 10 are discussed in the following (Fig.3.19); a total of 200 consecutive experiments have, in particular, been considered.

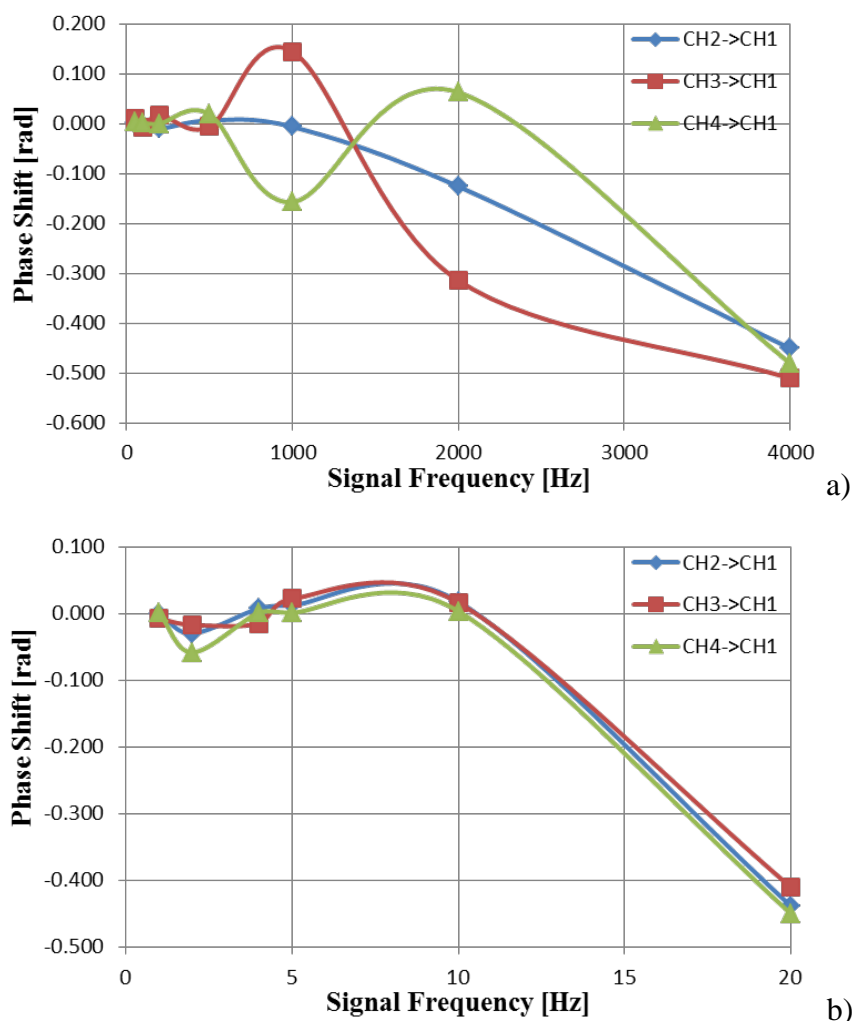


Fig.3.19 Measured phase shift for the four channels versus the signal frequency: a) sampling frequency equal to 10kS/s; b) sampling frequency equal to 50 S/s. The compressed acquisition approach is involved.

It is possible to appreciate how the proposed acquisition approach deeply reduces the measured phase shift; in particular, a maximum phase shift equal to 0.5 radians is experienced for a sample rate equal to 10 kS/s, lower than that experienced with the multiplexed acquisition in the same operating condition. In addition, it is possible to highlight that, independently from the sample rate, typical phase shifts within  $\pm 0.1$  radian have been experienced. This shifts are very good if compared to those typically experienced in the multiplexed acquisition when the sample rate is greater than 1 kS/s.

### 3.6 Conclusions

The second step of the research activity has dealt with the definition and implementation of an acquisition approach, based on compressive sampling, for simultaneous data acquisition,

which turns out to be mandatory when poly-phase systems for power distribution are taken into account. The approach exploits some attractive features of the CS, along with the availability of a common time basis, to randomly digitize a reduced number of samples and successively reconstruct the desired input signals without introducing fake phase shifts among the channels. The approach has proved particularly addressed to typical sequential data acquisition systems, such as those usually included in low-cost measurement solutions based on microcontrollers, FPGAs and similar intended to be adopted for the final smart grid meter.

A number of tests carried out both on numerical and actual sinusoidal signals highlighted and confirmed the promising performance of the proposed acquisition approach. Phase shifts,  $\Delta\varphi$ , among the reconstructed waveforms as low as few milliradians (about 0.016% of a whole period) have, in fact, been experienced in several measurement conditions, involving different values of the number of acquired samples, vertical resolution and input signal frequency, for 8-bit and 32-bit microcontrollers. Results not as good as the aforementioned ones have been achieved in tests conducted on FPGA; even though the phase shift proved to be lower than that obtained with pure sequential acquisitions, values of  $\Delta\varphi$  up to 0.5 rad have been encountered. Such a difference has to be ascribed to the non-efficient implementation (associated with the LabView environment) of the sampling algorithm.

### **3.7References**

- [1] F. Attivissimo, A. Di Nisio, N. Giaquinto and M. Savino, Measuring time base distortion in analog-memory sampling digitizers, *IEEE Transactions on Instrumentation and Measurement*, vol. 57, no. 1, pp. 55-62, Jan. 2008.
- [2] G. Betta, D. Capriglione, C. Landi, N. Pasquino, “Uncertainty and reproducibility in measuring the data acquisition system immunity to conducted disturbances,” *Measurement Science and Technology*, vol. 20, n. 5, May 2009.
- [3] G. Betta, D. Capriglione, C. Landi, N. Pasquino, “Uncertainty and reproducibility in measuring the data acquisition system immunity to conducted disturbances,” *Measurement Science and Technology*, vol. 20, n. 5, May 2009.
- [4] E. Candès, J. Romberg, and T. Tao, “Stable signal recovery from incomplete and inaccurate measurements,” *Comm. Pure Appl. Math.*, vol. 59, no. 8, pp. 1207–1223, Aug. 2006.

- [5] D. Mesecher, L. Carin, I. Kadar, R. Pirich, "Exploiting signal sparseness for reduced-rate sampling," *Systems, Applications and Technology. IEEE Long Island, Conference, 2009. LISAT '09*, pp 1-6, 2009.
- [6] C. Caione, D. Brunelli, L. Benini, "Distributed Compressive Sampling for Lifetime Optimization in Dense Wireless Sensor Networks, " *IEEE Transaction on Industrial Informatics*, VOL. 8, NO. 1, February 2012.
- [7] F. Chen, A.P. Chandrakasan, V.M. Stojanovic, "Design and Analysis of a Hardware-Efficient Compressed Sensing Architecture for Data Compression in Wireless Sensors, " *IEEE Journal of Solid-State Circuits*, VOL. 47, NO. 3, March 2012.
- [8] C. Luo, J.M. McClellan, "Compressive Sampling with a Successive Approximation ADC Architecture, " *In Proc. of IEEE International Conference on Acoustic, Speech and Signal Processing*, 22-27 May 2011.
- [9] P. K. Yenduri, A. Z. Rocca, A. S. Rao, S. Naraghi, M. P. Flynn, A. Gilbert, " A Low-Power Compressive Sampling Time-Based Analog-to-Digital Converter, " *IEEE Journal on Emerging and Selected Topics in Circuits and System*, Vol.2, N. 3, September 2012.
- [10] W. Guo, Y. Kim, A. Sanyal, A. Tewfik, N. Sun, "A single SAR ADC converting multi-channel sparse signals, " *In Proc. of IEEE International Symposium on Circuits and System*, 19-23 May 2013.
- [11] CVX: Matlab Software for Disciplined Convex Programming, Version 2.0 (beta), October 2013, <http://cvxr.com/cvx/>.
- [12] L. Angrisani, M. D'Arco, G. Ianniello, M. Vadursi, "An efficient pre-processing scheme to enhance resolution of band-pass signals acquisition,"*IEEE Trans. on Instrum. and Meas.*, vol. 61, no.11, pp.2932-2940, Nov. 2012.
- [13] L. Angrisani, F. Bonavolontà, M. D'Apuzzo, R. Schiano Lo Moriello, M. Vadursi, "A Compressive Sampling Based Method for Power Measurement of Band-Pass Signals," *Proc. of I2MTC 2013*, 7-9 May 2013, Minneapolis, pp. 102-107.

## 4 Sample Rate Enhancement In DASs For Low-Cost Sensing Nodes.

### 4.1 Introduction

In recent years, embedded systems (such as microcontrollers, field programmable gated arrays, digital signal processors and so on) have been playing a fundamental role in metrological applications. The availability of integrated systems capable of digitizing, processing and transmitting measurement results offers the opportunity of realizing nodes for distributed and/or portable measurement systems characterized by reduced costs and good performance. Typical application examples are smart meters for energy billing or analysis of electrical power quality [1]-[4], monitoring of environmental quantities of interest [5]-[8], control of complex production process [9]-[11].

Architectures based on successive approximation registers are usually chosen for the data acquisition section (DAS, mainly based on the ADC embedded in the measurements nodes), due to their straightforward implementation and a nominal vertical resolution that is suitable for most of the considered application. Nevertheless, some specific solutions for band-pass signals [12]-[14] and some dedicated solutions exploiting more performing ADCs ( $\Sigma\Delta$  or flash converters) are also available on the market [15].

The most significant parameters commonly used for characterizing and determining the performance of the DAS are:

- *nominal vertical resolution*: usually expressed in bits, it defines how many distinct output codes the DAS can produce; depending on the specific architecture of the ADC, typical resolution varies between 10 and 14 bits;
- *maximum sample rate*: it defines the capability of the DAS of rapidly sampling and converting the input signal and directly determines the maximum spectral component that can be alias-free sampled. Typical actual values for low cost microcontrollers range from few tens of kilohertz up to 5 MHz;
- *memory depth*: combined with the sample rate, it determines the maximum observation interval the microcontroller can acquire for successive processing. Values from few kilobytes up to some megabytes are usually found;
- *input bandwidth*: determines the maximum frequency of spectral components that the ADC can receive as input without significant distortion; to assure alias-free

digitization of the input signal, it is usually set no higher than half maximum sample rate, even though some solutions dedicated to digital downconversion provide larger bandwidth [16].

For the proposed distributed monitoring systems of Power Quality, consisting of distributed acquisition nodes and a central computing unit that processes measurement data, improving the performance of the embedded DAS, in terms of sample rate enhancement, can be crucial for the improvement of the whole measurement system. To this aim, a new method based on compressive sampling (CS), which permits to increase the maximum sample rate of DAS integrated in low-cost microcontrollers, is proposed in the following. Some papers recently focused their attention on the possibility of exploiting CS to enhance the performance of ADC in terms of sample rate. In particular, in [17] CS is used to extend the traditional equivalent time sampling (ETS) scheme in order to reconstruct the input signal with a higher time resolution. However, a number of periods of the input signal much higher than those successively reconstructed are involved, which poses severe constraints on the stability of the time base. Such problem has been solved for random sampling CS-based ADC in [18] through an ad-hoc new circuit. An alternative is represented by CS-based ADCs exploiting random demodulation [19], which have been shown to have good performance for most measurement applications [20]. In particular, a significant improvement in terms of sample rate has been obtained, though at the expenses of architectural complexity, due to the presence of the analog mixing of the input signal with a pseudo-random sequence.

Differently from the abovementioned solutions, the method proposed hereinafter does not require any hardware modification (as external clock circuits and/or analog mixing stages) to increase the sample rate and turns out to be the optimal solution for the majority of already available ADCs integrated in embedded systems. The proposed acquisition strategy permits, in fact, to achieve a higher time resolution when digitizing a signal included in the ADC bandwidth in real-time, by combining the already available hardware section (constituted by the traditional ADC and the high resolution time basis) with a proper software procedure, which provides a suitable random sequence of sampling instants and reconstructs the signal of interest according to the CS theory.

#### ***4.2 Increasing the effective sample rate of embedded DAS***

For the sake of clarity, the key idea underlying the method is described and compared both to the traditional and compressive sampling approach.

### 4.2.1 Traditional Sampling Approach

In Fig.4.1 the traditional sampling approach, adopted by the majority of ADCs, is shown. The ADC operates at its highest sampling rate and input signal samples are uniformly taken with a sampling period equal to  $T_{conv}$ , which is the time interval required by the ADC to digitize (i.e. to sample and convert) a single sample. Alias-free sampling can be assured on signal whose maximum spectral content is lower than  $1/(2T_{conv})$ . It is useful to highlight that in the case of low cost microcontrollers, the limited memory depth (usually shorter than 10kSamples) permits to save only short time records of the input signal.

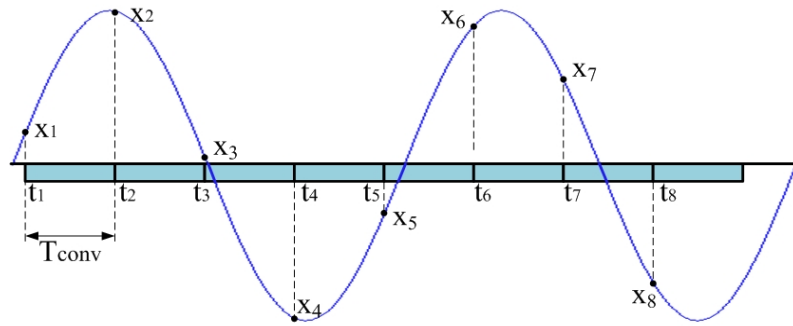


Fig. 4.1. Traditional approach for signal sampling; samples of the input signal of interest are uniformly digitized with constant period equal to  $T_{conv}$ .

### 4.2.2 CS-based Sampling Approach

As shown in Fig.4.2, if the samples (indicated by black dots) are randomly acquired throughout the observation interval, the signal of interest can accurately be reconstructed (samples marked by red dots) as it had been continuously digitized with a sampling period equal to  $T_{conv}$ .

It is worth noting that the desired reconstruction is achieved starting from a very limited number of random signal samples. It was shown that accurate reconstruction can be gained, with a compression ratio up to 98% for multicomponent signals (i.e. 10kSamples input signals were recovered starting from 200 acquired random samples).

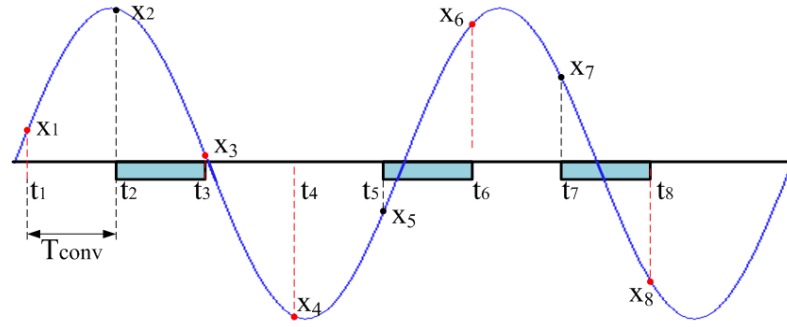


Fig.4. 2. Sampling strategy based on CS; only few samples are randomly digitized from which the input signal can be reconstructed with constant sampling period equal to  $T_{conv}$ .

### 4.2.3 Proposed Sample Rate Improvement

A new method (in the following referred to as new acquisition strategy) based on CS has been defined and implemented for increasing the effective sample rate of embedded DAS. The availability of a suitable time basis allows to finely set the random sampling instants (i.e. the time instants the ADC starts to convert a single sample, which are marked as black dots in Fig.4. 3), with a time resolution equal to  $T_c$ . Even though the conversion of a single sample takes a time  $T_{conv}$  greater than  $T_c$  ( $T_{conv} = 5 T_c$  in the example shown in Fig.4. 3), the proposed approach assures that the input signal will finally be reconstructed (red dots) at an effective sample rate equal to  $1/T_c$ . As it can be expected, the only constraint is that the time difference between two successive actual sampling instants should be greater than  $T_{conv}$ .

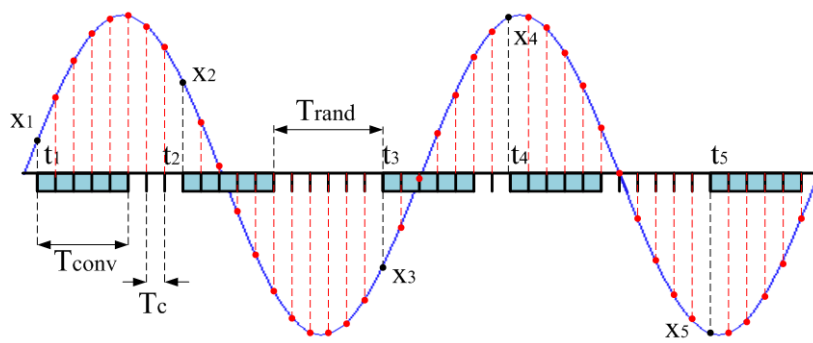


Fig.4. 3. Proposed acquisition strategy based on CS; thanks to the availability of a suitable time-basis, the input signal can be reconstructed with constant sampling period equal to  $T_c < T_{conv}$ .

### 4.3 Proposed Sampling Approach

To improve the sample rate of ADC in low-cost embedded systems, the traditional hardware for analog-to-digital conversion has been complemented with a proper digital signal

processing mandated to generate the random sequence of sampling instants and reconstruct the signal of interest from the acquired samples (Fig.4.4). In particular, the sequence of the random sampling instants is determined as a multiple of a high resolution time-basis,  $T_c$ , and exploited to control the start of conversion (SOC) signal of the ADC. The sequence of considered instants and the corresponding samples (digitized at lower rate, equal to  $1/T_{conv}$ , by the ADC) are given as input to the CS-based algorithm for the successive signal reconstruction, with a time resolution equal to that of the adopted time basis. Specific details about the determination of the random sampling instants along with some guidelines for the reconstruction algorithm are given in the following.

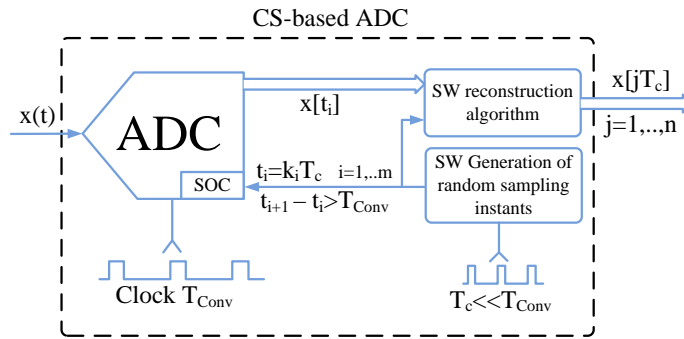


Fig.4. 4. Block diagram of proposed solution for improving ADC sample rate.

### 4.3.1 Sampling Instants Determination

The first step of the new acquisition strategy is the determination of the actual sampling instants. According to the random sampling approach [21], the sampling instants  $t_i$  are randomly chosen throughout the considered observation interval  $T_w$  equal to  $n$  times  $T_c$ . The key idea underlying the proposed sampling strategy is that the considered instants can be expressed as an integer multiple of the high resolution time basis  $T_c$

$$t_i = k_i T_c, \quad k_i \in [0, n - 1] \text{ and } i = 1, \dots, m \quad (4.1)$$

This way, the final signal reconstruction will be obtained with the same time resolution, thus granting a suitable enhancement of the nominal ADC sample rate. In order to assure proper operations of the CS-based ADC, the sampling instants  $t_i$  have to satisfy the following expression (Fig.4.3)

$$t_i = t_{i-1} + T_{conv} + T_{rand} \quad (4.2)$$

where  $T_{rand}$  is the random interval between the end of a conversion and the start of the successive one; the considered constraint assures that no new conversion will start until the pending one is over. Moreover, a specific software procedure has been implemented in order to assure the generation of a pseudo-random sequence of multiples  $k_i$  capable of assuring the full coverage of the observation with a suitable grade of randomness. In particular, let  $fr$  the value of the ratio between  $T_{conv}$  and  $T_c$ ; the pseudo-random sequence generator has to assure the determination of  $m$  sampling instants within the interval from 0 up to  $nT_c$  each of which far at least  $frT_c$  from the successive one. To this aim, the procedure enlists the following steps:

1. Evaluation of a suitable acceptance threshold  $tsh$ , equal to  $m/n$  (only  $m$  sampling instants among  $n$  possible values have to be determined) in the first iteration;
2. Current sampling instant index  $k_i$  is initially equal to 0;
3. A pseudo-random number is generated according to uniform random distribution within the interval from 0 up to 1;
4. If the obtained pseudo-random number is lower than the acceptance threshold, then  $k_i$  is retained in sampling sequence and its value is updated by adding  $fr$ ;
5. If the obtained pseudo-random number is greater than the acceptance threshold, then  $k_i$  is dropped and its value is incremented by one;
6. If the number of sampling instants included in the sequence is lower than  $m$  and  $k_i$  is lower than  $n-1$  return to step 3;
7. If  $k_i$  is not lower than  $n$  but the sampling instants sequence is not yet full, a new acceptance threshold has to be calculated; this is particularly likely when the value  $m \cdot fr$  is close to  $n$ . To assure a fast convergence of the procedure, a threshold increment by 20% was adopted, i.e. the new value of  $tsh$  is 1.2 times the old  $tsh$  value; once updated the  $tsh$  value, return to step 2;
8. If the number of sampling instants included in the sequence is equal to  $m$  and  $k_i$  value is lower than  $n-1$ , the sampling instants sequence is complete and can be adopted to acquire the samples of the input signal.

With regard to  $T_{conv}$ , since it is generated from the same fundamental clock, it usually is a multiple of the adopted time basis; if this is not the case, the first multiple of  $T_c$  immediately greater than  $T_{conv}$  is used, thus granting that condition (4.1) always holds.

According to the CS approach, and following the procedure described in the previous chapters, once the samples have been digitized, the input signal is reconstructed with the high resolution time basis  $T_c$ .

#### 4.4 Numerical Results

To preliminarily assess the performance of the proposed sampling strategy, several tests have been executed by means of numerical simulations. The effect of the most influencing parameters, such as number of acquired samples  $m$ , ADC sample rate  $f_{conv}$ , ADC vertical resolution  $n_{bit}$ , signal-to-noise ratio  $SNR$ , jitter and input signal sparsity  $S$ , has been evaluated. Parameters value has been chosen as close as possible to those provided by the cheapest microcontrollers [22] or granted by most of the embedded systems [23] that are currently available on the market. Similar values will be selected in the successive actual experimental tests. With regard to the number of acquired samples  $m$ , it has always been lower than typically available memory depth. On the contrary, the number of samples  $n$  granted for the signal reconstruction has been even much greater than memory depth, thanks to the CS-based approach.

As an example, some of the obtained results are presented in the following. Unless otherwise indicated, the input signal for tests has been a pure unipolar sinusoidal signal whose full scale amplitude and frequency were equal respectively to  $2^{n_{bit}}-1$  codes and 5 kHz; 80 random samples have been digitized with an effective vertical resolution of 12 bits at an ADC sample rate  $f_{conv}$  equal to 10 kS/s, and the signal has been reconstructed over a time sequence of 10,000 samples at an effective sample rate  $f_c$  of 1 MS/s. For the sake of clarity, the parameters values are summarized in Table I.

Table I. Parameters values typically adopted in numerical tests.

Number of acquired samples	80
Number or reconstructed samples	10000
$f_{conv}$ [kS/s]	10
$n_{bit}$	12
$f_c$ [MS/s]	1
Input signal frequency [kHz]	5
Input signal amplitude [Codes]	$2^{n_{bit}} - 1$

The reconstruction error has been used to assess the performance of the acquisition strategy. It is defined as:

$$\varepsilon = \frac{\|\hat{x} - x\|}{\|x\|} \cdot 100 \quad (4.3)$$

where  $\hat{x}$  is the reconstructed signal and  $x$  is the original one.

#### 4.4.1 ADC Sample Rate and Vertical Resolution

A first set of tests aimed at verifying the dependence of the performance of the proposed acquisition strategy on the ADC conversion period and effective number of bits. Several nominal values of ADC sample rate  $f_{conv}$  and vertical resolution  $n_{bit}$  have been taken into account.

As an example, Fig.4.5 shows the input signal, the acquired samples and the reconstructed signal (which completely overlies the input signal) when  $n_{bit}$  and  $f_{conv}$  were equal respectively to 12 and 10 kS/s. It is worth noting that 80 samples are randomly taken throughout 50 periods of the input signal; the acquired sequence clearly violates the Nyquist theorem. To better appreciate the performance of the proposed acquisition strategy, point-by-point differences  $\Delta x$  between the reconstructed signal  $\hat{x}$  and the input signal  $x$  is shown in Fig.4.6. Differences greater than 1 code have never been found, thus assuring a reconstruction error as low as 0.007%.

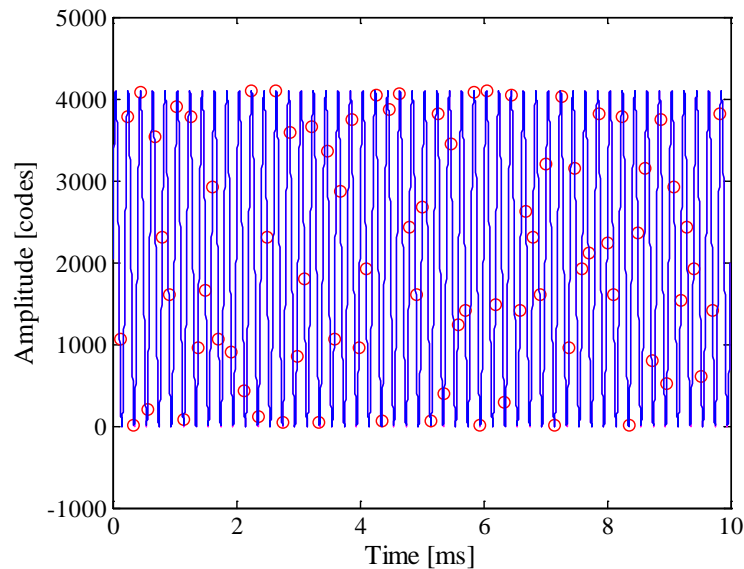


Fig.4. 5. Example of input signal, acquired samples (red circles), and reconstructed signal.

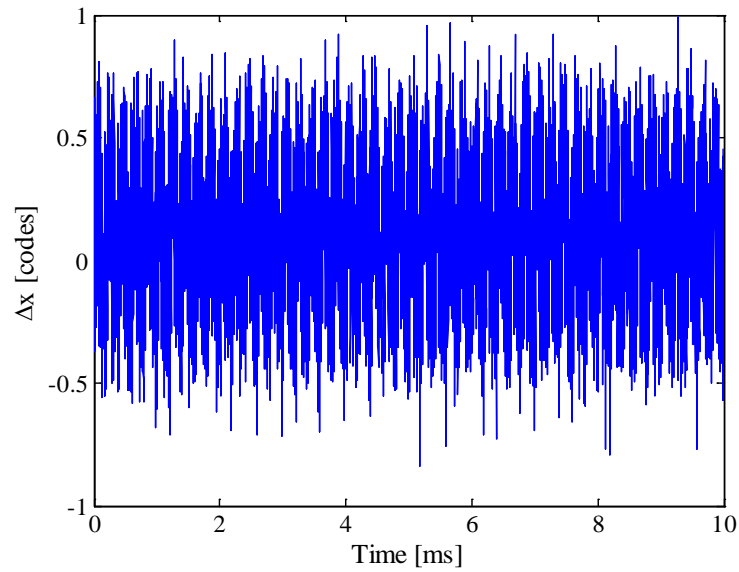


Fig.4. 6. Point-by-point differences between reconstructed and input signal.

Some results of the executed tests are summarized in Fig.4.7. As it can be seen, the performance of the acquisition strategy turned out to be almost independent from the nominal ADC sample rate. This way, the desired acquisition can be carried out by exploiting the ADC with the lowest available sample rate. It is so possible to make the ADC working in less critical conditions, thus allowing to take advantage of most of its effective number of bits. Moreover, for each test configuration in terms of  $n_{bit}$  and  $f_{conv}$ , reconstruction error proved to be lower than the associated least significant bit (LSB), thus assuring that no harmful artifacts have been introduced by the proposed strategy. Finally, to compare the performance of the proposed acquisition strategy with that granted by the traditional CS approach [24], the same test has been executed with a  $t_{conv}$  equal to  $t_c$  for each value of  $n_{bit}$ . The obtained values (i.e. the markers corresponding to a nominal ADC sample rate of 1 MHz in Fig.4.7) highlighted that no significant difference can be appreciated whatever the vertical resolution of ADC; this behavior can be easily explained if the equations system (5) is taken into account. Even though a suitable procedure for the generation of the random sequence of sampling instants has been defined, this choice involves no significant differences in solving the system (5). In other words, any random sequence is as good as any other from a theoretical point of view; only a negligible degradation in the mean performance is experienced, due to the time difference constraint (2) that slightly reduce the possible randomness of the sequence indexes. Similar considerations hold also in the other investigated test conditions.

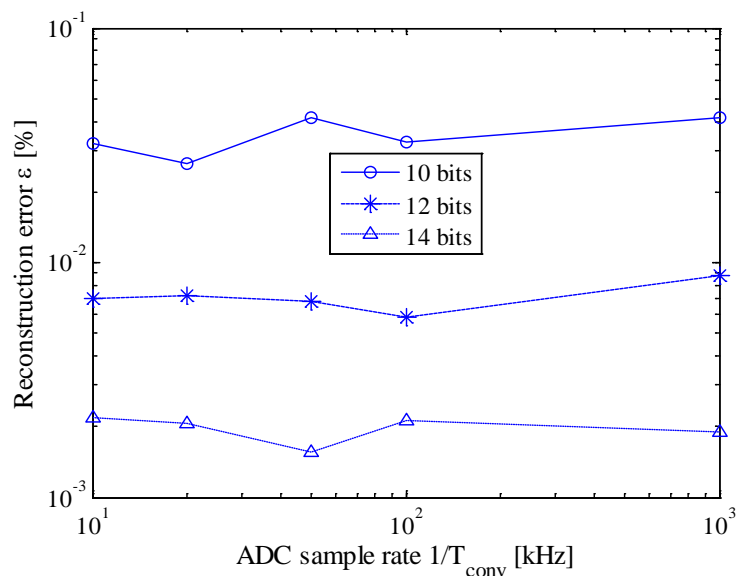


Fig.4. 7. Reconstruction error versus the ADC sample rate for different values ADC vertical resolutions; markers associated with an ADC nominal sample rate of 1MS/s accounts for traditional CS approach.

#### 4.4.2 Noise

The influence of the noise on the performance has successively been investigated. For each value of SNR, 1000 pseudo-random sequences generated according to an additive white Gaussian noise (AWGN) have been added to the input signal; the average value of reconstruction errors have been evaluated. As an example, some results, obtained for different values of effective number of bits, are shown in Fig.4.8. As expected, the higher the SNR, the better the performance of the proposed acquisition strategy. In particular, reconstruction error similar to those given in Fig.4.7 have been achieved only for the higher values of SNR.

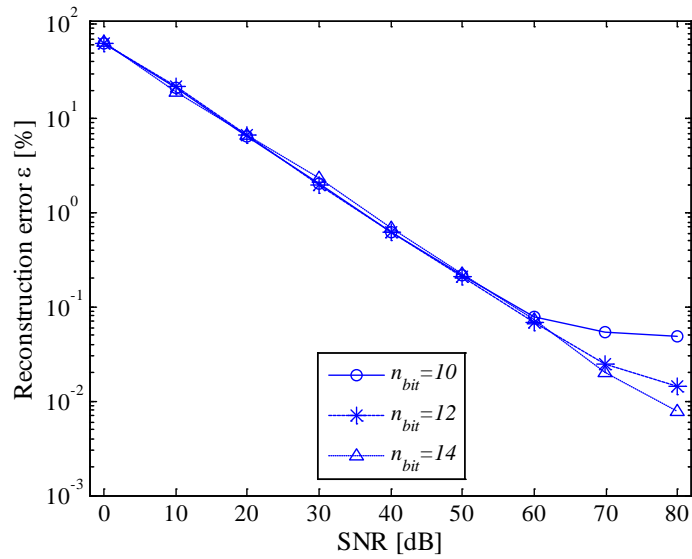


Fig.4. 8. Reconstruction error versus SNR; for different values of effective number of bits,  $n_{bit}$ .

#### 4.4.3 Number of Acquired Samples and Effective Sample Rate

A number tests have then been performed for different combinations both of number of random samples  $m$  and effective sampling frequency  $f_c$ . As an example, some results are summarized in Fig.4.9. As it can be appreciated, the difference between reconstructed and original signal is always lower than 1 LSB, including when only 20 random samples are acquired, i.e. in the presence of a compression ratio  $(1 - \frac{m}{n}) \cdot 100$  equal to 99.8%.

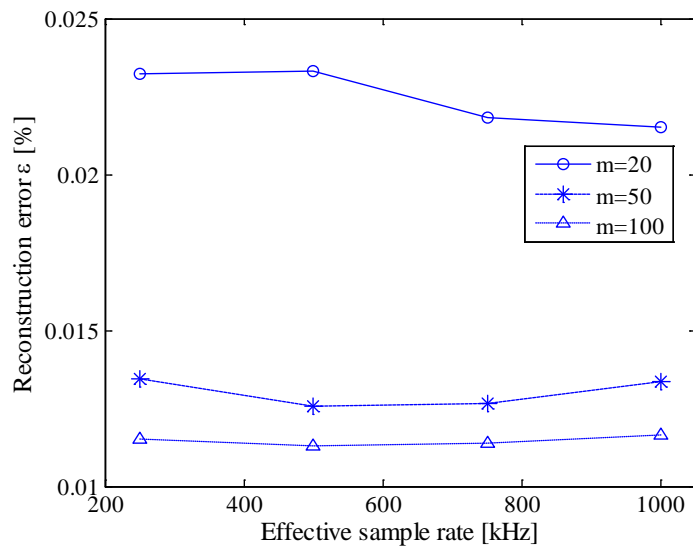


Fig.4. 9. Reconstruction error versus the effective sample rate  $f_c$  for different values of number  $m$  of randomly acquired samples.

#### 4.4.4 Jitter

As stated above, all the clock signals (included the high resolution time basis adopted by the proposed acquisition strategy) of an embedded system are derived from a fundamental clock, usually referred to as instruction cycle clock,  $f_{Ck}$ . Due to the specific architecture of the microcontroller and the software implementation of the time basis, a random difference between the nominal sampling instant and the effective one can occur. Such difference can be expressed in terms of number instruction cycles and typically assume integer values within 0 and 10 [23]. In other words, from the nominal SOC instant to its actual execution, a random number of instruction cycles could occur, due to latency or uninterruptable instructions problems. It is worth noting that this drawback can be mitigated but not completely eliminated and acts as a jitter on the high resolution time basis. Moreover, the actual jitter of the fundamental clock can be neglected in the following analysis, since its value is much lower than that associated to the instruction cycles. For the sake of the clarity, Fig.4.10a and Fig.4.10b show the actual SOC events (point-dashed lines) associated with a difference of two instruction cycles ( $T_{Jt}$ ) from the nominal SOC event (dashed line) in the presence of ratios  $f_{Ck}/f_c$  equal respectively to 1 and 4; the effect of the jitter on the actual digitized sample (circle marker) on the input signal (full line curve) is clearly reduced.

To analyze the effect of jitter, several scenarios have been simulated in terms of different values of ratio between instruction cycle clock frequency and effective sample rate. As an example, obtained results are presented in Fig.4.11 and Fig.4.12 for jitter values of 10 (worst case) and 2 (reduced jitter) instruction cycles, respectively.

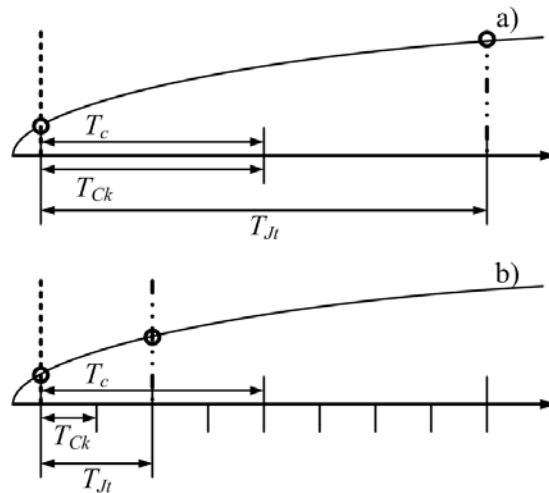


Fig.4. 10. Effect of instruction cycle jitter for different values of  $f_{Ck}/f_c$ .

As it can be appreciated in Fig.4.11, 10 instruction cycles jitter highly degrades the performance of the proposed acquisition strategy. As expected, the worst results have been experienced when the effective sample rate matched the instruction cycle clock frequency; in this case, a difference with respect to the nominal value up to ten sampling instants can occur. Better results have been obtained for higher values of the ratio  $f_{CK}/f_c$ . However, values of reconstruction error never lower than 0.1% have been encountered. The performance of the proposed acquisition strategy improves if the jitter is reduced down to 2 instruction cycles (Fig.4.12). Reconstruction errors of few hundredths can, in fact, be assured with a suitable level of ratio  $f_{CK}/f_c$ .

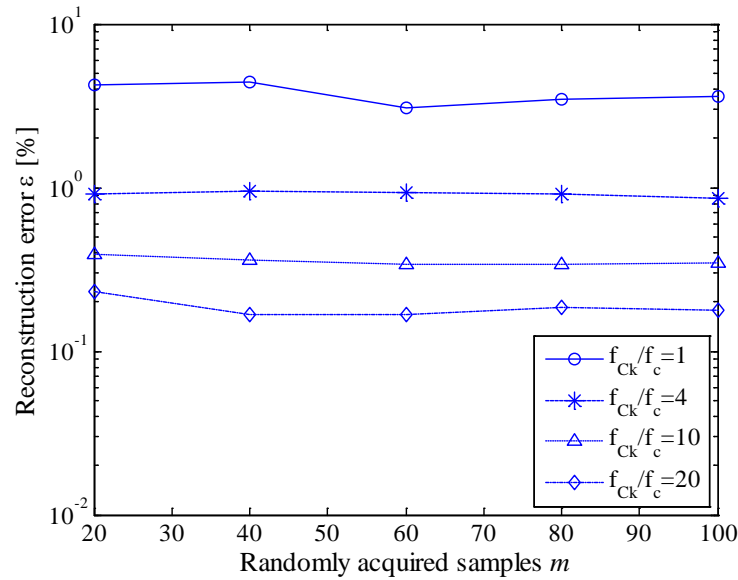


Fig.4. 11. Reconstruction error versus the number  $m$  of randomly acquired samples for different values of the ratio  $f_{CK}/f_c$ . when jitter equal to 10.

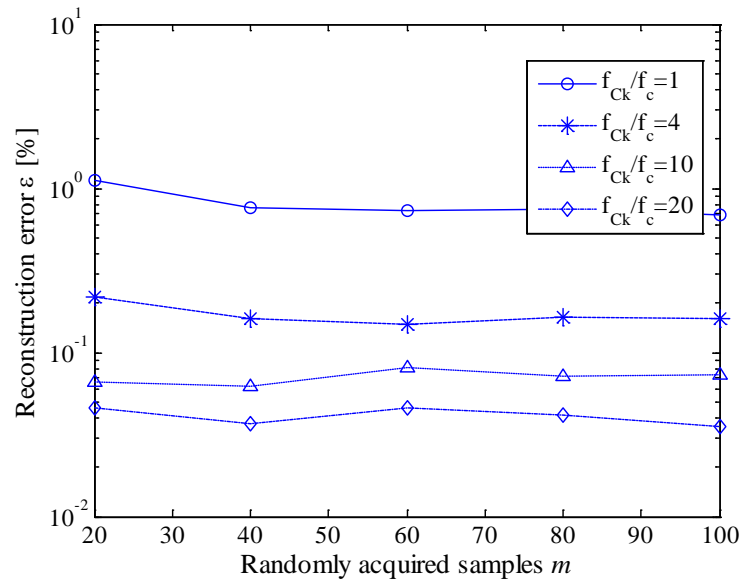


Fig.4. 12. Reconstruction error versus the number  $m$  of randomly acquired samples for different values of the ratio  $f_{Ck}/f_c$ , when jitter equal to 2.

#### 4.4.5 Input Signal Sparsity

Finally, the reconstruction error has been evaluated versus different values of number of acquired samples and number of spectral components included in the input signal (i.e. the signal sparsity in frequency domain). Specific test parameters are presented in Table II. As for the sparsity, its maximum value has been chosen according to eq.(14), once defined the highest number of random acquired samples. For each value of the signal sparsity 1000 numerical input signals have been generated by adding  $S$  spectral components whose amplitude, phase and location within the Nyquist band have randomly been selected. For each test configuration, minimum, average and maximum values of the reconstruction errors have been calculated in terms of  $m$  and  $S$ ; some of the results are reported in Table III.

**Table 2.** Parameters adopted in numerical tests conducted with different values of signal sparsity  $S$  and  $m$ .

Number of acquired samples $m$	[20, 40, 60, 80, 100]
Jitter [Instruction cycles]	2
SNR [dB]	50
$f_{Ck}/f_c$	20
Input signal sparsity $S$	[1,3,5,7,9,11]

As it can be expected, the higher the spectral content of the input signal, the higher the number of samples that have to be acquired in order to accurately reconstruct the signal. However, values of reconstruction error up to 10% has been experienced also when the input signal has been recovered from 100 random samples; this is mainly due to the effect of the considered jitter on spectral components characterized by higher frequency. This way, either the use of instruction cycle clocks with higher values of frequency or a greater number of random acquired samples is advisable to further mitigate this harmful effect.

**Table 3.** Reconstruction error, expressed in relative percentage value, obtained in numerical tests conducted with different values of signal sparsity  $S$  and  $m$ .

	$m=20$	$m=40$	$m=60$	$m=80$	$m=100$	
$S=1$	0.02	0.01	0.01	0.01	0.01	Min
	1.04	0.85	0.80	0.78	0.79	Avrg
	3.52	1.89	1.65	1.55	1.61	Max
$S=3$	0.28	0.05	0.05	0.05	0.05	Min
	10.86	1.32	0.59	0.54	0.52	Avrg
	22.45	11.88	1.56	1.38	1.32	Max
$S=5$	4.11	0.21	0.04	0.05	0.03	Min
	17.34	6.77	1.00	0.45	0.41	Avrg
	35.52	20.45	10.06	1.71	1.29	Max
$S=7$	12.15	1.41	0.25	0.11	0.08	Min
	21.55	13.28	5.69	0.61	0.38	Avrg
	51.58	22.71	17.26	2.47	1.11	Max
$S=9$	11.59	9.05	1.19	0.19	0.12	Min
	26.98	17.09	10.82	3.40	0.45	Avrg
	50.76	28.47	24.22	16.41	1.94	Max
$S=11$	11.61	9.06	5.82	0.90	0.19	Min
	28.10	19.15	14.49	8.34	2.28	Avrg
	56.48	26.18	25.37	19.26	9.48	Max

#### 4.5 Experimental Tests

A number of tests have finally been executed to assess the performance of the proposed acquisition strategy on two different cost-effective hardware architectures, characterized, respectively, by 8 and 32-bits core microcontrollers and specifications very close to those

presented in Section I and Section IV. A suitable measurement station has been setup (Fig.4.13), which includes:

- a microcontroller acting as DAS (either 8 or 32 bits);
- a dual-channel arbitrary function generator AFG3252C (maximum output frequency 240 MHz, 14 bits vertical resolution, 128 kSamples memory depth) by Tektronix;

a personal computer mandated to (i) generate the random sequence of sampling instants, (ii) transmit it to the low-cost DAS, (iii) receive back the acquired samples and (iv) process them by means of a free tool (namely CVX [25] and working in MATLAB™ environment).

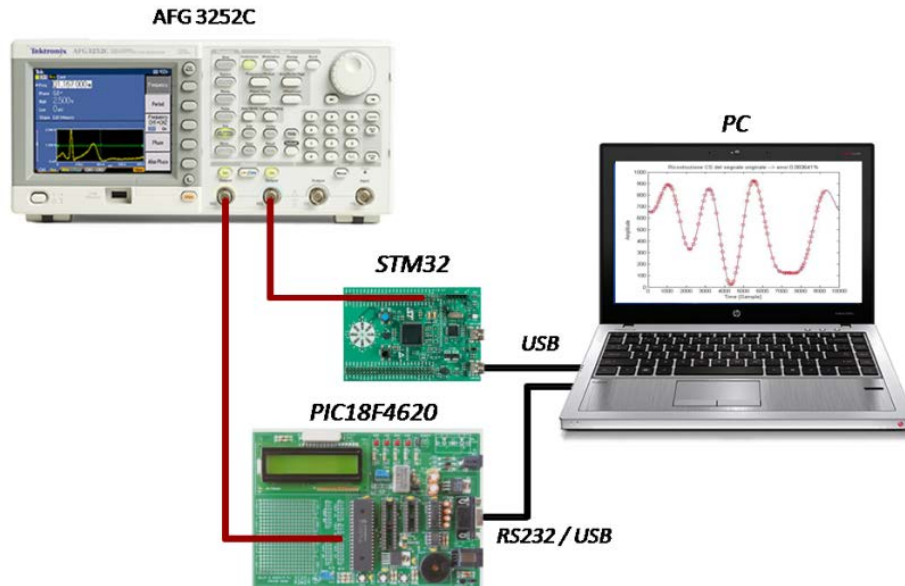


Fig.4. 13. Block diagram of the adopted measurement station.

Input signals characterized by several sparsity values have been taken into account. With specific regard to signals different from pure sinusoidal tones, the so-called optimized multisine [26], has been adopted as test signal. The optimized multisine can be expressed as the sum of cosine waveform according to:

$$x(t) = \sum_{h=1}^S A_h \cos(2\pi f_h t + \varphi_h) \quad (4.4)$$

where  $A_h$ ,  $f_h$ , and  $\varphi_h$  stand for the amplitude, frequency and phase of the  $h$ -th spectral component, respectively. Their values can easily be combined to generate a multitone signal whose amplitude is tailored to the ADC full scale range (3V and 5 V for 8 and 32-bits architecture respectively). In particular, for the considered application, the amplitude of the spectral components have been set to the same value in order to obtain a flat amplitude spectrum in the frequency region of interest. The phase of each component has been selected according to the criterion of crest factor (CF) minimization, thus assuring signals with suitable SNR in the whole observation interval. More specifically, Schroeder multisine [27] has been adopted; CF minimization was achieved by setting phase values according to the following expression:

$$\varphi_h = -\frac{h(h-1)}{S}\pi \quad (4.5)$$

As for the tests conducted in simulations, the reconstruction error has been adopted as the performance indicator. The best estimate of the input signal  $x$  has been gained through either the traditional four parameters sine-fit [28] or multisine interpolation [29] of the reconstructed signal, according to the corresponding test.

#### 4.5.1 Tests conducted on 32-bits microcontroller

The performance of the acquisition strategy have first been assessed on a STM32F303VCTM by STMicroelectronics, a microcontroller based on ARM Cortex M4 core. It is characterized by a maximum instruction cycle frequency  $f_{ck}$  equal to 72 MHz, data memory depth of 40 KB, four ADCs with selectable vertical resolution (6, 8, 10, and 12 bit) and full scale of 3 V [23]. The available values of  $T_{conv}$  consisted of the sum of:

- a constant term  $T_{SAR}$  equal to  $(n_{Bit}+0.5) T_{Ck}$  required for the execution of the operations of internal SAR ADC;
- a selectable term  $T_{Samp}$  ranging from 1.5 up to 601.5  $T_{Ck}$  accounting for the sampling time [23].

Unless otherwise indicated, the input signal for tests has been a pure unipolar sinusoidal signal whose full scale amplitude and frequency were equal respectively to 3 V<sub>pp</sub> and 1.2 kHz; 100 random samples have been digitized with a nominal vertical resolution of 12 bits and the input signal has been reconstructed over a time sequence of 10000 samples. The microcontroller was operated at its maximum instruction cycle frequency.

A first set of tests have been conducted to assess the influence of the nominal sample rate,  $f_{conv}$ , on the reconstruction performance of the proposed strategy. As expected, the higher the value of  $T_{conv}$ , (due to greater values of  $T_{Samp}$ ), the better the strategy performance, to the detriment of the ADC nominal sample rate. As an example, Table IV summarizes the results obtained on a sinusoidal signal with frequency equal to 6 kHz, for effective sample rate ranging from 1 MS/s and 12 MS/s: severe performance degradation has been experienced with the lowest value of  $T_{conv}$  (195 ns). This is mainly due to limited duration of the associated sampling time; this way, largest  $T_{conv}$  (usually  $32 T_{Ck}$ ) have been adopted in the successive experimental tests.

**Table 4.** Effect of  $T_{conv}$  (expressed in terms of multiple of fundamental instruction clock  $t_{Ck}$ ), on mean reconstruction errors and experimental standard deviation for different conditions of effective sample rate.

	m=20			m=50			m=100			$t_{Conv} [t_{Ck}]$
	14	32	194	14	32	194	14	32	194	
$f_c = 1 \text{ MS/s}$	0.278	0.057	0.076	0.235	0.078	0.079	0.124	0.083	0.080	<b>Avrg</b>
	0.068	0.008	0.019	0.047	0.024	0.021	0.021	0.008	0.007	<b>Std</b>
$f_c = 2 \text{ MS/s}$	0.267	0.075	0.066	0.168	0.079	0.081	0.100	0.081	0.079	<b>Avrg</b>
	0.053	0.017	0.009	0.021	0.015	0.012	0.014	0.015	0.009	<b>Std</b>
$f_c = 4 \text{ MS/s}$	0.243	0.073	0.060	0.116	0.075	0.072	0.109	0.081	0.078	<b>Avrg</b>
	0.045	0.019	0.010	0.057	0.006	0.010	0.059	0.006	0.003	<b>Std</b>
$f_c = 12 \text{ MS/s}$	0.125	0.069	0.069	0.087	0.081	0.089	0.094	0.079	0.083	<b>Avrg</b>
	0.051	0.016	0.012	0.047	0.011	0.009	0.021	0.011	0.007	<b>Std</b>

More exhaustive tests have been carried out on pure sinusoidal signals in different conditions of input signal frequency  $f_s$ , number of acquired samples  $m$ , ADC actual sample rate  $f_{conv}$  and frequency ratio  $f_{Ck}/f_c$ . For each test configuration, 100 acquisitions have been made and the reconstruction error has been evaluated in terms of its mean and standard deviation values. In order to compare the results of the different configurations, the same sequence of random sampling instants has always been adopted. As an example, Fig.4.14 shows some results obtained when  $T_{conv}$  and  $f_c$  were equal respectively to  $2.7 \mu\text{s}$  and 12 MS/s. Similar results have been gained in the other tests configurations. The reconstruction error got

worse for higher values of input signal frequency; the main reason for this was the effect of the instruction cycle jitter, as it can be noticed in Fig.4.14 and Table V.

In particular, Fig.4.15 reports the evolution of the mean reconstruction error versus the effective sample rate of the converter for 6 kHz input signal; as it can be noticed, the higher the effective sample rate, the better the reconstruction error, since the jitter effect is reduced. The jitter effect is more evident from the results reported in Table V, which refer to a sinusoidal signal with frequency equal to 60 kHz, while the fundamental instruction clock adopted for the time basis was equal either to 12 and 72 MS/s.

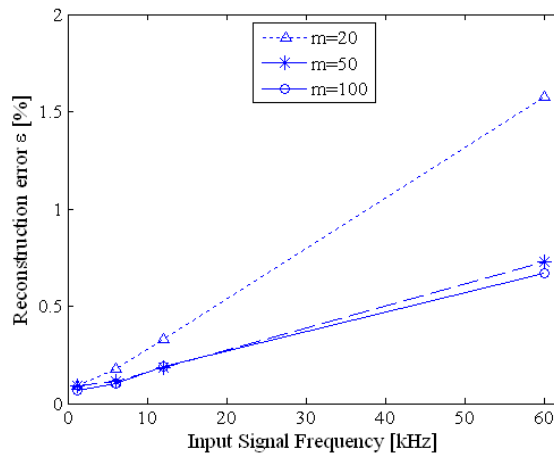


Fig.4.14. Reconstruction error versus the input signal frequency for different number  $m$  of randomly acquired samples.

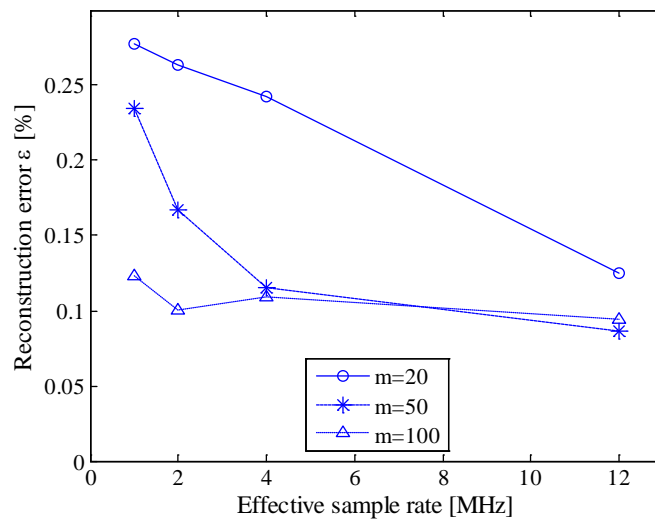


Fig.4. 15. Reconstruction error versus the effective sample rate for different number  $m$  of randomly acquired samples.

A specific feature of the arbitrary function generator has been exploited to assess the performance of the acquisition strategy in the presence of noisy signals. To this aim, wideband AWGN signals (characterized by different amplitude levels and 240 MHz bandwidth) have been generated and added to the signal of interest. Fig.4.16 shows the results obtained when  $T_{conv}$  and  $f_c$  were equal, respectively, to 2.7  $\mu$ s and 12 MS/s; results similar to those achieved without noise are granted only for SNR higher of 50 dB, i.e. the SNR value corresponding to the effective quantization noise of the adopted ADC.

**Table 5.** Mean reconstruction errors and experimental standard deviation for different conditions of effective sample rate and fundamental instruction cycle clock.

	<b>m=20</b>	<b>m=50</b>	<b>m=100</b>	
<b><math>f_c = 1MS/s</math></b>	6.5	1.94	1.85	<b>Avrg</b>
<b><math>f_{Ck}=12\text{ MHz}</math></b>	1.2	0.34	0.30	<b>Std</b>
<b><math>f_c = 1MS/s</math></b>	3.3	0.97	0.93	<b>Avrg</b>
<b><math>f_{Ck}=72\text{ MHz}</math></b>	0.9	0.12	0.13	<b>Std</b>
<b><math>f_c = 2MS/s</math></b>	4.4	1.18	1.12	<b>Avrg</b>
<b><math>f_{Ck}=12\text{ MHz}</math></b>	0.8	0.12	0.11	<b>Std</b>
<b><math>f_c = 2MS/s</math></b>	2.5	0.76	0.72	<b>Avrg</b>
<b><math>f_{Ck}=72\text{ MHz}</math></b>	0.6	0.08	0.07	<b>Std</b>
<b><math>f_c = 4MS/s</math></b>	3.2	1.13	1.08	<b>Avrg</b>
<b><math>f_{Ck}=12\text{ MHz}</math></b>	0.6	0.11	0.10	<b>Std</b>
<b><math>f_c = 4MS/s</math></b>	2.1	0.72	0.68	<b>Avrg</b>
<b><math>f_{Ck}=72\text{ MHz}</math></b>	0.4	0.13	0.10	<b>Std</b>
<b><math>f_c = 12MS/s</math></b>	1.9	0.71	0.73	<b>Avrg</b>
<b><math>f_{Ck}=12\text{ MHz}</math></b>	0.4	0.08	0.07	<b>Std</b>
<b><math>f_c = 12MS/s</math></b>	1.6	0.62	0.67	<b>Avrg</b>
<b><math>f_{Ck}=72\text{ MHz}</math></b>	0.3	0.06	0.05	<b>Std</b>

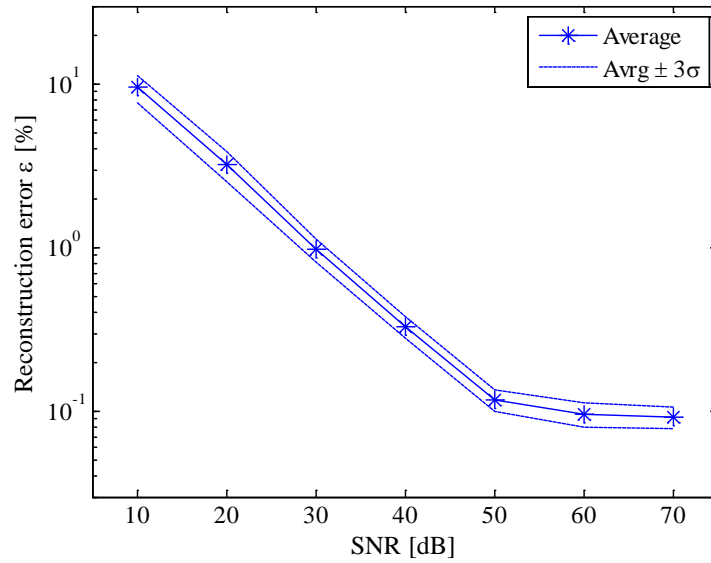


Fig.4.16. Reconstruction error versus signal-to-noise ratio.

The effect of the input sparsity has, finally, been investigated by means of the aforementioned multisine signal. To this aim, signals composed by different harmonic components have been taken into account. As an example, the results obtained for input signal involving up to 11 spectral components when  $T_{conv}$  and  $f_c$  were equal respectively to 444 ns and 12 MS/s, which are given in Fig.4.17, show that the higher the spectral content, the worse the reconstruction error. Nevertheless, satisfying results ( $\epsilon < 1\%$ ) are granted in the whole analysis range.

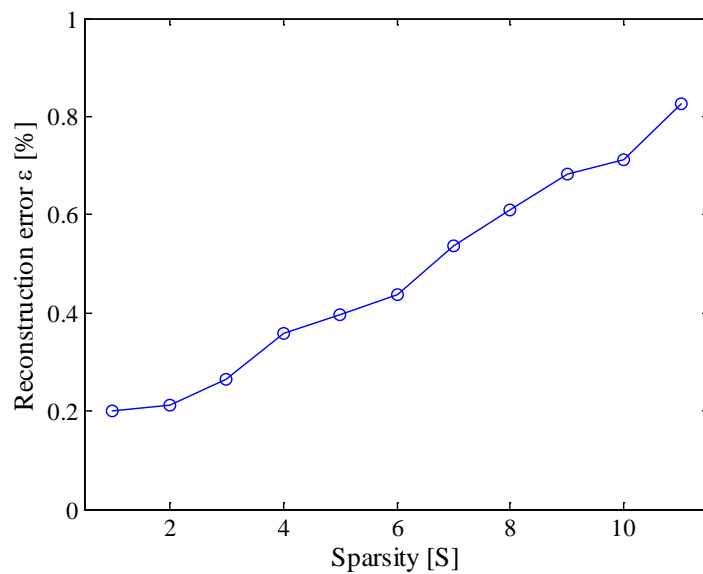


Fig.4. 17. Reconstruction error versus the sparsity of the signal

### 4.5.2 Tests conducted on 8-bits microcontroller

Further experiments have been carried out on PIC18F4620 by Microchip, a typical example of very low cost, low performance 8-bit microcontroller. It is characterized by a maximum instruction cycle frequency  $f_{ck}$  equal to 10 MHz, data memory depth of 4 kB, a single ADC with selectable vertical resolution (8 and 10 bit) and full scale of 5 V [22].

With regard to the considered configuration, a traditional external 4 MHz clock has been adopted, thus granting an effective  $f_{ck}$  equal to 1 MHz. Similarly to the 32-bits microcontrollers, the nominal conversion interval  $T_{conv}$  is given by the sum of a constant term equal to  $11 T_{ck}$  (needed for the digitization of the single sample) and a tunable sampling time ranging from 2 up to  $20 T_{ck}$  [22]. Tests have been conducted to the minimum  $T_{conv}$  (i.e. 15  $\mu$ s) capable of assuring reliable conversion of the input signal, thus granting a theoretical maximum sample rate of about 66 kS/s. Unfortunately, the actual sample rate was limited to 20 kS/s due to some instructions (beyond the traditional registers move) needed to implement the random acquisition strategy. Even in the presence of highly optimized assembly implementation of the code, no new acquisitions could start before the considered instructions have been executed. Thanks to the CS-based approach, the considered drawback has not only been recovered, but also overcome with sample rate values otherwise unavailable on the device.

A first set of measurements involved different conditions of input signals frequency and number of acquired samples. Experiments have been conducted at an effective sampling rate  $f_c$  equal to 1 MS/s (i.e. the worst condition in terms of instruction jitter) and nominal vertical resolution  $n_{bit}$  equal either to 8 or 10 bits. As for the successive tests, signal amplitude has been set to match the ADC full scale (5V). For each test configuration, 100 successive random sequences have been acquired; as for the 32 bits microcontroller, the same sequences of sampling instants have been adopted in order to compare the performance throughout the different configurations. Some results, in terms of average reconstruction error and experimental standard deviation, are reported in Table VI and Table VII for 10 and 8 bits resolution, respectively.

Table 6. Mean reconstruction errors and experimental standard deviation with nominal vertical resolution of 10 bits.

<b>fs (Hz)</b>	<b>m=20</b>	<b>m=50</b>	<b>m=100</b>	
100	0.47	0.32	0.04	<b>Avrg</b>
	0.16	0.10	0.01	<b>Std</b>
500	2.9	2.3	0.28	<b>Avrg</b>
	0.2	0.2	0.01	<b>Std</b>
1000	4.4	4.4	0.55	<b>Avrg</b>
	0.4	0.3	0.02	<b>Std</b>

As it could be expected, the highest the number of acquired samples, the better the reconstruction performance. This is particularly true for signals characterized by the highest frequency values, in correspondence of which the effect of instruction cycle jitter proved to be worse; jitter influence was so high in such conditions that similar results have been achieved for both vertical resolutions. As for the 32-bits microcontroller, its effect should be mitigated by setting higher values of instruction cycle frequencies.

Table 7. Mean reconstruction errors and experimental standard deviation with nominal vertical resolution of 8 bits.

<b>fs (Hz)</b>	<b>m=20</b>	<b>m=50</b>	<b>m=100</b>	
100	0.48	0.36	0.18	<b>Avrg</b>
	0.15	0.09	0.01	<b>Std</b>
500	2.9	2.2	0.32	<b>Avrg</b>
	0.3	0.2	0.03	<b>Std</b>
1000	4.4	4.3	0.58	<b>Avrg</b>
	0.4	0.4	0.03	<b>Std</b>

The effect of noise on reconstruction performance has then been assessed by means of several tests conducted with different levels of AWGN signals and number of acquired samples. The test signal was a pure sinusoidal tone whose frequency has been set to 100 Hz. As an example, some results obtained for SNR values varying upon the interval from 20 up to 50 dB are shown in Table VIII. As it can be noticed, obtained results are better than those achieved in tests conducted through numerical simulations. Experienced improvement mainly

relies on the reduced input bandwidth of the considered ADC (few tens of kHz), capable of cutting most of the high bandwidth (240 MHz) added noise.

Further tests have finally been conducted with optimized **multisine** input signals. Different conditions of signal sparsity and number of acquired samples have been taken into account. As an example, Fig.4.18 shows estimated input signal, acquired samples and the reconstructed signal when  $S$  and  $m$  were equal respectively to 5 and 100. More details can be appreciated in Fig.4.19, where the point-by-point differences between reconstructed and input signal is plotted. Some results are given in Table IX. No reliable results were obtained with a number of acquired samples lower than 20, while 50 samples allowed to reconstruct the input signal with no more than 7 spectral components; as it can be expected, the best results were achieved only when at least 100 random samples were acquired.

**Table 8.** Mean reconstruction errors and experimental standard deviation in different noise conditions.

<b>SNR (dB)</b>	<b>m=20</b>	<b>m=50</b>	<b>m=100</b>	
20	1.5	1.5	1.5	<b>Avrg</b>
	0.2	0.2	0.2	<b>Std</b>
30	0.62	0.58	0.52	<b>Avrg</b>
	0.10	0.11	0.05	<b>Std</b>
40	0.51	0.36	0.20	<b>Avrg</b>
	0.15	0.10	0.03	<b>Std</b>
50	0.53	0.35	0.14	<b>Avrg</b>
	0.14	0.09	0.02	<b>Std</b>

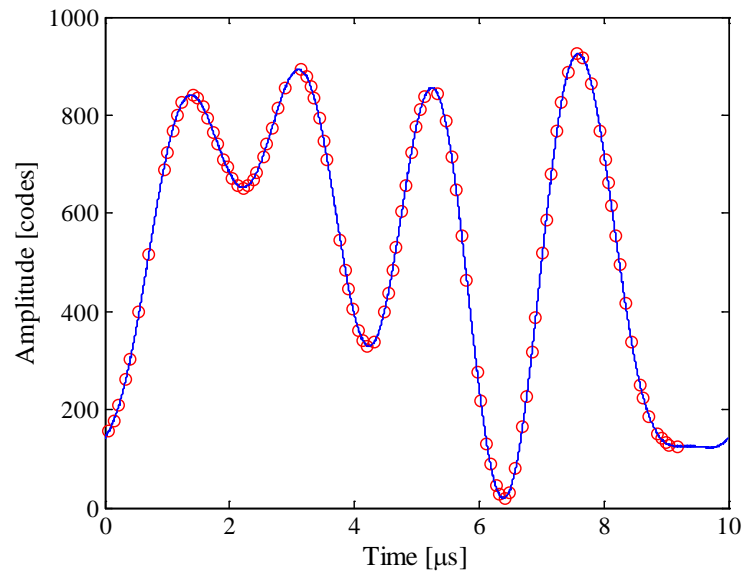


Fig.4. 18. Example of estimated input signal, acquired samples (red circles), and reconstructed signal in the presence of 5-components multisine.

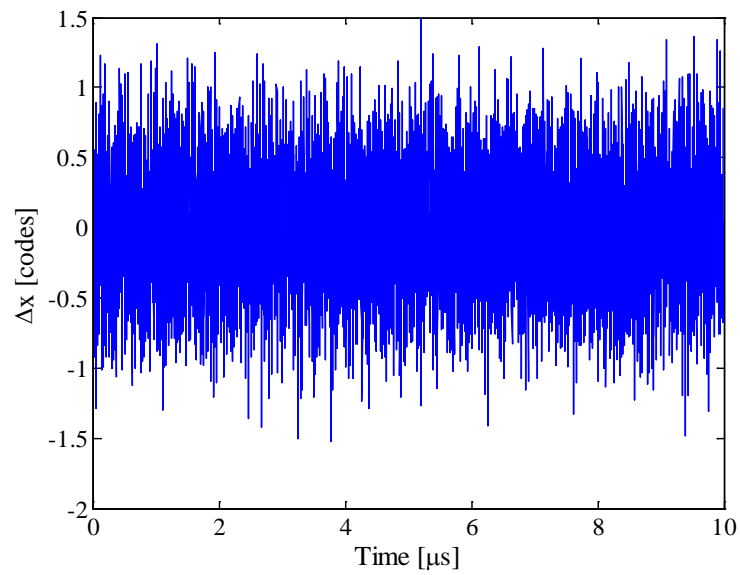


Fig.4.19. Point-by-point differences between reconstructed and input signal.

**Table 9.** Mean reconstruction errors and experimental standard deviation in different conditions of input signal sparsity.

Sparsity	m=50	m=100	
3	0.60	0.09	<b>Avrg</b>
	0.22	0.01	<b>Std</b>
5	2.5	0.29	<b>Avrg</b>
	0.8	0.04	<b>Std</b>
7	4.6	0.35	<b>Avrg</b>
	1.2	0.11	<b>Std</b>
9	-	0.53	<b>Avrg</b>
	-	0.16	<b>Std</b>
11	-	0.62	<b>Avrg</b>
	-	0.21	<b>Std</b>

#### 4.6 Conclusions

In this Chapter a new acquisition strategy, based on compressive sampling, for the improvement of the effective sampling rate of ADC usually integrated in microcontrollers or embedded systems has been presented. The proposed strategy is tailored on cost-effective embedded systems characterized by reduced performance in terms of data acquisition block, and exploits the availability of a high resolution time basis to finely set the sampling instants of the random samples acquired through a low-rate ADC. Thanks to the adopted CS approach, the signal of interest can be reconstructed with the same time basis, thus enhancing the sample rate.

Preliminary tests conducted in simulations highlighted the promising effective performance of the proposed strategy in the presence of signals characterized by different amplitude and spectral contents. Experimental tests have also been carried out on microcontrollers characterized by different internal architecture and operating specifications. It is worth highlighting that satisfying results were obtained with both embedded systems, with increase of effective sample rate up to 50 times with respect of the actual ADC sample rate. Different measurement conditions in terms of input signal and noise have been taken into account as well as several configurations of acquisition parameters, such as effective sample rate, nominal number of bits and number of acquired random samples. The results obtained

and discussed can be adopted as guidelines in choosing the proper trade-off between desired reconstruction error and computational burden.

#### **4.7References**

- [1] Landi, C.; Luiso, M.; Pasquino, N.; A remotely controlled onboard measurement system for optimization of energy consumption of electrical trains. *IEEE Transactions on Instrumentation and Measurement* 2008, Volume 57, n. 10, pp. 2250-2256.
- [2] Sarkar, A.; Sengupta, S.; Design and implementation of a low cost fault tolerant three phase energy meter. *Measurement: Journal of the International Measurement Confederation* 2008, Volume 41, n.9, pp.1014-1025.
- [3] Adamo, F.; Attivissimo, F.; Cavone, F.; Di Nisio, A.; Spadavecchia, M.; Channel Characterization of an Open Source Energy Meter. *IEEE Transactions on Instrumentation and Measurement* 2014, Volume 63, n.5, pp.1106-1115.
- [4] Demirci, T. et al., Nationwide real-time monitoring system for electrical quantities and power quality of the electricity transmission system. *IET Generation, Transmission & Distribution* 2011. Volume 5, n.5, pp.540 - 550.
- [5] Gallo, D.; Landi, C.; Pasquino, N.; An instrument for objective measurement of light flicker. *Measurement: Journal of the International Measurement Confederation* 2008, Volume 41, n.3, pp.334-340.
- [6] Lamonaca, F.; Nastro, V.; Nastro, A.; Grimaldi, D.; Monitoring of indoor radon pollution. *Measurement: Journal of the International Measurement Confederation* 2014, Volume 47, pp.228-233.
- [7] D'Apuzzo, M.; Liccardo, A.; Bifulco, P.; Polisiero, M.; Metrological issues concerning low cost EMG-controlled prosthetic hand. In *Proceedings of IEEE International Instrumentation and Measurement Technology Conference*, Graz, Austria, May, 13-16, 2012, pp. 1481-1486.
- [8] Melillo, P.; Santoro, D.; Vadursi, M.; Detection and compensation of inter-channel time offsets in indirect Fetal ECG sensing. *IEEE Sensors Journal* 2014, Volume 14, n. 7, pp. 2327-2334.
- [9] Baccigalupi, A.; D'Arco, M.; Liccardo, A.; Vadursi, M. ; Testing high resolution DACs: a contribution to draft standard IEEE P1658. *Measurement: Journal of the International Measurement Confederation* 2011, Volume 44, pp.1044-1052.

- [10] Buonanno, A.; D'Urso, M.; Prisco, G.; Felaco, M.; Angrisani, L.; Ascione, M.; Schiano Lo Moriello, R.; Pasquino, N.; A new measurement method for through-the-wall detection and tracking of moving targets. *Measurement: Journal of the International Measurement Confederation* 2013, Volume 46, n.6, pp. 1834-1848.
- [11] Ascione, M.; Buonanno, A.; D'Urso, M.; Angrisani, L.; Schiano Lo Moriello, R.; A New Measurement Method Based on MUSIC Algorithm for Through-the-Wall Detection of Life Signs. *IEEE Transactions on Instrumentation and Measurement* 2013, Volume 62, n.1, pp.13-26.
- [12] Angrisani, L.; D'Arco, M.; Ianniello, G.; Vadursi, M.; An Efficient Pre-Processing Scheme to Enhance Resolution in Band-Pass Signals Acquisition. *IEEE Transactions on Instrumentation and Measurement* 2012, Volume 61, pp. 2932-2940.
- [13] Angrisani, L.; Vadursi, M.; On the optimal sampling of bandpass measurement signals through data acquisition systems. *Measurement Science & Technology* 2008, Volume 19, n. 4, pp. 1-9.
- [14] D'Arco, M.; Genovese, M.; Napoli, E.; Vadursi, M.; Design and Implementation of a Preprocessing Circuit for Bandpass Signals Acquisition. *IEEE Transactions on Instrumentation and Measurement* 2014, Volume 63, pp. 287-294.
- [15] Texas instruments, "MSP430F42xA Mixed Signal Microcontroller," Datasheet, Feb. 2008.
- [16] Analog Devices, "AD9244, 14-Bit, 40 MSPS/65 MSPS A/D Converter Rev.C," Datasheet, 2005.
- [17] Zhao, Y.; Hu, Y. H.; Wang, H.; Enhanced Random Equivalent Sampling Based on Compressed Sensing. *IEEE Transactions on Instrumentation and Measurement* 2012, Volume 61, n.3, pp.579-585.
- [18] Trakimas, M.; D'Angelo, R.; Aeron, S.; Hancock, T.; Sonkusale, S. ; A Compressed Sensing Analog-to-Information Converter With Edge-Triggered SAR ADC Core. *IEEE Transactions on Circuits And Systems* 2013, Volume 60, n.5, pp. 1135-1148.
- [19] Chen, X.; Yu, Z.; Hoyos, S.; Sadler, B. M.; Silva-Martinez, J.; A Sub-Nyquist Rate Sampling Receiver Exploiting Compressive Sensing. *IEEE Transactions on Circuits And Systems* 2011, Volume 58, n.3, pp. 507-520.

- [20] Bao, D.; Daponte, P.; De Vito, L.; Rapuano, S.; Defining frequency domain performance of Analog-to-Information Converters. In Proceedings of 19th Symposium IMEKO TC-4, Barcelona, Spain, July, 18-19, 2013, pp. 748-753.
- [21] Candès, E.; Romberg, J.; Tao, T.; Robust uncertainty principles: Exact signal reconstruction from highly incomplete frequency information. *IEEE Transactions on Information Theory* 2006, Volume 52, n. 2, pp. 489–509.
- [22] PIC18F4620 Data Sheet, 28/40/44-Pin Enhanced Flash Microcontrollers with 10-Bit A/D and nano Watt Technology, Microchip.
- [23] RM0316 Reference Manual, “STM32F302xx, STM32F303xx and STM32F313xx advanced ARM-based 32-bit MCUs,” Mar. 2013 STMicroelectronic.
- [24] Chen, X.; Yu, Z.; Hoyos, S.; Sadler, B. M.; Silva-Martinez, J.; A Sub-Nyquist Rate Sampling Receiver Exploiting Compressive Sensing. *IEEE Transactions on Circuits And Systems* 2011, Volume 58, n.3, pp. 507-520.
- [25] CVX: Matlab Software for Disciplined Convex Programming, Version 2.0 (beta), October 2013, <http://cvxr.com/cvx/>.
- [26] Carnì, D.L.; Grimaldi, D.; Voice quality measurement in networks by optimized multi-sine signals, *Measurement: Journal of the International Measurement Confederation* 2008, Volume 41, n.3, pp. 266-273.
- [27] Schroeder, M. A.; Synthesis of low peak-factor signals and binary sequences of low autocorrelation. *IEEE Transaction on Information Theory* 1970, Volume 16, pp. 85–89.
- [28] Standard IEEE 1241-2010, IEEE Standard for Terminology and Test Methods for Analog-to-Digital Converters, 2011.
- [29] Ramos, P.M.; Serra, A.C.; Least-squares multiharmonic fitting: convergence improvements. *IEEE Transaction on Instrumentation and Measurement* 2007, Volume 56, n. 4, pp. 1412–1418

## **5 Compliance assessment of the CS based architecture in Harmonic and Interharmonic Measurements.**

### **5.1 Introduction**

Recently, the increasing use of electronic devices and the large use of renewable energy sources in the transmission grid are leading to the generation of power quality disturbances. Consequently, in order to evaluate the power quality in a grid, the capability of measuring disturbances and the identification of their sources is becoming very relevant. The measurement system of the grid electrical quality has to be distributed, with the measurement nodes that locally acquire the signals, process the sample in order to calculate the quantities of interest, and send them back to a central collecting and processing unit.

As it can be expected, the number of measurement nodes increases according to the extension of the monitored grid. Even though the cost of the single nodes should not be excessive (ranging from 10 k€ for high performance meter down to few hundreds of euro for devices not compliant with the current measurement standards), deploying thousands of such devices turns rapidly to be very expensive.

To overcome the considered limitation, the research activities presented in the previous chapters suggest evidenced the possibility to move towards a different approach for monitoring grid deployed on wide geographical areas, exploiting the advantages of an innovative measurement approach: the Compressed Sampling. In particular, the proposed architecture consists of low cost nodes mandated only to acquire and digitize a limited number of input signal samples and transmit them to a central measurement unit, saving, thus, the costs related to large memory supports and expensive digital processing units. Once the samples have been received, the central unit recovers the signal spectrum thanks to CS-based algorithm and carries out the desired measurements. In the following, a number of numerical and experimental tests assessed that the measurement node based on CS approach is compliant with the current Power Quality standard. In particular, the capability of CS-based acquisition approach of correctly measuring root-mean-square amplitude of harmonic and interharmonic voltage pollution has been verified.

## 5.2 The proposed approach

The standard IEC 61000-4-7 (*Electromagnetic compatibility (EMC) Part 4: Testing and measurement techniques Section 7: General guide on harmonics and interharmonics measurements and instrumentation, for power supply systems and equipment connected thereto*) suggests a method of interharmonics measurement based on the concept of the so-called “grouping”. Its basis is Fourier analysis performed in a time-window equal to 10 cycles of the fundamental frequency (50Hz), i.e. approximately 200 ms. Sampling is synchronised with the power supply frequency by means of a phase-locked loop. The result is a spectrum with 5 Hz resolution.

The sample rate, according to the Nyquist theorem, has to be set equal or greater than 10 kS/s, whereas the number of samples has to be equal or greater than 2000, since 100 harmonics are spread over 1000 bins. In order to exploit the Fast Fourier Transform (FFT) algorithm, a number of samples equal to a power of two is usually preferred. Successively, the spectrum is further processed according to the standard, in order to estimate the harmonics and interharmonics pollution affecting the measured voltage.

In particular, as recommended by the IEC 61000-4-7 standard, the process is based on grouping and subgrouping of spectral components. These operations allows to measure the harmonic and interharmonic amplitudes even in the presence of slight fluctuation of frequency, which causes that the energy of a harmonic component spreads over different bins of the spectrum. The grouping operation for the estimation of harmonics amplitude is shown Fig. 5.1a, whereas the subgrouping one is shown in Fig. 5.1b. With regard to the harmonic components, if  $k_h$  is the frequency bin associated to the the  $h^{\text{th}}$  order component, the amplitude of the  $h^{\text{th}}$  harmonic group  $X_{hg,h}$  is obtained by taking into account the amplitudes  $X$  of the ten nearest bins, according to the formula:

$$X_{hg,h} = \sqrt{\frac{1}{2}X_{k_h-5}^2 + \sum_{i=-4}^4 X_{k_h+i}^2 + \frac{1}{2}X_{k_h+5}^2} \quad (5.1)$$

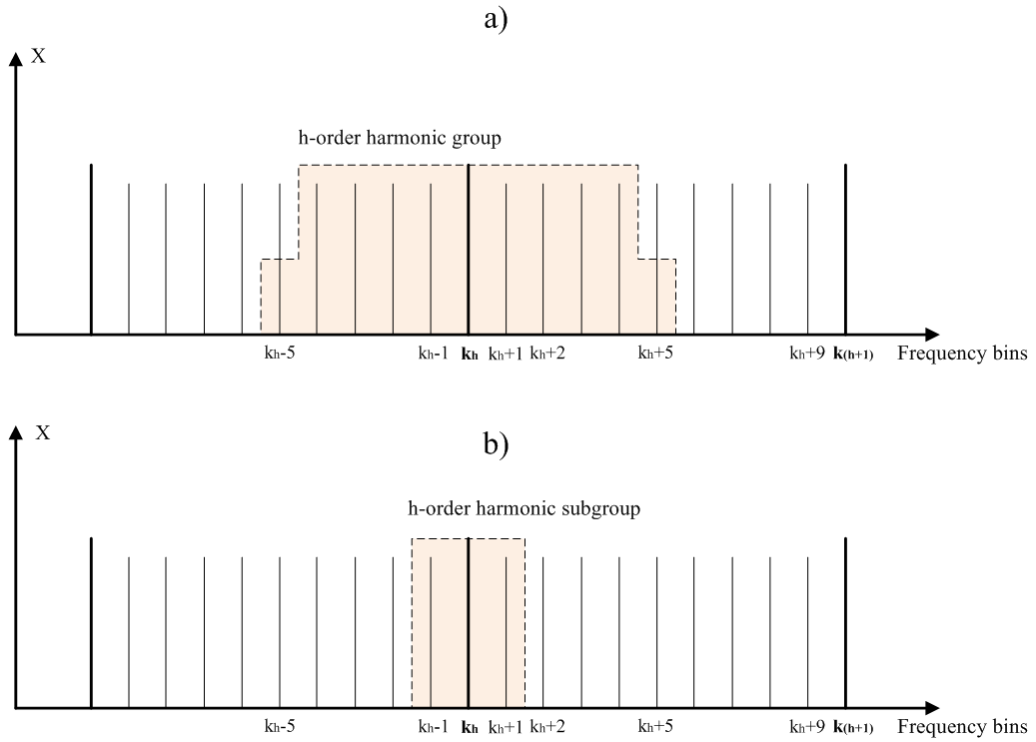


Fig.5.1 a) Harmonic group b) Harmonic subgroup.

The amplitude of the harmonic subgroup  $X_{hsg,h}$ , of the  $h^{\text{th}}$  order, instead, is obtained by taking into account the two nearest bins:

$$X_{hsg,h} = \sqrt{\sum_{i=-1}^1 X_{k_h+i}^2} \quad (5.2)$$

Similarly, the amplitude of the  $h$ th interharmonic group  $X_{ig,h}$  is defined according to:

$$X_{ig,h} = \sqrt{\sum_{i=1}^9 X_{k_h+i}^2} \quad (5.3)$$

The amplitude of the  $h$ th interharmonic subgroup group  $X_{isg,h}$  is given by:

$$X_{isg,h} = \sqrt{\sum_{i=2}^8 X_{k_h+i}^2} \quad (5.4)$$

For the sake of clarity, a graphical representation of interharmonic group and subgroup is shown in Fig. 5.2.

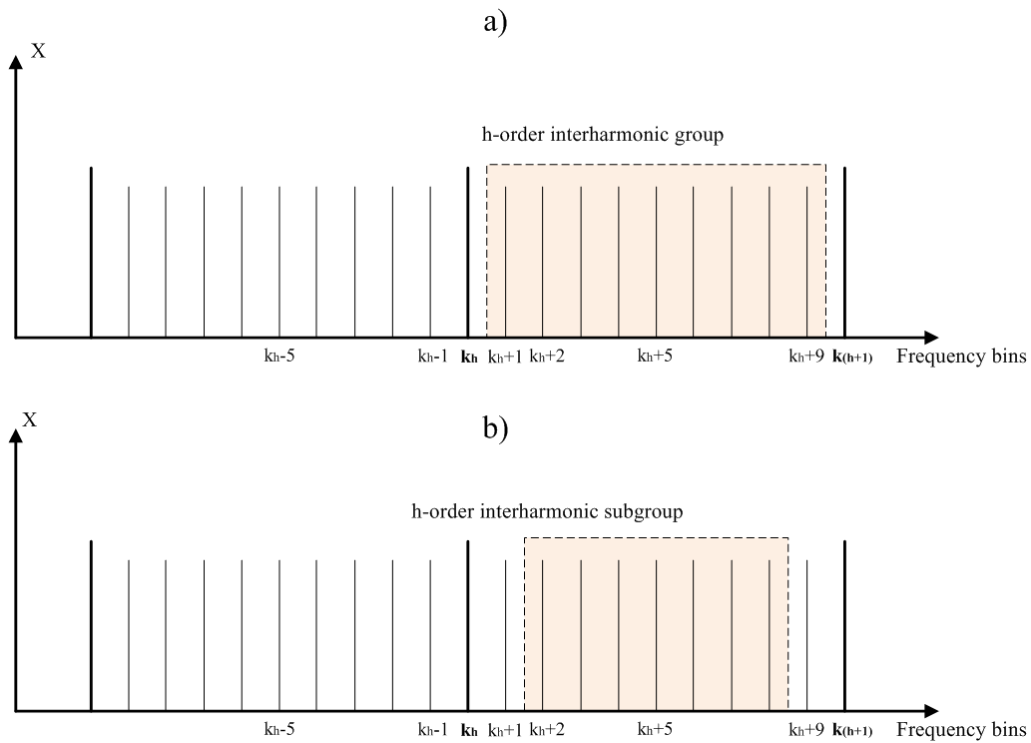


Fig.5.2 a) Interharmonic group b) Interharmonic subgroup.

In the proposed approach, instead, only  $M \ll N$  samples of the input signal are digitized; but in order to assure the frequency resolution compliant to the standard, the sampling process still have to be synchronized with the fundamental input frequency with the aim of acquiring an observation interval involving exactly 10 periods of the input signal.

To this aim, the internal architecture of the proposed CS-based Sensor Node is shown in Fig.5.3

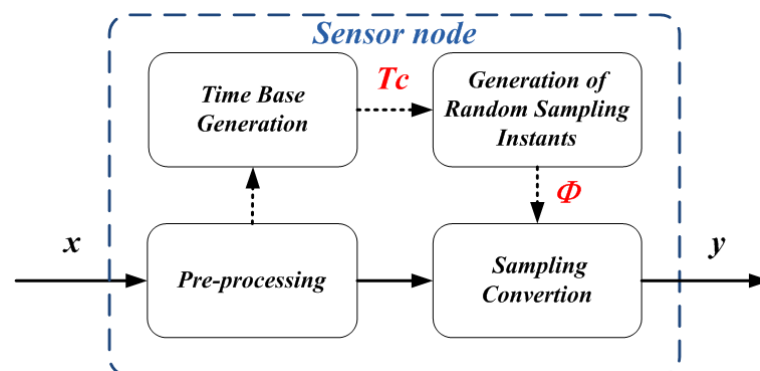


Fig.5.3 Scheme of the CS-based Sensor Node.

The pre-processing block receives in input the signal of interest, usually characterized by nominal amplitude of  $230 V_{RMS}$ , and adapts the voltage levels to the range of the ADC. The

Time Base Generation Block determines the time base resolution  $T_c$ , locked to the signal carrier frequency, in order to assure a synchronous sampling and prevent spectral leakage phenomena. However, the required sampling frequency is lower than that 10 kS/s, since the time base  $T_c$  is only used for generating the random sampling instants.

The Generation of Random Sampling Instants Block, in fact, receives  $T_c$ , and determines the sampling matrix  $\Phi$ . In particular, this block randomly generates  $M$  integer numbers  $k_i$  and obtains the  $M$  sampling instants  $t_i$  as random integer multiple of the resolution time bases  $T_c$  [1]:

$$t_i = k_i T_c, \quad k_i \in [0, N - 1] \text{ and } i = 1, \dots, M \quad (5.5)$$

Finally, the Sampling Conversion Block acquires and converts the reduced number of samples according to the received sampling instant and stores them.

The acquired  $M$  samples are sent, then, to the Central Measurement Unit, together with the sampling instants, that are necessary for the CS-based spectrum reconstruction.

The CMU has to perform the following tasks: (i) recovering of the magnitude spectrum of the input signal  $x$ , by means of a proper routine (CS-Solver) able to solve the convex minimization problem; (ii) estimation of harmonic and interharmonic disturbances according to IEC 61000-4-30 standard; (iii) data aggregation over 10 minutes intervals; and (iv) storage of the spectrum reconstructed through the samples received by all the sensing nodes deployed within the monitored grid.

Since the samples are stored in the CMU memory, it is not necessary to aggregate them. Therefore, time domain waveform of the input signal can be easily recovered at any time, if required by the operator (for example, if a fault has occurred). This capability is a further considerable advantage, with respect to traditional architecture, especially if diagnostics issues of the grid are taken into account.

### 5.3 Test Assessment

#### 5.3.1 Aims of the tests

Several tests, both numerical and experimental have been performed in order to assure that the measurement system based on CS is compliant to the standard. The tests have been carried out by means of the following steps: (i) a proper source supplies a voltage waveform affected

by harmonics and interharmonics whose order and amplitude are determined a priori, (ii) the measurement device performs the measurements of the groups and subgroups as defined in (5), (6), (7), and (8) and (iii) verifies that the deviation between the imposed values and those measured is lower than the recommended limit.

As regards the measurement of harmonic and interharmonic disturbances, the IEC 61000-4-30 standard refers to IEC 61000-4-7, that provides the accuracy requirements. The uncertainty limits associated with the harmonic subgroups measurements are reported in Tab. I for different conditions of meter class and component amplitude ( $U_m$ ) with respect to the rated RMS voltage ( $U_{nom}$ ) of the power system.

Tab.I Limits of desired uncertainty related to class A and B meters according to the standard IEC 61000-4-7.

Class	Measurement	Conditions	Maximum error
A	Voltage	$U_m \geq 1\% U_{nom}$	$\pm 5\% U_m$
		$U_m < 1\% U_{nom}$	$\pm 0.05\% U_{nom}$
B	Voltage	$U_m \geq 3\% U_{nom}$	$\pm 5\% U_m$
		$U_m < 3\% U_{nom}$	$\pm 0.15\% U_{nom}$

Numerical tests have been carried out through a suitable algorithm developed in Mathworks Matlab® programming language. The script allows to synthetize 2048 samples of a discrete-time reference signal  $\mathbf{x}$ , with a time period of 20 ms and an associated sampling rate of 10.24 kS/s, made by sums of sinusoidal wave shapes at harmonic and interharmonic frequencies. It is possible to set the nominal amplitude of each harmonic and interharmonic component.

Also the acquisition system has been simulated in Matlab, through a proper sampling and quantizing function, which allows to select: (i) the resolution time base  $T_c$  for the random sequence of sampling instants; (ii) the resolution (i.e. the number of bits) of the simulated ADC; (iii) the number of samples  $M$  and the number of reconstructed samples  $N$ , which both determine the compression ratio

$$CR = \left(1 - \frac{M}{N}\right) \cdot 100 \quad (5.6)$$

The digitized samples are then supplied to the reconstruction algorithm, in order to estimate the magnitude spectrum of the input signal. At this aim, one of the free available CS-Solvers, CVX, is used [2], with the aim of finding the sparse solution of the convex optimization problem.

As performance factor, the difference between measured and nominal amplitude of each harmonic and/or interharmonic subgroup has been evaluated and compared with the maximum error defined in the IEC 61000-4-7 for class A meters.

### **5.3.2 Selection of the Test Signal**

It is worth noting that particular attention has to be paid to the selection of the harmonic content of the generated test voltage. The number of test voltage sets, in fact, could be theoretically infinite due to the degrees of freedom associated to the number of harmonic and interharmonic components, to their frequency and to their amplitude.

According to condition (1.10) the performance of the CS approach depend on the sparsity of the input signal; the higher is the number of frequency components (i.e. the sparsity  $S$ ), the higher is the number of required samples  $M$  for accurately reconstruct the input signal. Therefore, the reference input signal has been selected in order to assess the proposed approach in the worst operating conditions. At this aim, the harmonic and interharmonic components have been set according to the maximum values reported in the standard EN 50160, which defines the main voltage characteristics of electricity supplied by public distribution network under normal operating conditions.

With specific regard to spectral harmonic content, during the period of a week, the 95% of RMS values of each individual harmonic voltage up to the 25<sup>th</sup> order, aggregated over time intervals of 10 minutes, shall be less than or equal to the values given in Tab. II. Moreover, the total harmonic distortion of the supply voltage (including harmonics up to the order 40) shall be less than or equal to 8%.

Tab.II – Limit values of individual harmonic voltages at supply terminals for order up to 25 given in per cent of the fundamental amplitude  $u_1$

Odd harmonics				Even harmonics	
Not multiples of 3		Multiples of 3			
Order h	Relative amplitude $u_h$	Order h	Relative amplitude $u_h$	Order h	Relative amplitude $u_h$
5	6.0 %	3	5.0 %	2	2.0 %
7	5.0 %	9	1.5 %	4	1.0 %
11	3.5 %	15	0.5 %	6 ... 24	0.5 %
13	3.0 %	21	0.5 %		
17	2.0 %				
19	1.5 %				
23	1.5 %				
25	1.5 %				

Therefore, the signal  $x$  has been obtained by combining all the spectral harmonics up to 25<sup>th</sup> order. The amplitudes of the harmonic components have been set equal to the limits provided by EN 50160, with the purpose of assessing the proposed approach with the input signal affected by the maximum pollution admitted on the transmission networks. The harmonic content of the test signal is shown in Fig.5.4, where the amplitudes are referred to the rated RMS voltage  $U_{nom}$  of 230 V.

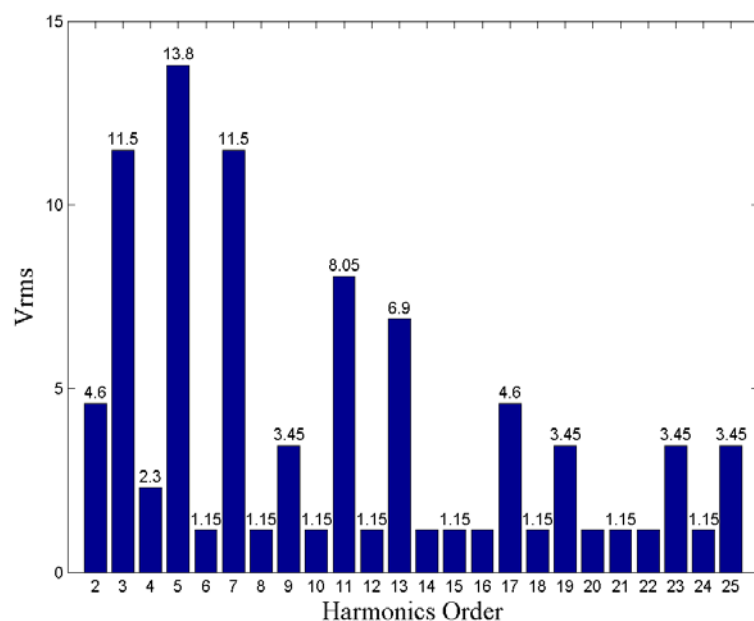


Fig.5.4 Harmonic content of the test signal

Several tests have been performed by varying the characteristics of the acquisition system (resolution and number of acquired samples), in order to establish the proper trade-off between hardware costs and compliance to the uncertainty limits stated by the standard.

### 5.3.3 Simulation Results

As an example, Fig.5.5, shows the test signal and the acquired samples, highlighted by means of red markers. As can be observed, samples have been taken uniformly at random in the observation time window of 200 ms.

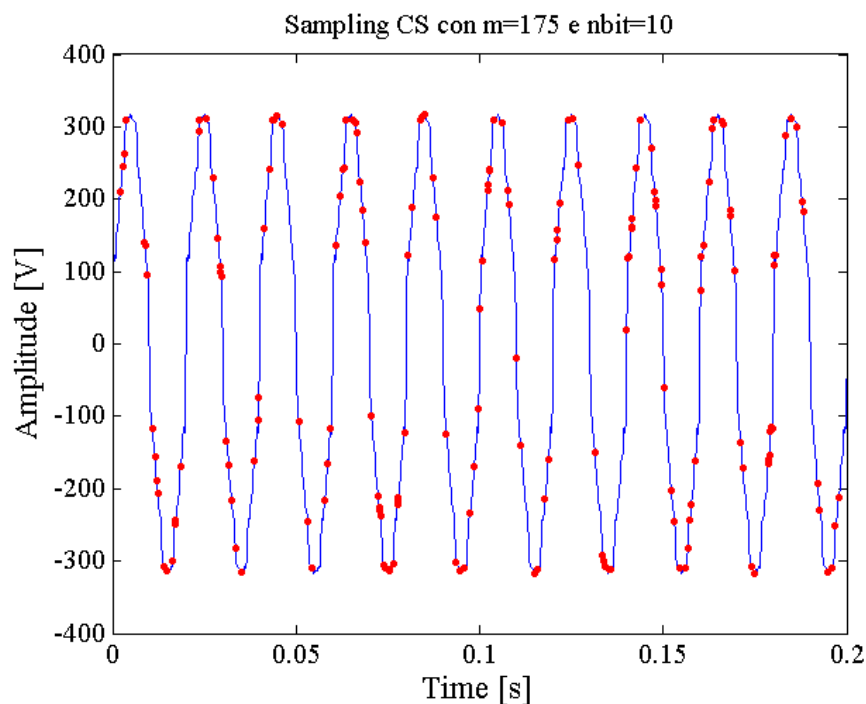


Fig.5.5 The test signal in time-domain (blue line) and the acquired random samples (red dots)

The amplitude spectrum of the test signal has been reconstructed by means of CS-based spectrum estimation by taking 125, 150, 175 random samples with a vertical resolution of 10 bits. The 3D-bar plot in Fig.5.6 shows the differences between measured and nominal amplitude of each harmonic subgroup. The red surface shapes the maximum error allowed according to IEC 61000-4-7 for each harmonic subgroup. As it can be appreciated, most of the amplitude measured with only 125 and 150 random samples are not compliant with the limits of desired uncertainty (the relative 3D-bar plot passes the red surface). On the contrary, by increasing the number of acquired samples up to 175, an accurate estimate of the RMS amplitude of each harmonic subgroup can be gained. The numerical results prove that the CS-based PQ instrument is able to measure the polluted voltage of actual electrical power

delivery systems by means of the acquisition of only 175 samples, rather than the 2048 samples necessary to traditional PQ instruments (i.e. a compression ratio of 91.45% is obtained), with notable reduction of the involved memory depth.

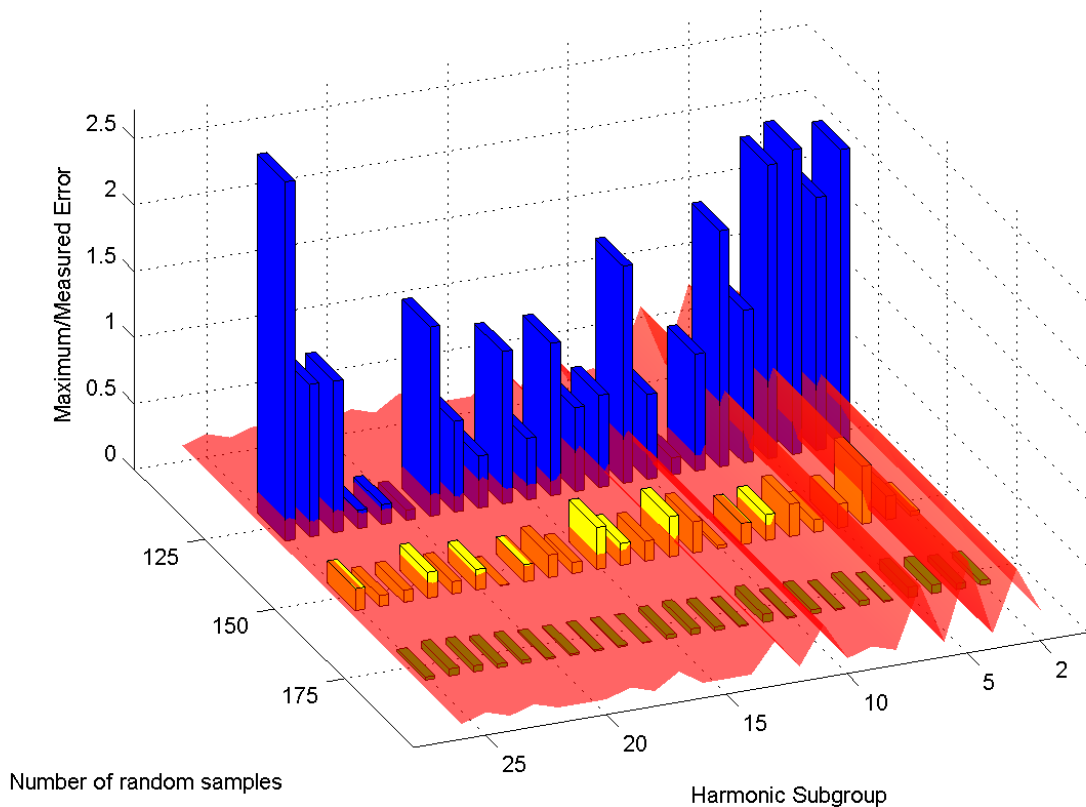


Fig.5.6 Measured error for each harmonic subgroup for different number of random samples.

In order to assess the performance in actual operating conditions the influence of the noise has been successively investigated by means additional tests. As an example, results with a Signal to Noise Ratio (SNR) of 60 dB and for different values of effective number of bits, are shown in Fig.5.7.

The amplitude spectrum of the test signal has been reconstructed by means of CS-based algorithm by taking 250 random samples with a resolution of 10, 12, 14 bits. In this instance, the relative 3D-bar plot proves that if the number of bits is equal to 10, some RMS amplitudes of harmonic subgroups are not correctly measured. On the contrary, a resolution at least equal to 12 effective bits is suitable to perform harmonics measurements compliant with standard IEC 61000-4-7.

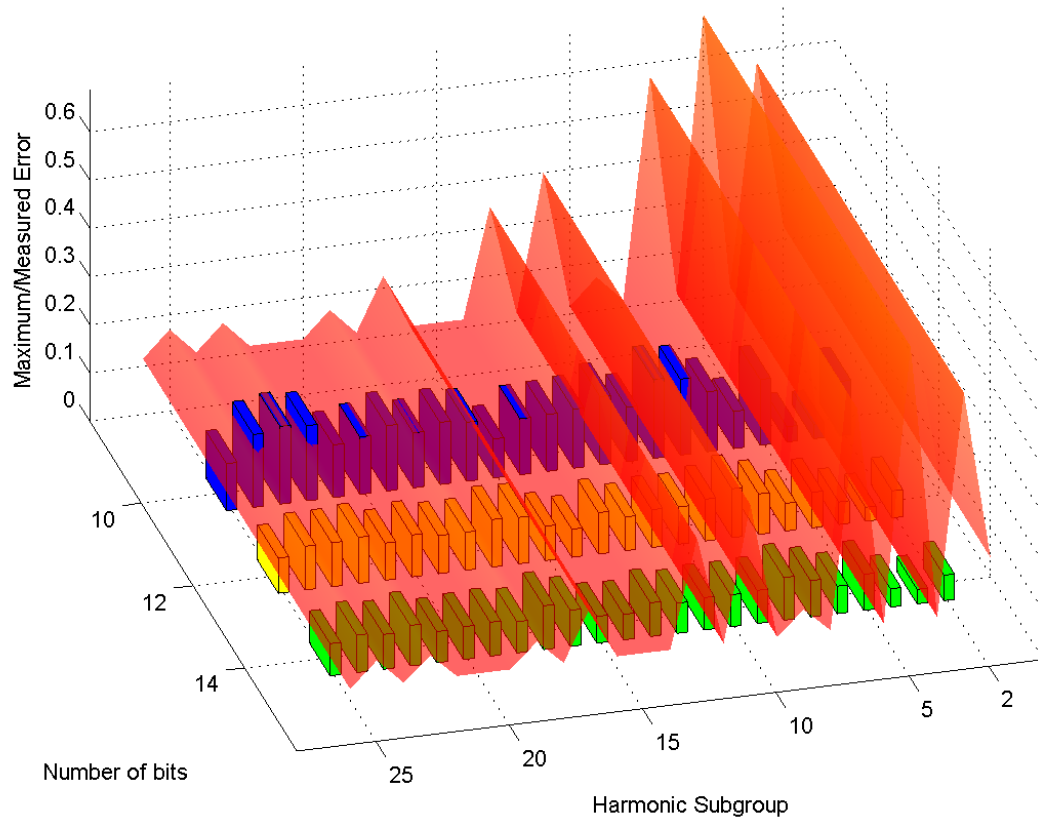


Fig.5.7 Measured error for each harmonic subgroup for different ADC resolutions.

### 5.3.3.1 Issue concerning interharmonic components

Most of the instruments performing PQ measurements make use of a phase locked loop in order to synchronize the acquisition with the fundamental frequency of the input signal so that exactly 10 cycles are obtained. This approach is, obviously, not suitable for the measurement of interharmonics component, whose frequency is not an integer multiple of the fundamental frequency. Since the observation interval does not include an integer number of periods of the interharmonic components, the magnitude spectrum suffers from spectral leakage. Traditional PQ instruments usually mitigate this effect by applying a suitable window to the input signal.

The proposed CS-based PQ instrument also takes advantage from a proper windowing technique; in particular, the Hanning window is applied to the acquired samples.

In order to assess the performance of proposed method also if interharmonic components occur, a suitable number of tests have been conducted. In Fig.5.8, the signal obtained by combining the test signal in Fig.5.4 with two interharmonics is shown. In this instance, the

interharmonic frequencies have been set equal to 75.5 and 775.5 Hz, whereas the amplitudes have been set equal to 30 Vrms

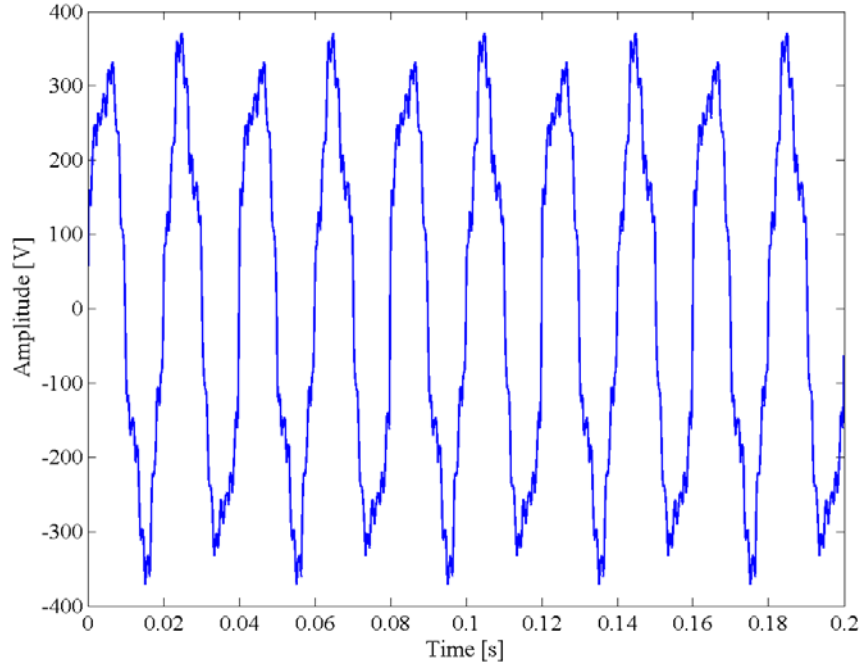


Fig.5.8 Test signal used to assess the proposed method also in presence of interharmonic components.

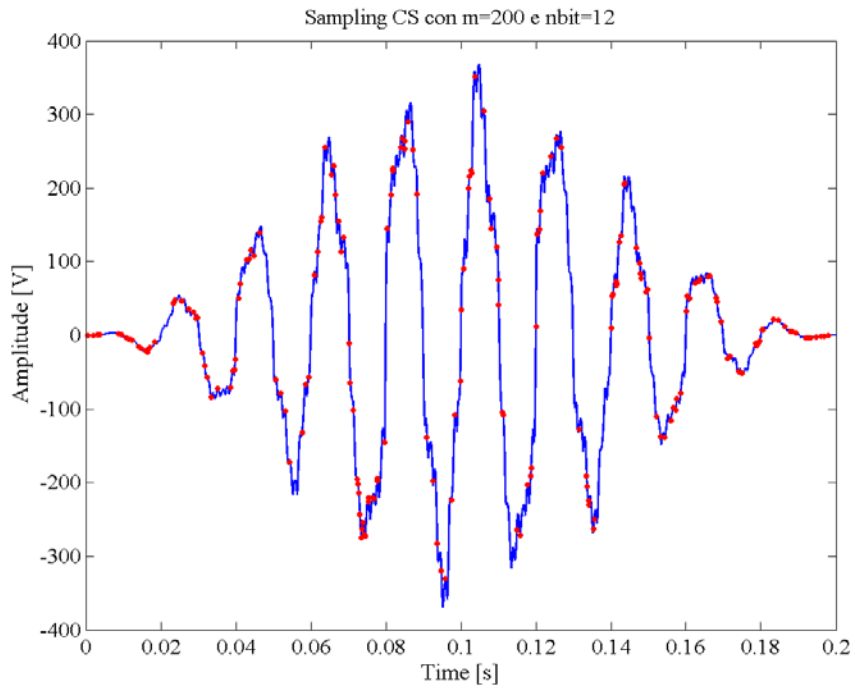


Fig.5.9 Signal windowed through Hanning function.

and 15 Vrms respectively. For the sake of clarity, the samples acquired according to the CS strategy and processed through the Hanning window, are shown in Fig.5.9, marked with red dots.

The 3-D bar plot in Fig.5.10 shows that for the considered test signal, windowed with a Hanning function, an accurate estimate of the RMS amplitude of each interharmonic subgroup can be gained by means of no less than 350 samples, slightly greater than required when the considered test signal is obtained by combining all the spectral harmonics up to 25<sup>th</sup> order. This results could be expected, since the test signal used in order to assess the performance of the proposed method in occurrence of interharmonic pollution, have been obtained adding to test signal of Fig.5.4 two interharmonic components, thus increasing the sparsity  $S$  of the input signal.

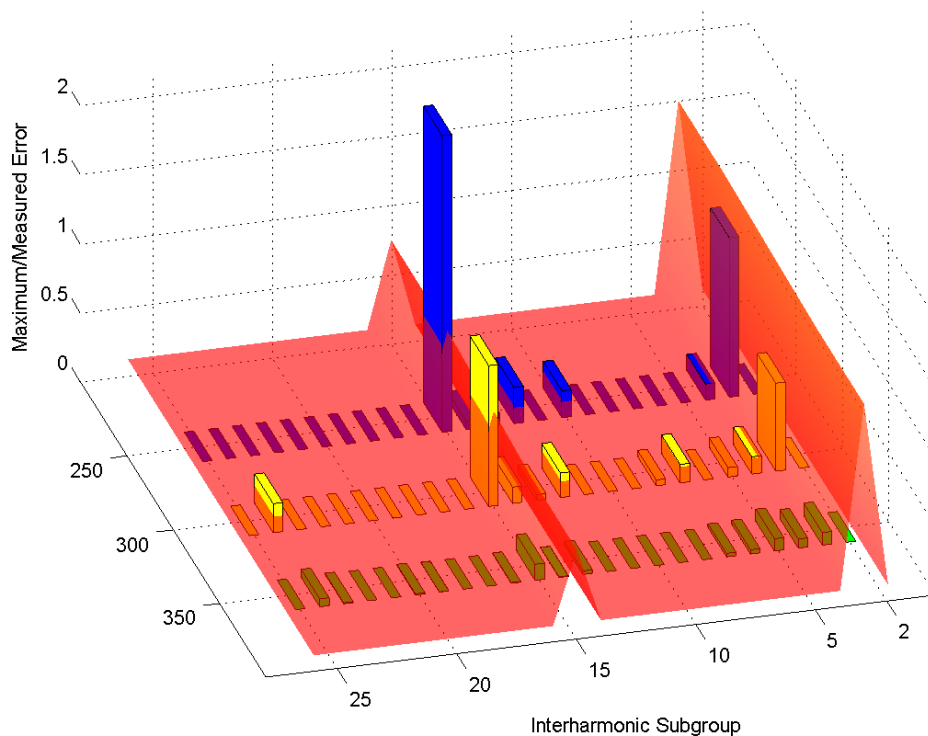


Fig.5.10 Measured error .in presence of interharmonic components for different number of random samples.

### 5.3.4 Experimental Results

Numerical results have provided fundamental information about the characteristics that the acquisition system has to meet, in terms of vertical resolution (effective number of bits) and number of samples. In particular, an ADC characterized by 12-bit resolution and able to acquire about 250/350 random samples (depending on the occurrence of interharmonic

components), over an observation time interval of 200 ms, should be adopted in order to assure measurement results compliant with IEC 61000-4-7 standard.

The performances of the proposed approach have been further assessed also in actual operating conditions, through the realization of a proper test station, that has been set up exploiting high-performance components, in order to evaluate the performance of the reconstruction algorithm regardless the uncertainty introduced by the hardware devices.

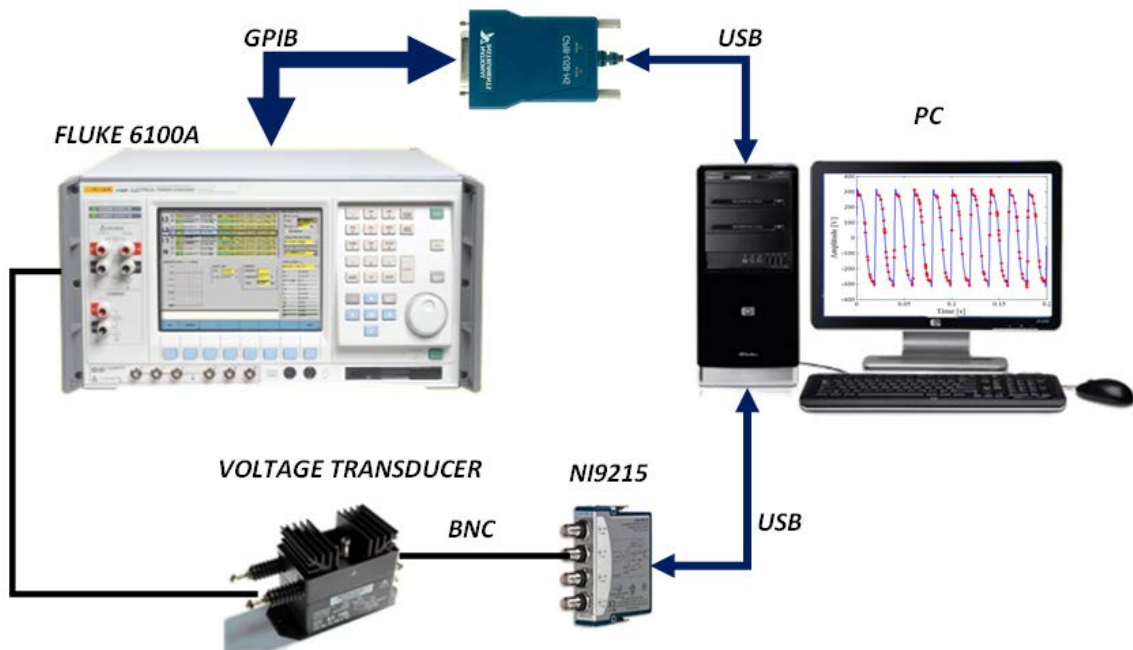


Fig.5.11 Set up for experimental tests.

In particular, the measurement station (Fig. 5.11), involves:

- A Data Acquisition System (DAS) NI9215, by National Instruments, characterized by a sample rate of 10 kS/s for each channel, an input voltage ranges of  $\pm 10.4$  V and a nominal vertical resolution of 16 bit.
- An electrical power calibrator FLUKE 6100A [3], able to generate a wide variety of complex signals, including harmonic and interharmonic components; the calibrator FLUKE 6100A has been configured in order to provide the same signal adopted in the numerical tests.
- A voltage transducer LEM CV 1000, characterized by an extended bandwidth from DC up to 500 kHz, with a conversion ratio equal to 100, and an overall accuracy of 0.1%, mandated to adapt the output signal of the calibrator.

- A Personal Computer (PC) mandated to: (i) set calibrator FLUKE 6100A by means of a proper user interface; (ii) set parameters of the data acquisition system and start the acquisition process; (iii) receive and process the digitized samples in order to reconstruct the input signal.

Since the available DAS executes only traditional uniform sampling, the random sampling, necessary for exploiting the CS-based approach, has been obtained through a proper decimation process, performed by a software application. As reported in the flow chart of Fig.5.12, the DAS acquires  $N$  samples according to its constant sampling rate  $f_c$  and sends them to the PC, where a suitable function, "Random Sampling", randomly extracts the desired number  $M$  of samples from the measurements vector of size  $N$ . As matter of practice, this operation is equivalent to perform a random sampling of  $M$  samples of the input signal acquired at  $M$  random instants that are integer multiple of  $T_c=1/f_c$  in the observation time interval. In order to assure a frequency resolution equal to 5 Hz and the reconstruction of the spectral components up to the 100<sup>th</sup> harmonic, 2000 samples have been acquired during an observation interval of 200 ms.

As for the numerical tests, the performances of the proposed approach are quantified through the comparison with results obtained through the traditional DFT algorithm. The amplitude of the frequency components measured through DFT, in fact, is considered as the reference values. In the left side of the flow chart in Fig.5.12, the reference harmonic amplitudes are obtained by processing the complete vector of 2000 samples according to the traditional Fourier analysis. In the right side of the flow chart, the compressed vector of  $M$  samples is given as input to the CS-based reconstruction algorithm. Both the two approach compute the magnitude spectrum on 2000 bins and determine the amplitude of harmonic and interharmonic subgroups. Successively, for each harmonic and/or interharmonic order, the difference between the amplitudes measured by means of CS-based spectrum estimation and that measured by means of DFT (referred to as measured error) has been evaluated and compared with the maximum error defined in the IEC 61000-4-7 for class A meters. Also in this instance, the algorithm has been implemented through Mathworks Matlab® programming language.

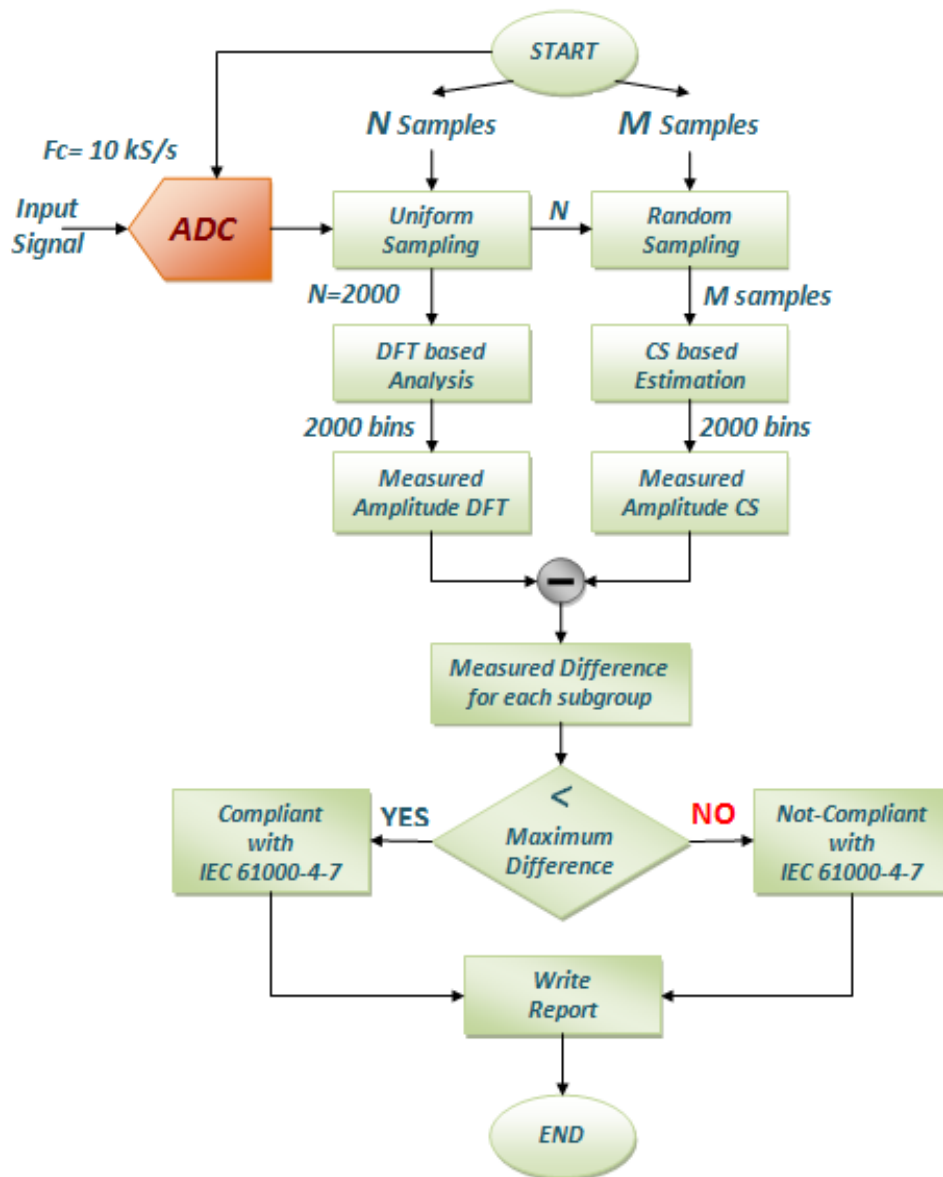


Fig.5.12 Flow chart illustrating the operation of the experimental assessment.

Also in these tests, compliance with IEC 61000-4-7 standard has been evaluated versus different values of number of random samples  $M$ . For each test configuration, 100 acquisitions have been performed and the difference between amplitudes measured by means CS-based spectrum estimation and reference amplitudes of each harmonic and/or interharmonic subgroup has been evaluated in terms of mean and standard deviation.

According to a worst-case approach, the maximum value observed within the 100 repeated acquisitions of the measured error has been evaluated for each harmonic subgroup and for different number  $M$  of samples. The results are shown in Fig.5.13. As it can be noticed, the non-idealities characterizing the actual acquisition process affect the accuracy of the CS-based

reconstruction algorithm. In fact, in this instance the minimum number of samples required in order to assure the compliance to the standard for each frequency component is  $M=450$ , causing the increase of the compression ratio up to 77%.

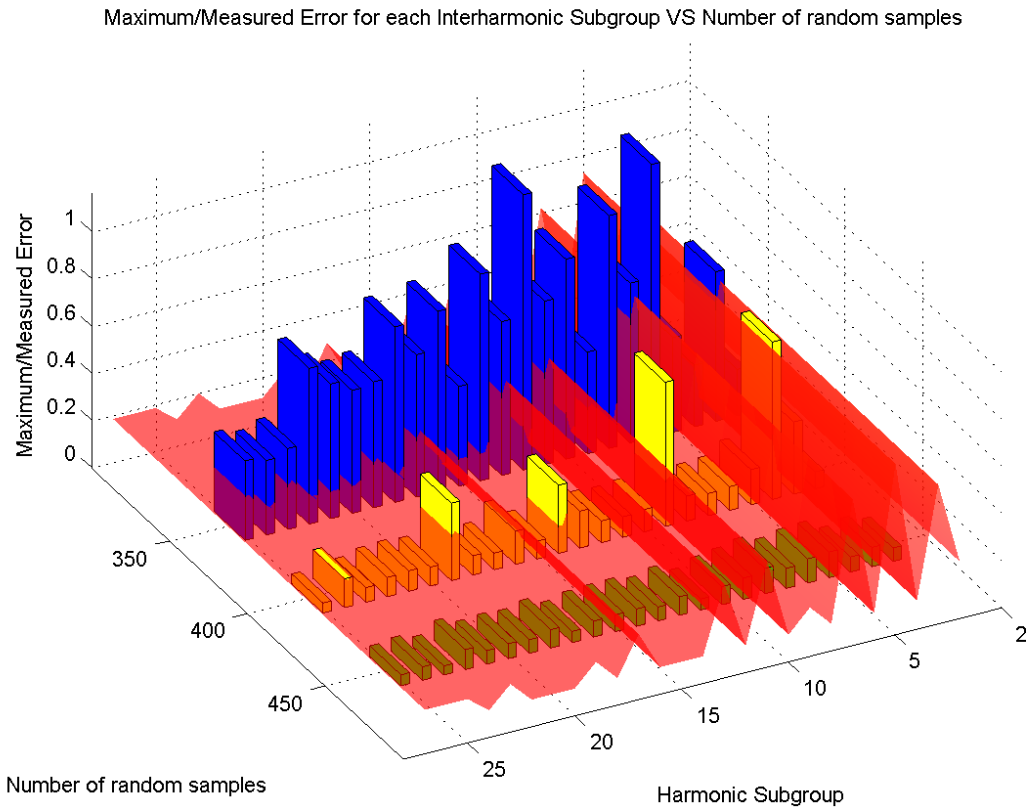


Fig.5.13 Maximum measured error within 100 repeated acquisitions for different number of samples in experimental tests.

Additional information about the experimental characterization is given in Tab. III, where, for each harmonic group and for three values of  $M$ , have been estimated: (i) the error limit stated by the standard, (ii) the mean the error measured on 100 repeated acquisition, (iii) the maximum observed error, and (iv) the number of trials (in terms of percentage of 100 acquisitions) in which the maximum measured error is lower than the allowed limit (i.e. the error is compliant to the standard).

Tab.III – Experimental results for different number of samples.

Order	limit [V]	M=350			M=400			M=450		
		mean [V]	max [V]	compliance to standard	mean [V]	max [V]	compliance to standard	mean [V]	max [V]	compliance to standard
2	0,235	0,044	0,198	100%	0,035	0,570	99%	0,025	0,074	100%
3	0,580	0,049	0,633	99%	0,031	0,305	100%	0,027	0,082	100%
4	0,119	0,044	0,261	93%	0,036	0,667	99%	0,022	0,083	100%
5	0,694	0,055	0,669	100%	0,032	0,207	100%	0,027	0,108	100%
6	0,115	0,063	1,156	91%	0,036	0,776	98%	0,024	0,102	100%
7	0,579	0,057	0,916	97%	0,041	0,581	100%	0,025	0,087	100%
8	0,115	0,067	0,985	91%	0,032	0,112	100%	0,027	0,108	100%
9	0,178	0,054	0,696	95%	0,034	0,611	98%	0,024	0,119	100%
10	0,115	0,054	0,846	94%	0,030	0,113	100%	0,027	0,090	100%
11	0,406	0,062	0,914	97%	0,042	0,573	99%	0,031	0,101	100%
12	0,115	0,063	1,166	91%	0,034	0,522	99%	0,029	0,089	100%
13	0,350	0,059	1,087	97%	0,038	0,271	100%	0,031	0,102	100%
14	0,115	0,064	0,875	91%	0,036	0,289	98%	0,028	0,074	100%
15	0,115	0,058	1,077	93%	0,034	0,290	99%	0,027	0,109	100%
16	0,115	0,059	0,764	92%	0,036	0,336	98%	0,028	0,109	100%
17	0,235	0,063	0,948	96%	0,041	0,477	99%	0,031	0,117	100%
18	0,115	0,058	0,744	93%	0,031	0,120	99%	0,026	0,078	100%
19	0,176	0,054	0,660	95%	0,035	0,327	99%	0,028	0,080	100%
20	0,115	0,048	0,520	93%	0,036	0,253	99%	0,025	0,080	100%
21	0,115	0,053	0,777	95%	0,037	0,184	98%	0,027	0,088	100%
22	0,115	0,048	0,660	93%	0,032	0,161	99%	0,022	0,085	100%
23	0,176	0,054	0,623	97%	0,036	0,105	100%	0,031	0,092	100%
24	0,115	0,045	0,393	94%	0,036	0,224	97%	0,028	0,093	100%
25	0,178	0,052	0,336	98%	0,045	0,153	100%	0,036	0,120	100%

As it can be expected, the higher the number of random acquired samples, the better the performance of the proposed approach in terms of both maximum error and number of compliant results; some deviations from this general enhancement, however, have been noted (e.g. 2<sup>nd</sup> and 4<sup>th</sup> harmonic orders). Such a behavior is related to the reconstruction quality that depends on the number of acquired samples; according to what stated in [4], correct reconstructions are granted “with overwhelming probability” only if eq. (1.10) is strictly satisfied. If this is not the case, unpredictable outliers can likely occur also if the number of acquired samples is close to the required value (depending on the specific random sequence of acquired samples). When 450 random samples are taken into account, the proposed approach always assured convergent reconstruction and, as a consequence, reliable results; no outliers have been evidenced throughout the tests in the considered experimental configuration.

As confirmation, Fig.5.14 shows the measured errors obtained for the 11<sup>th</sup> harmonic group in the different considered acquisition conditions. In particular, for each value of  $M$ , both the scattered plot of the measured errors and the corresponding empirical probability density functions (EPDFs) are drawn. Most of the measured errors (approximately 94%) were spread out in a limited interval equal for all the values of  $M$  and the width of main lobe of the EPDFs were roughly the same. The EPDF corresponding to 350 and 400 presented spurious samples

i.e. “outliers” far from the mean value causing the experienced worsening of the maximum error.

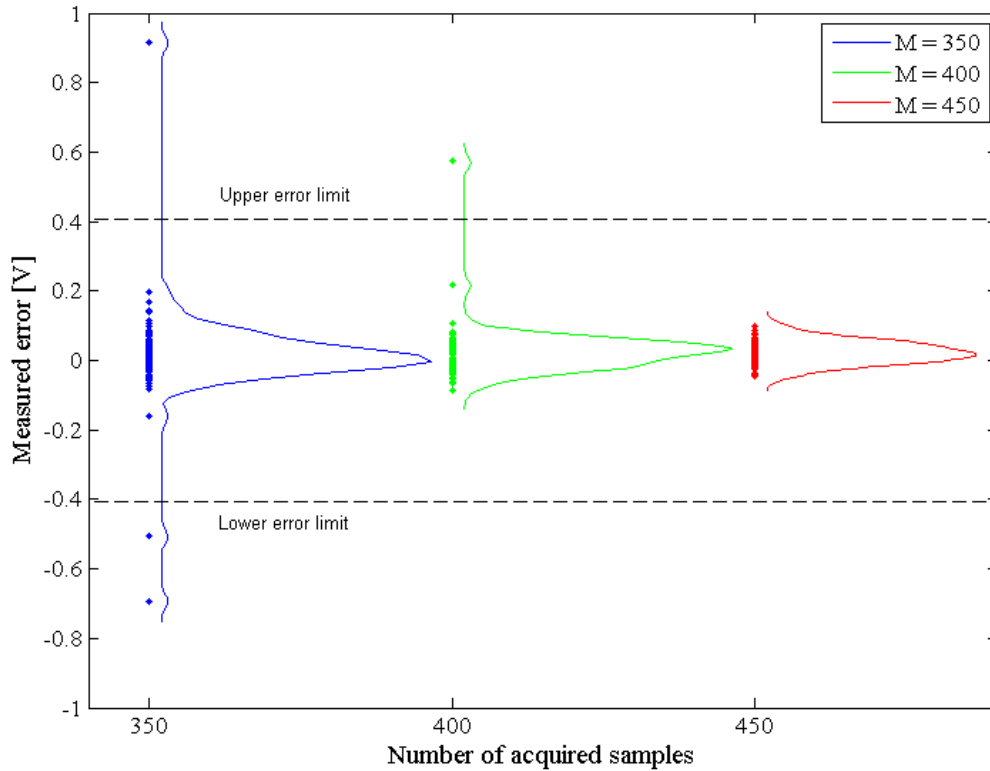


Fig.5.14 Scattered plot and EPDF of measured error for different number of samples.

#### 5.4 Conclusions

The results experienced in both numerical and actual experiments highlighted that by means of the CS-based approach the measurement of harmonic and interharmonic disturbances, compliant with the error limits stated by the current standards, can be obtained through the acquisition of a reduced number of samples, achieving a compression ratio equal to 77%. Thanks to these features, it is possible to exploit a cost-effective architecture for monitoring harmonic and interharmonic pollution on wide grid. The opportunity of acquiring a reduced number of samples not only makes possible the employment of low-cost devices, but it also allows to store in the memory of the CMU the minimal information for successive full reconstruction of the time domain waveforms if required for diagnostic issues.

## **5.5 References**

- [1] F. Bonavolontà, M. D'Apuzzo, A. Liccardo, M. Vadursi, "New approach based on compressive sampling for sample rate enhancement in DASs for low-cost sensing nodes", *Sensors*, Vol. 14, N. 10, pp. 18915-18940, 2014.
- [2] CVX: Matlab Software for Disciplined Convex Programming, Version 2.0 (beta). Available online: <http://cvxr.com/cvx/>.
- [3] Fluke 6100 Electrical Power Quality Calibrator, Specification, Note 3499335, available at [www.fluke.com](http://www.fluke.com).
- [4] E.J. Candès and J. Romberg, "Sparsity and incoherence in compressive sampling", *Inverse Problems*, Vol. 23, N. 3, pp. 969-985, 2007.

## **Conclusions and Future Developments**

The research activity, presented in this Ph.D. final work, suggests the possibility to move towards a different approach for monitoring grid deployed on wide geographical areas, exploiting the advantages of an innovative measurement approach: the Compressed Sampling. In particular, the proposed architecture consists of low cost nodes mandated only to sample and digitize a limited number of input signal samples and transmit them to a central measurement unit, saving, thus, the costs related to large memory supports and expensive digital processing units. Once the samples have been received, the central unit recovers the signal spectrum thanks to CS-based algorithm and carries out the desired measurements. In other words, thanks to the CS-based approach, it has been possible to design and realize a measurement node, characterized by reduced memory depth and only one ADC that allows meeting the requirements of a distributed measurement system suitable for Smart Grid environment.

In Chapter 2, a new method for the measurement of electrical power quality based on the new paradigm of compressive sampling has been presented. In particular, the attention has been focused on the measurement of the root means square (RMS) voltage whatever the harmonic content of the input signal. It has been proved that by using a compressive sampling approach, a notably reduction of the required memory depth to perform long-time analysis has been obtained. In Smart Grid applications, the measurement node is required to simultaneously acquire a defined number of quantities (e.g. voltage and current acquisition for smart metering applications). This requirement cannot be met on most of the traditional low-cost platforms, since they multiplex input physical channels to reduce the cost of the ADC section (i.e. one of the most expensive), thus allowing only sequential data acquisition to be performed. Therefore, overall measurement performance is limited, because an unwanted phase displacement turns out to be imposed on the acquired signals. This phase shift is mainly due to the inter-channel delay the multiplexer spends to acquire two samples on different channels, and proves to be a deep constraint that typically reduces the applicability of low-cost measurement nodes. To overcome the considered limitations, in chapter 3 a novel acquisition approach, based on CS, capable of carrying out multichannel simultaneous data acquisition also through inherently sequential DASs has been presented. The approach exploits a unique time-basis for all the input channels adopted, along with a compressive random sampling, in order to assure the reconstruction of desired signals without any artefact

due to the inter-channel delay and/or sequential acquisition scheme. A number of tests carried out both on numerical and actual sinusoidal signals highlighted and confirmed the promising performance of the proposed acquisition approach. Phase shifts among the reconstructed waveforms as low as few milliradians (about 0.016% of a whole period) have, in fact, been experienced in several measurement conditions, involving different values of the number of acquired samples, vertical resolution and input signal frequency, for 8-bit and 32-bit microcontrollers.

For the proposed distributed monitoring systems, improving the performance of the embedded DAS, in terms of sample rate enhancement, can be crucial for the improvement of the whole measurement system. To this aim, a new method based on compressive sampling (CS), which permits to increase the maximum sample rate of DAS integrated in low-cost microcontrollers, has been proposed in Chapter 4. Preliminary tests conducted in simulations highlighted the promising effective performance of the proposed strategy in the presence of signals characterized by different amplitude and spectral contents. Experimental tests have also been carried out on microcontrollers characterized by different internal architecture and operating specifications. It is worth highlighting that satisfying results were obtained with different embedded systems, with increase of effective sample rate up to 50 times with respect of the actual ADC sample rate.

Finally, in the Chapter 5, the compliance of the measurement node based on CS approach with the current Power Quality standard has been assessed by means of numerical and experimental tests. In particular, the capability of CS-based acquisition approach of correctly measuring root-mean-square amplitude of harmonic and interharmonic voltage pollution has been verified.

The results provided by means of the CS-based approach experienced in both numerical and actual experiments highlighted that the measurement of harmonic and interharmonic disturbances, compliant with the error limits stated by the current standards, can be obtained through the acquisition of a reduced number of samples, achieving a compression ratio equal to 77%. Thanks to these features, it is possible to exploit a cost-effective architecture for monitoring pollution on smart grid.

Future research activities can be addressed to:

1. performance comparison, in terms of computational burden, among the different tools available for the solution of the optimization problem,

## *Conclusions and Future Developments*

2. identification of optimal random sequence capable of making the proposed strategy with the lowest reconstruction error,
3. exploitation of transformation matrix based on wavelet transforms in order to perform reconstruction of non stationary signals
4. the implementation of the whole smart meter on a low-cost embedded system.